

LOAN DOCUMENT

PHOTOGRAPH THIS SHEET

①

DTIC ACCESSION NUMBER

LEVEL

INVENTORY

WL-TR-95-4066

DOCUMENT IDENTIFICATION

may 95

DISTRIBUTION STATEMENT

ADDITIONAL INFO	
NTIS	ORAM
DTIC	TRAC
UNANNOUNCED	
JUSTIFICATION	
BY	
DISTRIBUTION/	
AVAILABILITY CODES	
DISTRIBUTION	AVAILABILITY AND/OR SPECIAL
A-1	

DISTRIBUTION STAMP

DTIC	
ELECTE	
AUG2 1995	
C	D

DATE ACCESSIONED

DATE RETURNED

REGISTERED OR CERTIFIED NUMBER

19950728 050

DATE RECEIVED IN DTIC

PHOTOGRAPH THIS SHEET AND RETURN TO DTIC-FDAC

H
A
N
D
L
E

W
I
T
H

C
A
R
E

WL-TR-95-4066

HIERARCHICAL PROCESS CONTROL OF
CHEMICAL VAPOR INFILTRATION



PALAITH D., SAYLOR J., (TA&T)
GARRETT P., JONES J. (UC)

T&T
133 DEFENSE HWY, SUITE 212
ANNAPOLIS, MD 21401

MAY 1995

FINAL REPORT FOR 05/01/95-05/31/95

APPROVED FOR PUBLIC RELEASE; DISTRIBUTION IS UNLIMITED.


MATERIALS DIRECTORATE
WRIGHT LABORATORY
AIR FORCE MATERIEL COMMAND
WRIGHT PATTERSON AFB OH 45433-7734


NOTICE


When Government drawings, specifications, or other data are used for any purpose other than in connection with a definitely Government-related procurement, the United States Government incurs no responsibility or any obligation whatsoever. The fact that the Government may have formulated or in any way supplied the said drawings, specifications, or other data, is not to be regarded by implication, or otherwise in any manner construed, as licensing the holder, or any other person or corporation; or as conveying any rights or permission to manufacture, use, or sell any patented invention that may in any way be related thereto.

This report is releasable to the National Technical Information Service (NTIS). At NTIS, it will be available to the general public, including foreign nations.

This technical report has been reviewed and is approved for publication.


LT JOHN BUSBEE, Engineer
Materials Process Design
Integration & Operations Division
Materials Directorate


STEVEN R. LECLAIR, Chief
Materials Process Design
Integration & Operations Division
Materials Directorate


JOHN R. WILLIAMSON
Integration & Operations Division
Materials Directorate

If your address has changed, if you wish to be removed from our mailing list, or if the addressee is no longer employed by your organization please notify WL/MLIM, Wright Patterson AFB, OH 45433 to help maintain a current mailing list.

Copies of this report should not be returned unless return is required by security considerations, contractual obligations, or notice on a specific document.

REPORT DOCUMENTATION PAGE			FORM APPROVED OMB NO. 0704-0188	
Public reporting burden for this collection of information is estimated to average hour per response, including the time for reviewing instructions, searching existing data sources, gathering and maintaining the data needed, the complete and review the collection of information. Send comments regarding this burden estimate or any other aspects of this collection of information, including suggestions and reducing this burden to Washington Headquarters Services, Directorate for Information Operations and Reports, 1215 Jefferson Davis Highway, Suite 1204, Arlington, VA 22202-4302, and to the Office of Management and Budget, Paperwork Reduction Project (08704-0188, Washington, DC 20503.				
1. AGENCY USE ONLY (Leave Blank)		2. REPORT DATE May 1995		3. REPORT TYPE AND DATES COVERED May 1995 - May 1995
4. TITLE AND SUBTITLE Hierarchical Process Control of Chemical Vapor Infiltration			5. FUNDING NUMBERS C: F33615-94-D-5809 PE: 65502F PR: 2418 TA: 90 WU: 01	
6. AUTHOR(S) Palaith D., Saylor J., (TA&T) Garrett P., Jones J. (UC)				
7. PERFORMING ORGANIZATION NAME(S) AND ADDRESS(ES) TA&T 133 Defense Hwy, Suite 212 Annapolis, MD 21401			8. PERFORMING ORGANIZATION REPORT NUMBER	
9. SPONSORING MONITORING AGENCY NAME(S) AND ADDRESS(ES) Materials Directorate Wright Laboratory Air Force Materiel Command Wright Patterson AFB OH 45433-7734			10. SPONSORING/MONITORING AGENCY REP NUMBER WL-TR-95-4066	
11. SUPPLEMENTARY NOTES -				
12a. DISTRIBUTION/AVAILABILITY STATEMENT Approved for public release: distribution is unlimited.			12b. DISTRIBUTION CODE	
13. ABSTRACT <p>This is the final report on the Phase I STTR effort entitled "Hierarchical Process Control of Chemical Vapor Deposition." The work was performed jointly by Technology Assessment and Transfer and the University of Cincinnati (UC). It was shown that not only was process control for CVI feasible, but the anticipated improvements in product quality through increased densification and the reduction in processing time were substantial. Thus, the potential economic impact of this work is considerable, and could lead to a viable production technology. Specifically the University of Cincinnati developed a generic approach to the intelligent processing of materials (IPM), applied simulations of it to CIVI materials processing, and developed a rapid convergence artificial neural network and used it to discover improved regions of the CVI processing parameter space; also, the Technology Assessment & Transfer developed subprocess in situ state models for chemical vapor infiltration (CVI) of silicon carbide fiber preforms, and used them to identify in situ process sensors of considerable promise and as artificial neural network training pairs.</p>				
14. SUBJECT TERMS chemical vapor deposition, intelligence processing of materials (IMP), neural network, in situ state models, chemical vapor infiltration			15. NUMBER OF PAGES 62	
			16. PRICE CODE	
17. SECURITY CLASSIFICATION OF REPORT UNCLASSIFIED	18. SECURITY CLASS OF THIS PAGE. UNCLASSIFIED	19. SECURITY CLASS OF ABSTRACT UNCLASSIFIED	20. LIMITATION ABSTRACT UL	

HIERARCHICAL PROCESS CONTROL OF CHEMICAL VAPOR INFILTRATION

Contract No. DoD/Air Force F33615-94-C-5809

Draft Final Report
May 15, 1995

I INTRODUCTION

This is the Final Report on a Phase I STTR effort entitled "Hierarchical Process Control of Chemical Vapor Deposition." The work was performed jointly by Technology Assessment and Transfer and the University of Cincinnati (UC). It was shown that not only was process control for CVI feasible, but the anticipated improvements in product quality through increased densification and the reduction in processing time were substantial. Thus, the potential economic impact of this work is considerable, and could lead to a viable production technology. Specifically:

- *University of Cincinnati* developed a generic approach to the intelligent processing of materials (IPM), applied simulations of it to CVI materials processing, and developed a rapid convergence artificial neural network and used it to discover improved regions of the CVI processing parameter space;
- *Technology Assessment & Transfer* developed subprocess in situ state models for chemical vapor infiltration (CVI) of silicon carbide fiber preforms, and used them to identify in situ process sensors of considerable promise and as artificial neural network training pairs.

Nearly all ceramic matrix composite (CMC) processing today is performed under isothermal-isobaric conditions ranging from 900 to 1200°C and 5 to 20 Torr. Typical processing times for 6 mm-thick sections are measured in hundreds of hours. Processing geometries and methods of heating also result in large density gradients including premature surface pore closure and low ultimate density. Several methods have been proposed to eliminate these problems. Most notable among these has been the so-called "forced flow thermal gradient" method. While exhibiting considerable improvement in processing conditions, this method requires special fixturing for every part processed and is not, therefore, a method that holds great promise for mass production of CMCs.

TA&T has been exploring alternative technologies with special emphasis on microwave processing including methods of pulsed temperature and pulsed pressure. Two research microwave reactors have been built, and preliminary results have been encouraging. But if either method is to be successful it is clear that process controls are necessary. In fact, it will be shown in this report that dramatic improvement in both final density and processing time can be achieved by tracking an optimum processing trajectory in real-time. It also will be shown in this report that this optimum trajectory can be found and tracked using the hierarchical control methodologies that have been developed and expanded during the course of this work. Finally, it will be shown how in situ sensors have been identified and how they could be incorporated into a complete process control scheme for microwave CVI during a Phase II effort.

Production of advanced engineering materials requires a processing operation that is more tightly controlled than conventional systems that use variables defined at the process boundary. This requirement can be met by achieving accurate control of in situ process variables that are defined beyond process environmental boundaries. This goal is complicated by interactions among the variables -- interactions that may also be nonlinear -- as well as by measurement and actuation limitations. IPM was developed to reduce these processing difficulties by combining knowledge of material properties with process apparatus design in such a way as to compensate for these interactions.^{1 2} The IPM control architecture also was designed to exploit a comprehensive process knowledge representation in order to optimize goal trajectories for processing variables.

This work was conveniently divided into two initially independent paths. Along one path, the generic structure for the hierarchical process model was expanded and adapted for CVI (Tasks 1 and 2). Along the other path, models of the CVI process at the materials level were expanded to serve as subprocess in situ state models (Task 3), and to direct in situ sensor evaluation (Task 4). The interrelationship among these tasks is shown in Figure 1, reproduced from the original Phase I proposal. This figure also shows how the Phase I tasks lead naturally into a Phase II effort, and how that Phase II effort would be completed with transfer of the technology. All tasks were successfully completed, as was a detailed outline of a Phase II effort. This report comprises the following additional six section:

- II Survey and critique of commercially available IPM control systems;
- III Description of the IPM system that was developed during this Phase I work;
- IV In situ state model requirements;
- V Description of the in situ state model developed during the course of this Phase I effort, and of the preliminary computer simulations of the CVI process;
- VI Evaluation of potential in situ process control sensors, and their use in feedback control;
- VII Outline of a Phase II effort.

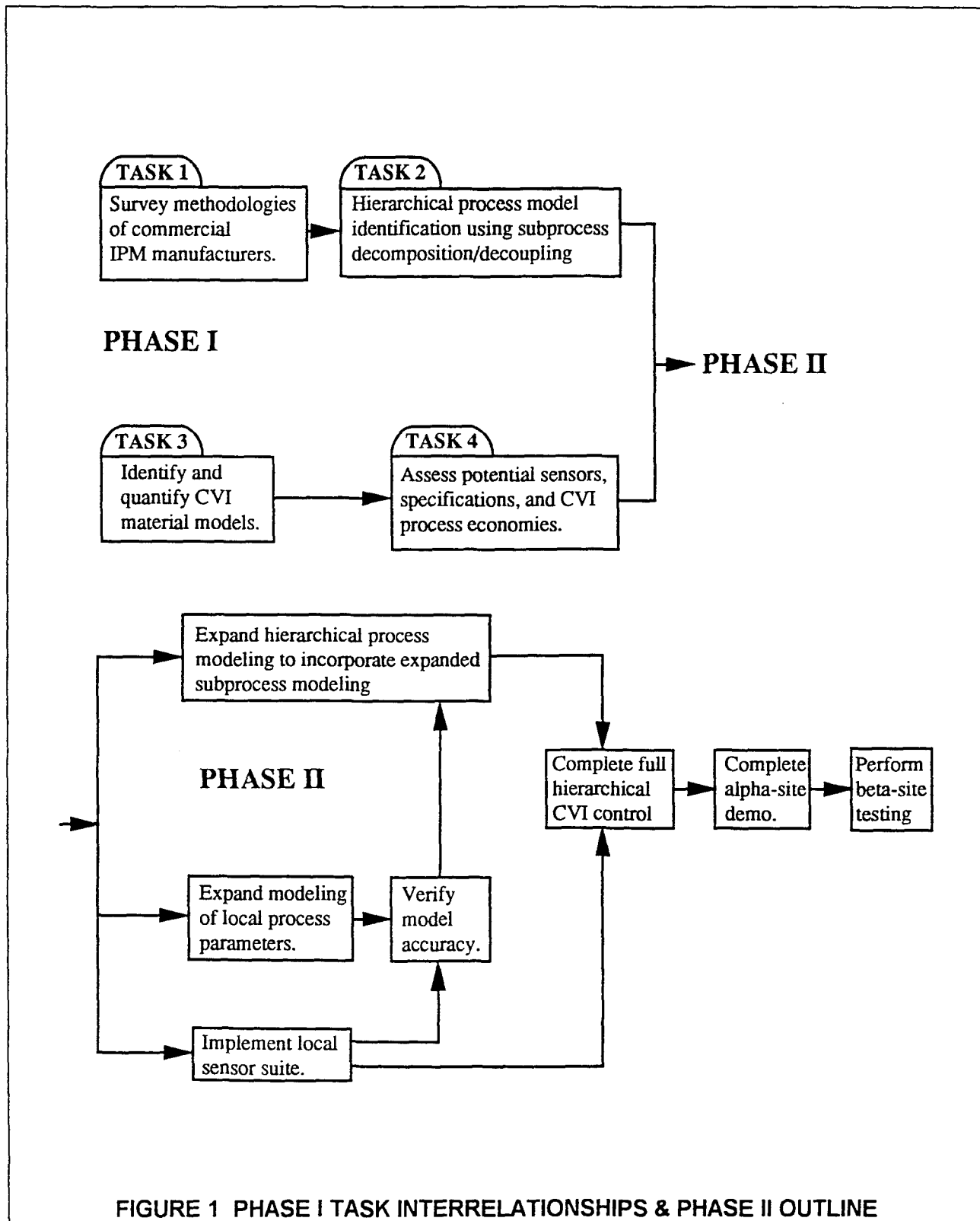
II SURVEY OF THREE COMMERCIALY AVAILABLE IPM CONTROL SYSTEMS

Although there exists a wide variety of materials processing techniques, nearly all of them exhibit certain common principles. For example, the transport of energy, mass, and momentum, and the goals of high uniformity and reproducibility, are essential elements of all materials processing approaches. An ideal process control system would be one that fundamentally addresses generic materials processing principles and eliminates the need for continuous control fine tuning for interacting process elements or for developing one-of-a-kind solutions for each processing case. Of course, processes capable of only marginal performance will be unlikely to produce premium products even with the most capable control system. This leads to the important, and often overlooked, conclusion that one focus of any processing research effort must be on upon improving the capability of the process apparatus

¹ "The Basics of the Intelligent Processing of Materials," Parrish, P. A. and Barker, W. G., J. Materials, July 1990.

² "Emerging Methods for the Intelligent Processing of Materials," Garrett, P. H., et al., J. Mat. Engineering and Performance, October 1993.

and the models that represent it in order to achieve the process controllability required for advanced engineered materials. Therefore, one aspect of this Phase I effort was to compare existing IPM systems developed by commercial process control manufacturers.



Typical of the design methods and perspectives for IPM systems are those developed independently by MTS Systems Corporation³, General Electric Research⁴, and United Technologies Research Center⁵. A preliminary evaluation of these processing systems, represented in Figures 2 through 4, suggested a nested process representation mated to a hierarchically partitioned control system whose levels are organized according to the principle of increasing control precision with decreasing materials properties intelligence^{6, 7}. Upper control levels are dedicated to managing product optimization with adaptation to process migration while minimizing disturbances and conflicts in the control space. This is typically implemented with a combination of quantitative process models and qualitative knowledge augmented by real-time sensor process data for the purpose of linking materials goals to product results.

The MTS system is typical.⁸ It utilizes a hierarchical control architecture that employs a heterogeneous knowledge representation system (HKRS) at the upper level to synthesize a nested process description model (see Figure 5). This process model then enables the derivation of process variable trajectories. These satisfy a cost function that is equal to the variance between actual and ideal material. Specific properties of the ideal quality material are distributed throughout the model state space by a dynamic process planner (DPP). The predictive attribute of this planner is necessary to accommodate the timing mismatch between slower model-based process variables and faster environmental variable actuation. Interpretation of process dynamics is provided by a fuzzy logic controller (FLC) that interfaces the DPP to the environmental control loops. This system is illustrated in Figure 5.

The HKRS is the repository for encodable process knowledge including process influences, mathematical algorithms, empirical variable, and process sensor data. It also includes support utilities such as an object-oriented language, relational database, and expert system shell. In characterizing complex materials variables, it frequently is necessary to use in situ sensor data to translate dimensional information into more interpretable units. (The MTS gas arc welding sensor is a typical example whereby an optimum mapping is achieved for the control of weld geometries that are obscured by debris.) The use of neural networks by MTS to transform such sensor data may be a nontransferable and process-specific approach. It warrants research to achieve more efficient generic data transformation solutions, using, for example, micromechanics, which offers promise for facilitating in situ data transformation in on-line materials characterization.

Process actuation is constrained to the environmental boundary in IPM systems, primarily due to incomplete understanding of how to implement in situ actuation. Thus, due to the serial process influence of process variables, the realization of minimum-variance process variables needs highly accurate trajectory planning for environmental variables. MTS material

³ Zappia, T., et al., "Fuzzy Logic, Neural Networks and the Spray Forming Process," MTS Systems Corporation, Eden Prairie, MN 55344.

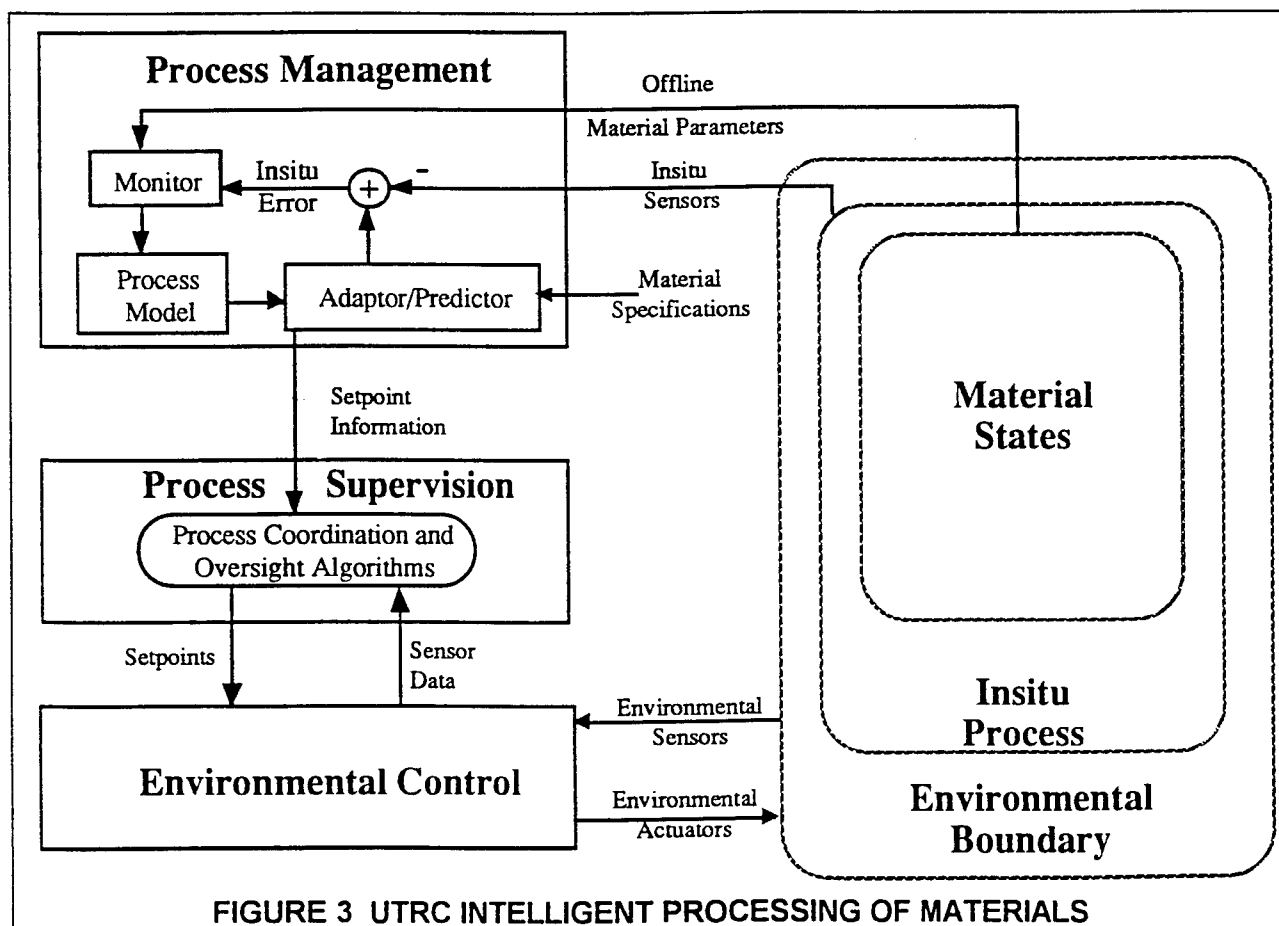
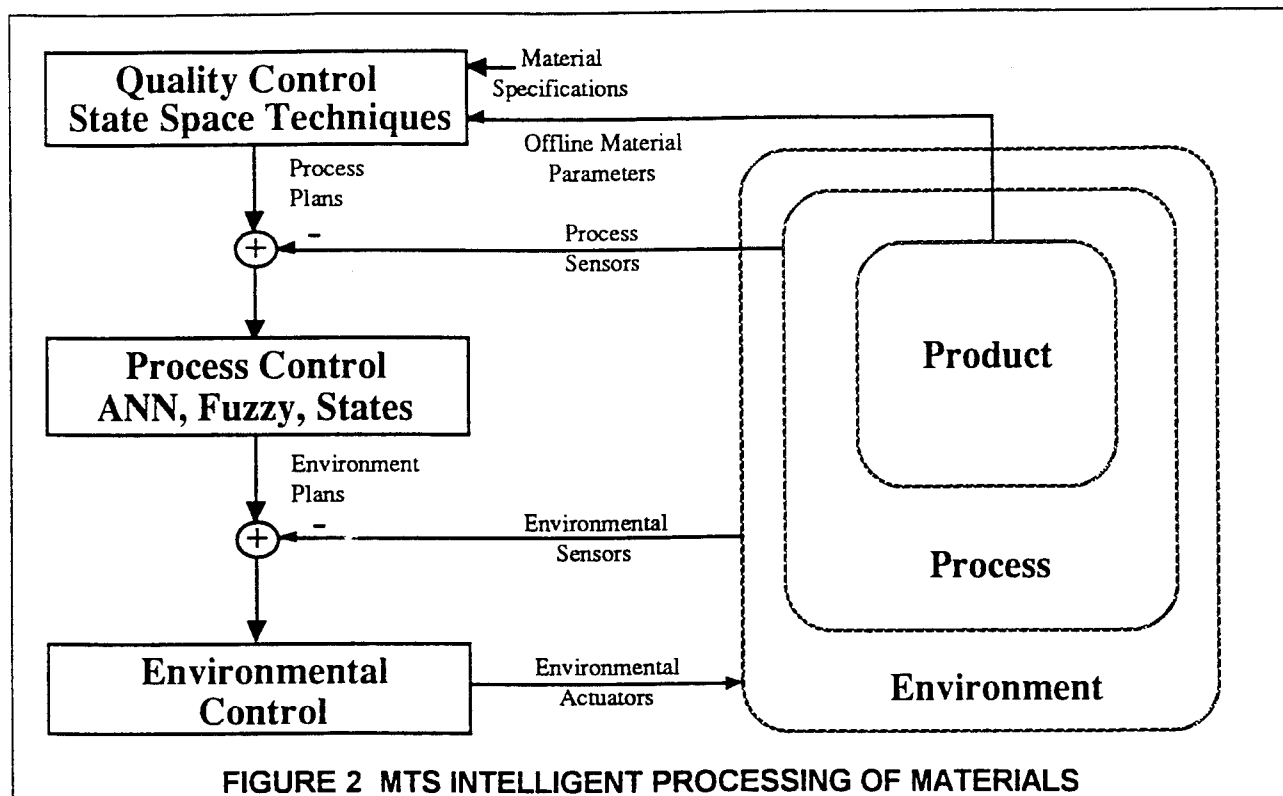
⁴ Wang, H. P., et al., "Intelligent Processing of Materials: Control Models for Induction-coupled Plasma Deposition," 120th TMS Annual Meeting, New Orleans, LA, February 1991.

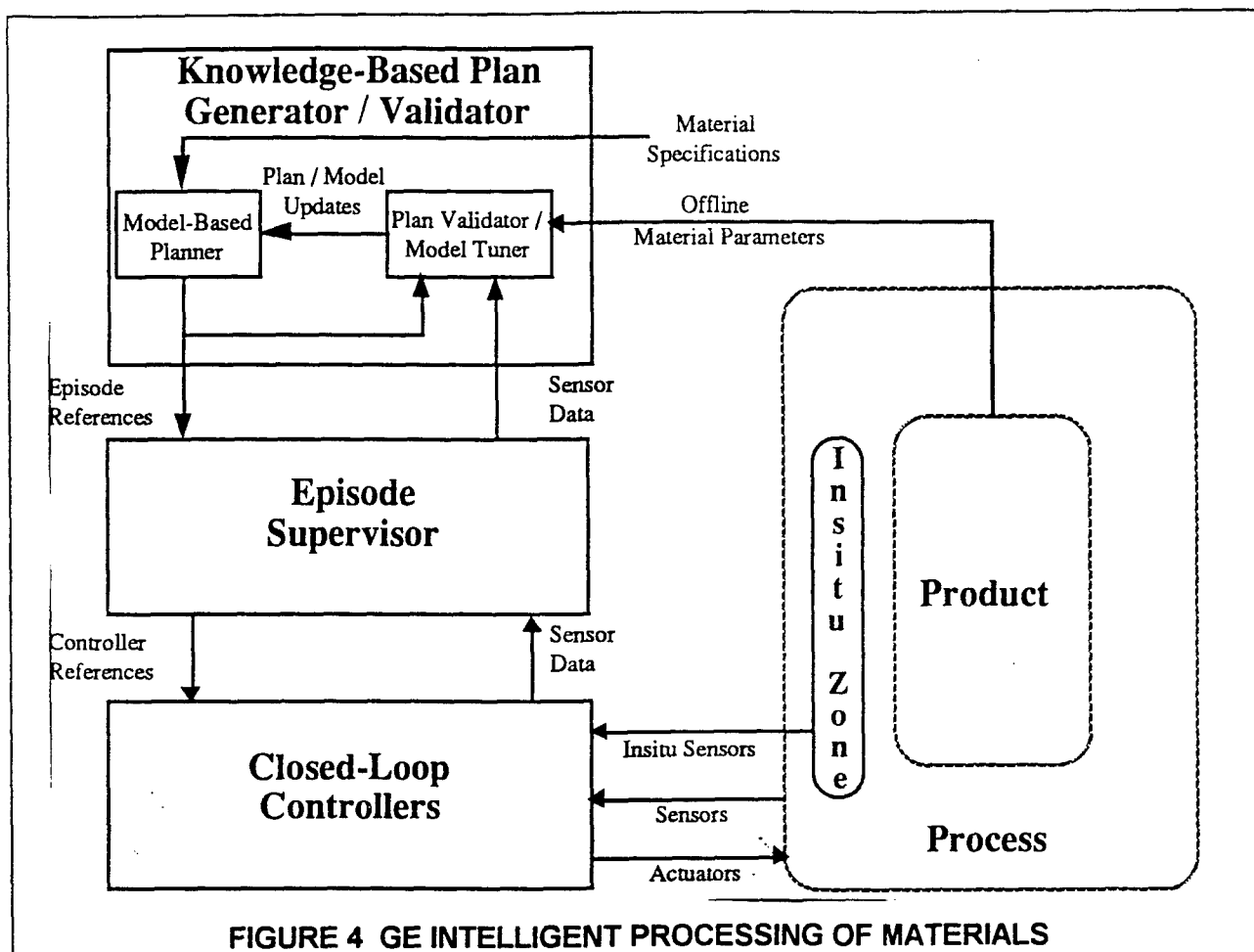
⁵ Bowen, P. S., et al., "Manufacturing Science of Silicon Nitride Chemical Vapor Deposition," United Technologies Research Center, East Hartford, CT 06106, R91-918220-14, April 30, 1991.

⁶ Saridis, G. H., "Analytic Formulation of the Principle of Increasing Precision with Decreasing Intelligence for Intelligent Machines," Int'l Federation of Automatic Control, Symposium on Robot Control, Karlsruhe, F.R.G., October 1988.

⁷ Meystel, A., "Multiresolutional Feedforward/Feedback Loops," 8th IEEE Int'l Symposium on Intelligent Control, August 1993.

⁸ MTS Systems Corporation and AMPI, Cleveland, B. A., MTS White Paper, May 1994.





quality is, therefore, largely determined by the simulation performance of the DPP, and of its capability for accurate planning of environmental and process variable trajectories based on the process description model synthesized by the HKRS. The weakness of this design is that the planning accuracy is directly proportional to simulation time. This is the same resource that must be allocated to provide environmental variable values sufficiently in advance to meet their real-time actuation requirements.

The effect of a knowledge-based process simulator consuming time resources in planning variable trajectories to a specified accuracy is shown in Figure 6. Typical simulation curves describe diminished performance with extended simulation times.⁹ This can make it difficult to satisfy timing constraints in multi-variable planning for complex processes. Concern arises over planning enhancement that may be achievable through evolution of the HKRS-DPP structure for multi-variable complex processes as opposed to enhancement achievable by alternative approaches. Research at the Air Force Materials Directorate by Laube and Stark has demonstrated the merit of a direct in situ process controller employing multi-variable process-state sensor feedback for linear control of process variables.¹⁰ This IPM

⁹ Johnson, C. D. and Thomas, D. W., "The Paralysis by Analysis Problem," 26th IEEE Conference on Decision and Control, LA, December 1987.

¹⁰ Laube, S. J. P. and Stark, E. F., "Artificial Intelligence in Process Control of Pulsed Laser Deposition," IFAC Proceedings, AIRTC, October 1994.

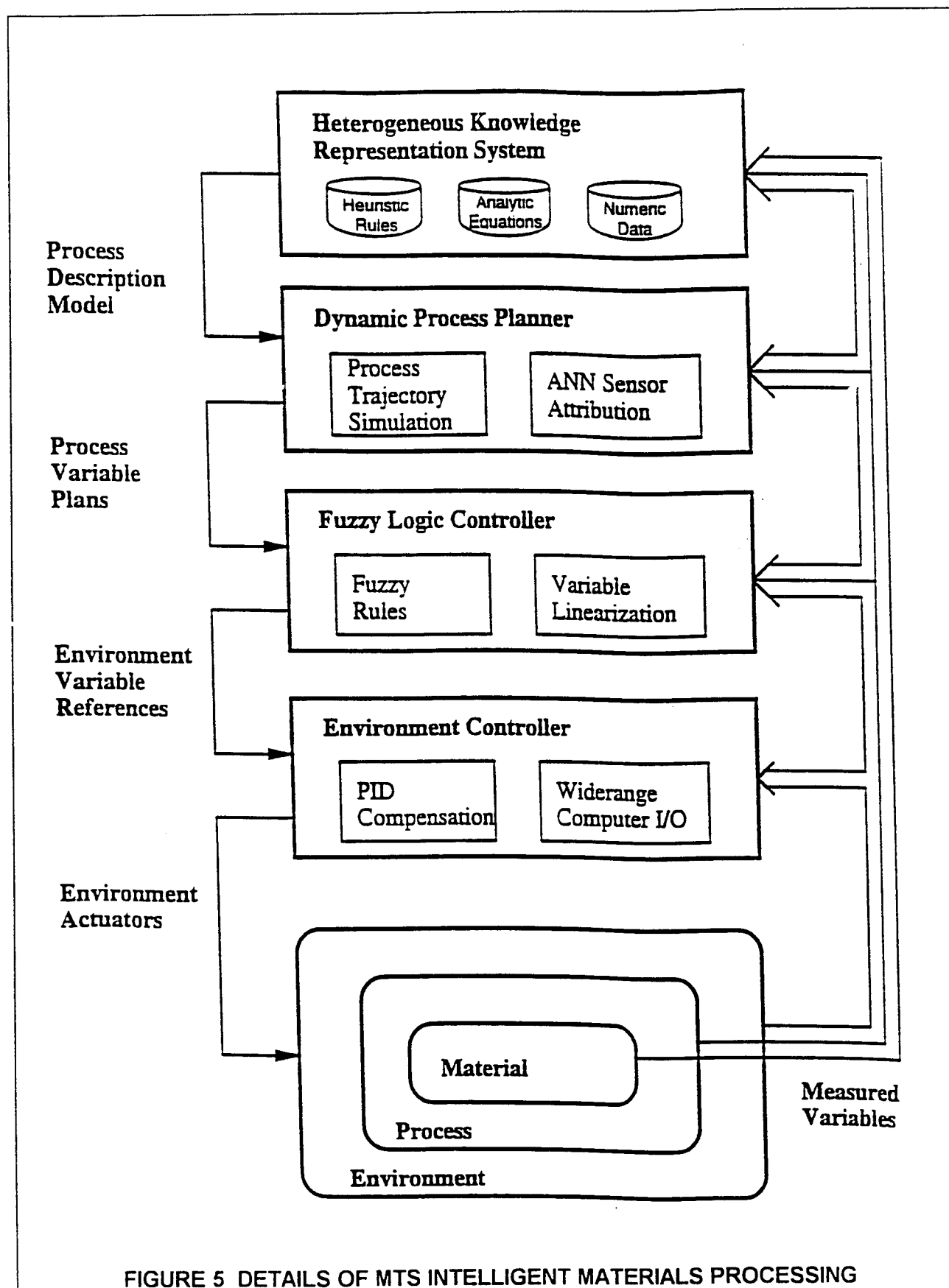
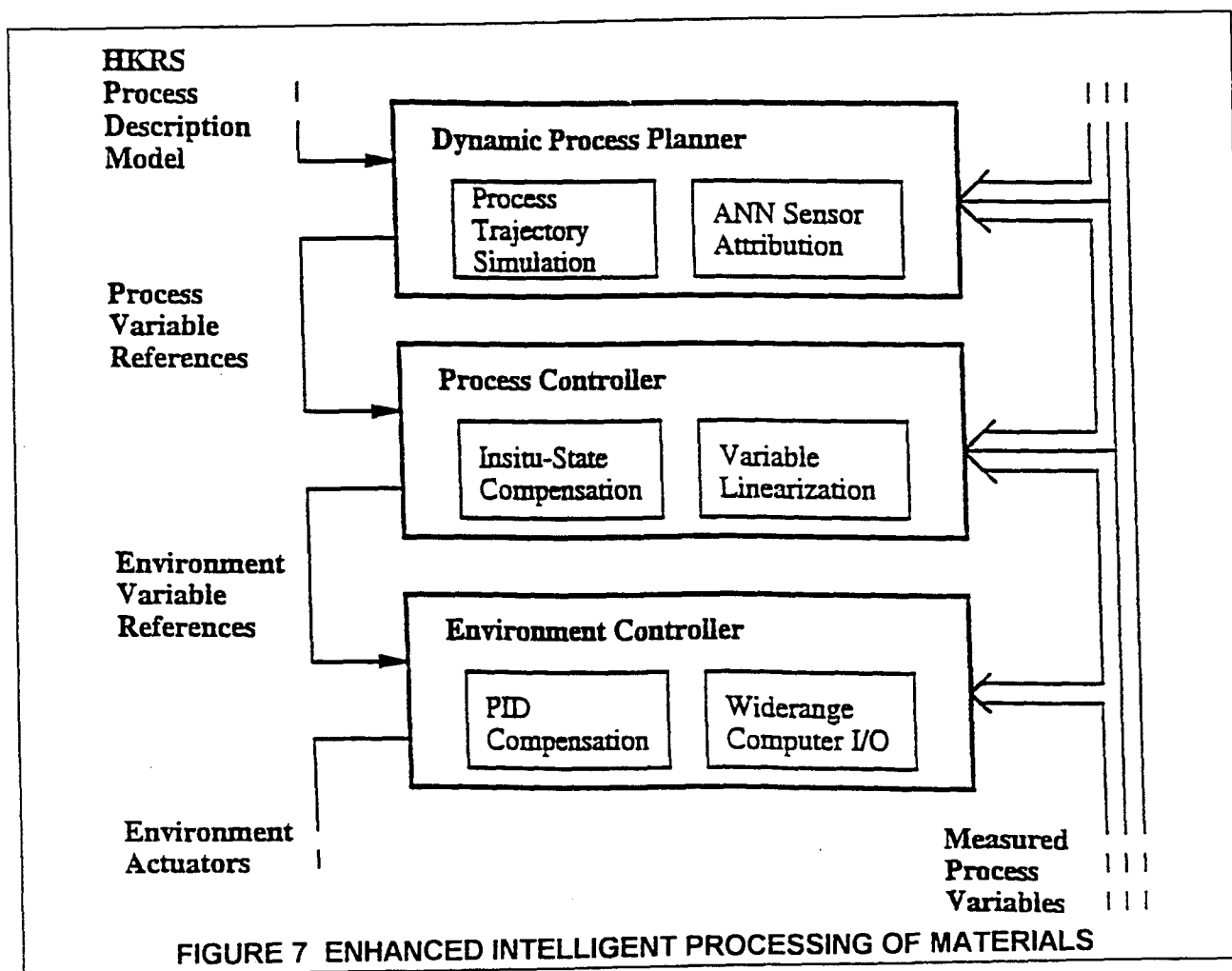
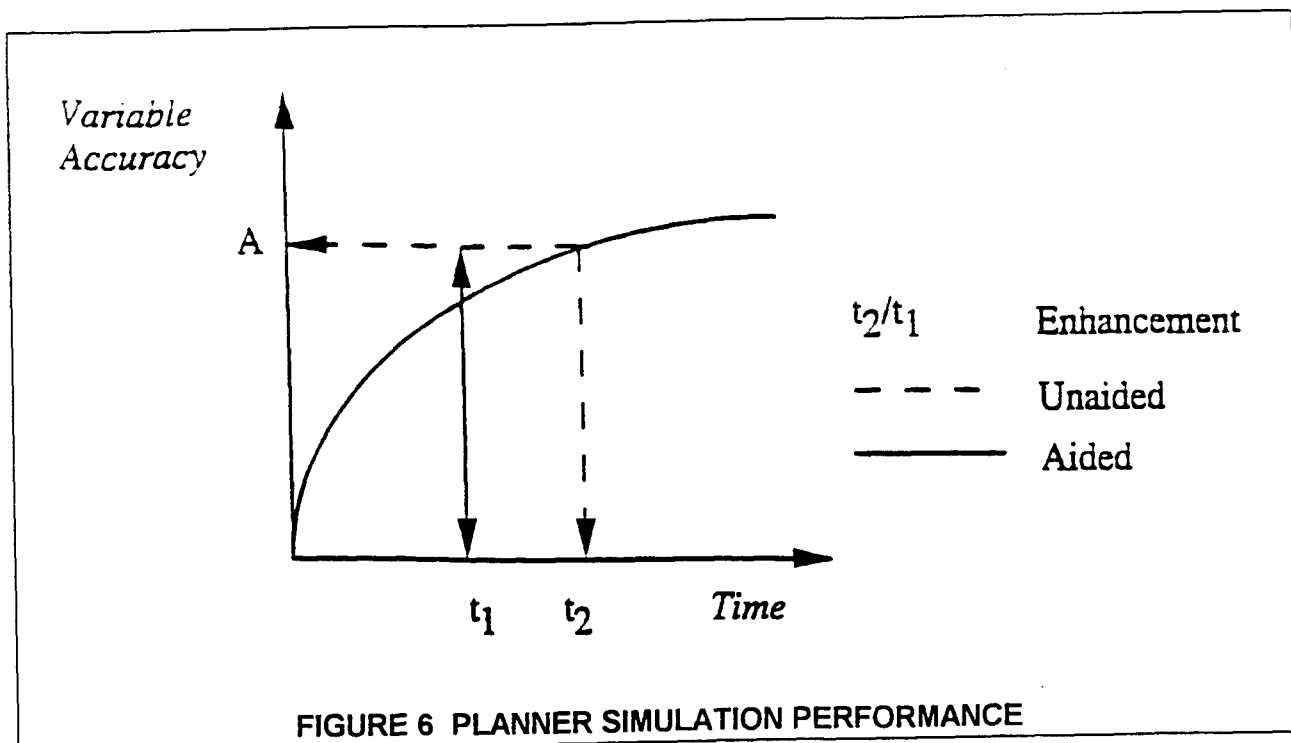


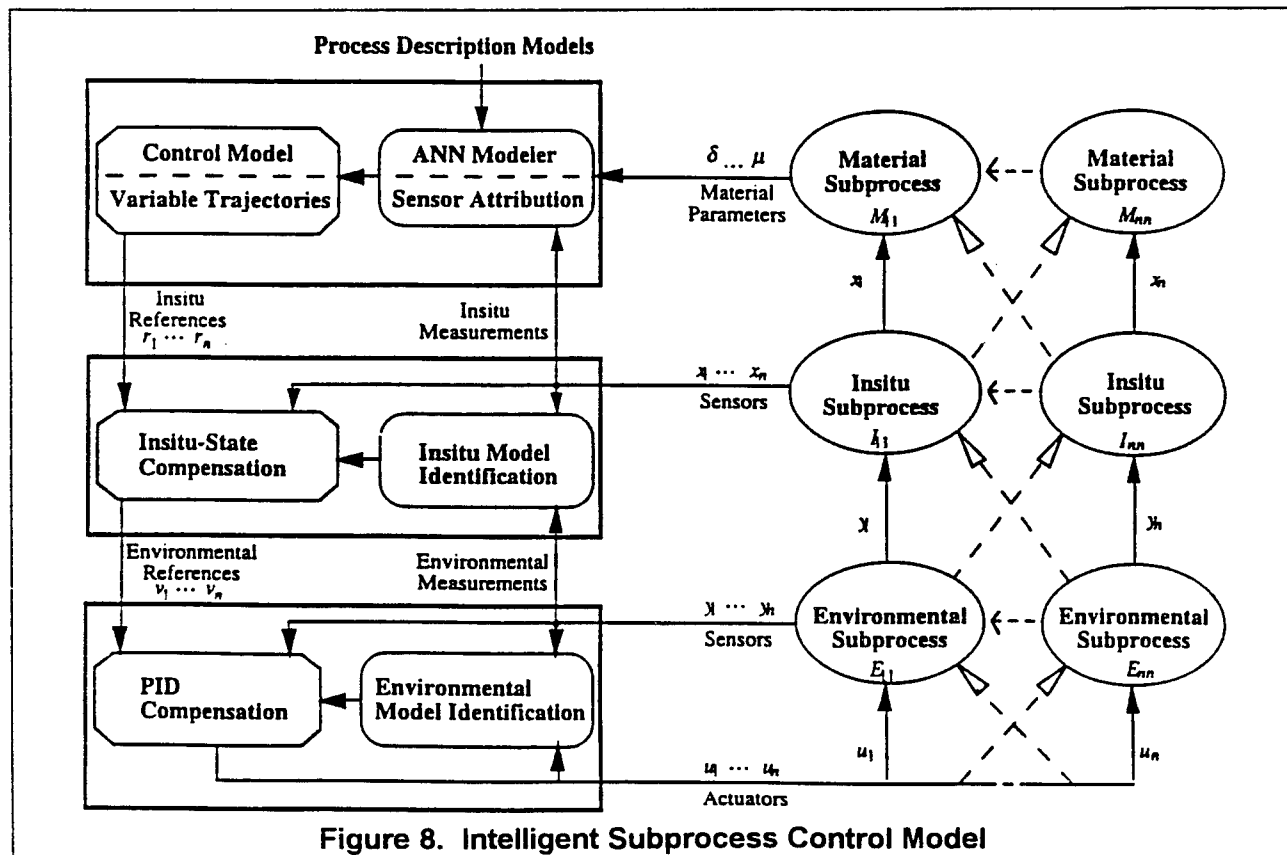
FIGURE 5 DETAILS OF MTS INTELLIGENT MATERIALS PROCESSING



enhancement is illustrated in Figure 7 where planner process variable references are combined with in situ-state compensation derived from intrinsic process domain knowledge to expedite real-time process control.

III CURRENT IPM IMPLEMENTATION

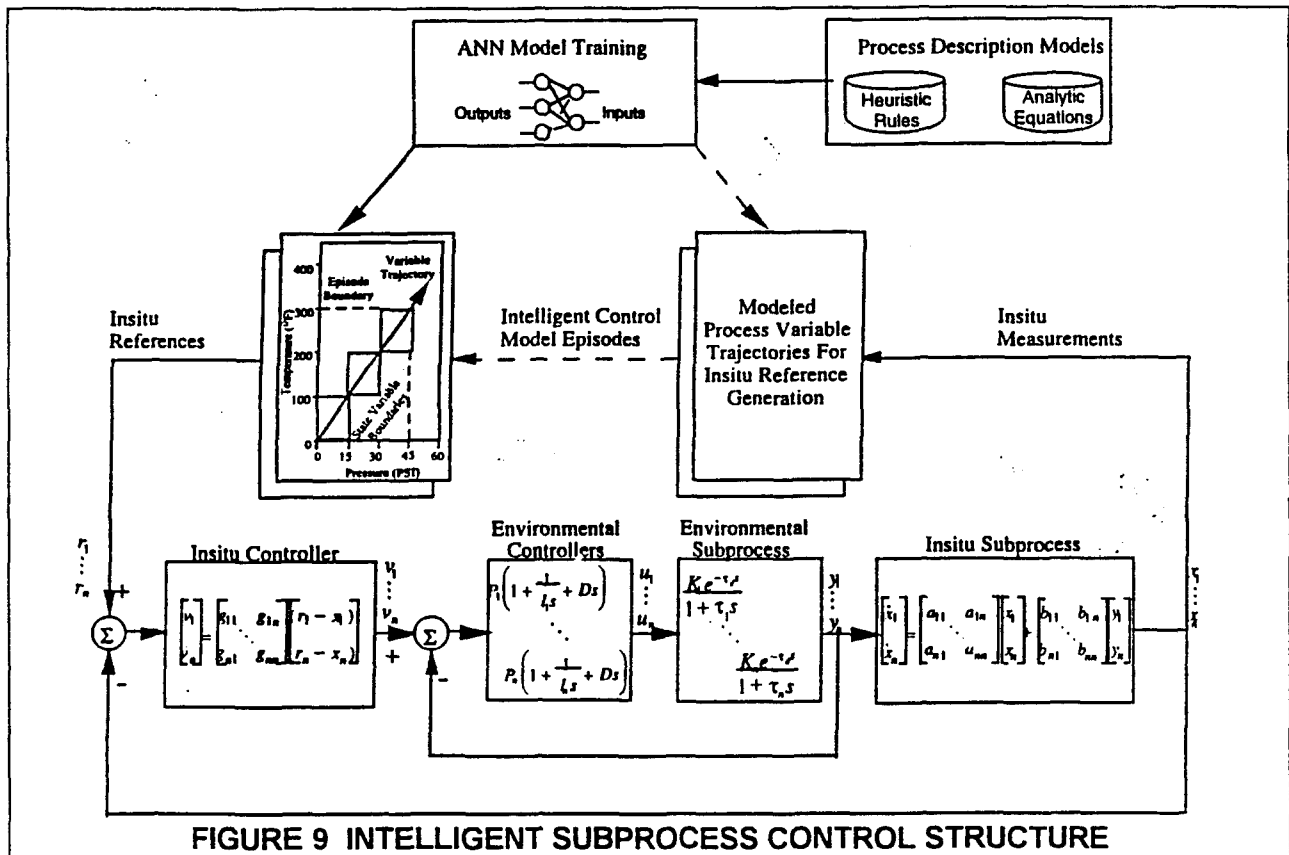
Several IPM research demonstration projects have been carried out at the Air Force Materials Directorate over the past five years to advance materials process design and control technologies.¹¹ An outcome achieved from this effort has been the evolution of an IPM approach defining a systematic blueprint for the manufacture of complex engineered materials. The intelligent subprocess control structure developed consistently provides reduced processing time, process disorder, and parameter variability over a range of material processes when compared to traditional process control systems defined at process boundaries. This system includes process decomposition into a hierarchy of subprocess with direct in situ compensation of controlled variables employing simultaneous multi-loop controllers that extend beyond process boundaries that are coordinated by an intelligent control model derived from an ANN trained with independent process description models. A diagram of this system is shown by Figure 8.



¹¹ P. H. Garrett, et al., "Intelligent Subprocess Control in Materials Manufacturing," submitted to IEEE Transactions on Semiconductor Manufacturing, October 1994.

The nested process representation utilized by MTS Systems Corporation and other IPM vendors is limited for accommodating process design advancements such as the independence axiom.¹² This axiom provides for the decoupling of processes through subprocess design such that iterative control interactions are substantially reduced. Decoupling provides the minimization of cross linkages for the subprocess elements of Figure 8. These linkages are represented by either diagonal or triangular coefficients in the mapping matrices of equation (1). The realization of reduced process disorder and accompanying control simplification are of substantial benefit. Challenge then arises in achieving sensor-actuator connections to subprocesses from hierarchical control elements and identification of appropriate controller compensation for each feedback loop of the control structure.

$$\begin{bmatrix} \delta \\ \vdots \\ \mu \end{bmatrix} = \begin{bmatrix} M_{11} & \cdots \\ \vdots & \ddots \\ & & M_{nn} \end{bmatrix} \begin{bmatrix} I_{11} & \cdots \\ \vdots & \ddots \\ & & I_{nn} \end{bmatrix} \begin{bmatrix} E_{11} & \cdots \\ \vdots & \ddots \\ & & E_{nn} \end{bmatrix} \begin{bmatrix} u_1 \\ \vdots \\ u_n \end{bmatrix} \quad \text{subprocess mapping} \quad (1)$$



¹² The Principles of Design, Suh, N. P. (1990, Oxford University Press).

Comprehensive measurement and actuation are necessary for the control of in situ variable trajectories. The attribution of in situ sensor data is a frequent requirement for translating the sensed characterization of materials into more interpretable dimensional units which is practical, but often require inefficient and process-specific solutions. Further, actuation of in situ subprocesses is generally relayed through the environmental controllers and their subprocesses because of presently inadequate implementation technologies for direct in situ actuation. Environmental in situ actuation is achievable because the coupling between environmental variables typically is minimum thereby permitting an approximate one-to-one correspondence between environmental references v_1 to v_n and environmental variables y_1 to y_n . These relationships are clearer when viewed from the control structure perspective of Figure 9.

Control compensation with the direct controller of Figure 9 defined by equation (2), requires process modeling capable of accurately describing process state information and its transition along trajectories including the aggregate of process influences. In situ model identification must provide for the accommodation of nonlinear state variables because of anticipated complex subprocess relationships. Continuous nonlinear models of the form of equation (3) can approximate the relationship between, x and y , where x is a vector of subprocess states and y of environmental variables input to the model identifier. The nonlinear identification approximation of equation (4) models f employing radial basis functions.¹³ The function parameters of Table 1 form a linear combination of Gaussian hypersurfaces whose proper values minimize the error between true state values and those estimated by f . Linearization about operating points of interest x_0 , y_0 may then be achieved when required by employing the partial derivative representation of equation (5) to provide required linear state estimates.

$$v = G(r - x) \quad \text{in situ controller} \quad (2)$$

$$\dot{x} = f(x, y) \quad \text{nonlinear in situ state model} \quad (3)$$

$$\dot{x}_k = \sum_{i=1}^n A_i \exp \left\{ - \sum_{j=1}^m \gamma_{ij} (x_j - \mu_{ij})^2 - \sum_{r=1}^p \rho_{ir} (y_r - \tau_{ir})^2 \right\} \quad \text{nonlinear identification} \quad (4)$$

$$\dot{x} \equiv f(x_0, y_0) + \left. \frac{\partial f}{\partial x} \right|_{x_0, y_0} \Delta x + \left. \frac{\partial f}{\partial y} \right|_{x_0, y_0} \Delta y \quad \text{model linearization} \quad (5)$$

¹³ Ibid

Following identification of the linear in situ state model of equation (6) an in situ compensator matrix G can be defined to provide necessary control commands v_1 to v_n that achieve in situ state trajectories of interest. Substitution of controller equation (2) into (6) yields a closed-loop state equation defining G matrix coefficient values in terms of in situ state model A and B matrix coefficients. A decoupled controller is further obtained when the G coefficient values can be selected to realize BG and $(A-BG)$ either as diagonal or triangular matrices. However, in situ regulation employing this direct state-sensor feedback and linear variable actuation may require periodic in situ model re-identification and re-linearization episodes as a processing cycle progresses in order to maintain the benefits of unconditional stability, reduced disorder, and speed of response.

$$\begin{aligned}\dot{\mathbf{x}} &= \mathbf{Ax} + \mathbf{By} \\ &= \mathbf{Ax} + \mathbf{BG}(\mathbf{r} - \mathbf{x}) && \text{in situ state model} \quad (6) \\ &= (\mathbf{A} - \mathbf{BG})\mathbf{x} + \mathbf{BGr}\end{aligned}$$

TABLE 1 RADIAL-BASIS FUNCTION PARAMETERS

\dot{x}_k	k th element of the nonlinear insitu state model f
A_i	output weight parameter
γ_i	state radial-basis function width parameter
μ_i	state radial-basis function center parameter
ρ_r	input radial-basis function width parameter
τ_r	input radial-basis function center parameter

The requirement for compensator design in the environmental control loops is to achieve tracking of controlled variables u_1 to u_n with references v_1 to v_n at minimum variability since all process parameters are influenced by error in these variables with reference to Figure 8. Conventional PID controllers are beneficially employed at this level in order to retain industry standard functions useful to process operations. With the product of subprocess K and controller P gains equaling unity of less around environmental control loops, unconditional stability is assured when P equals $1/K$. Controlled variable steady-state error minimization is concurrently achieved by the selection of a controller integral term adequate to cancel residual differences between reference inputs and process measurements. Contemporary feedback loop implementation permit a total controlled variable error approaching 0.1% error in y_1 to y_n can be approximated by averaging n identical measurement channels through sensor fusion to yield a total error of $1/\text{square root of } n$ times the error of a single measurement.¹⁴ This method

¹⁴ Advanced Instrumentation and Computer I/O Design, Garrett, P. H. (1992, IEEE Press).

is equally applicable for minimizing the error of in situ measurements x_1 to x_n and is compatible with any sensor device.

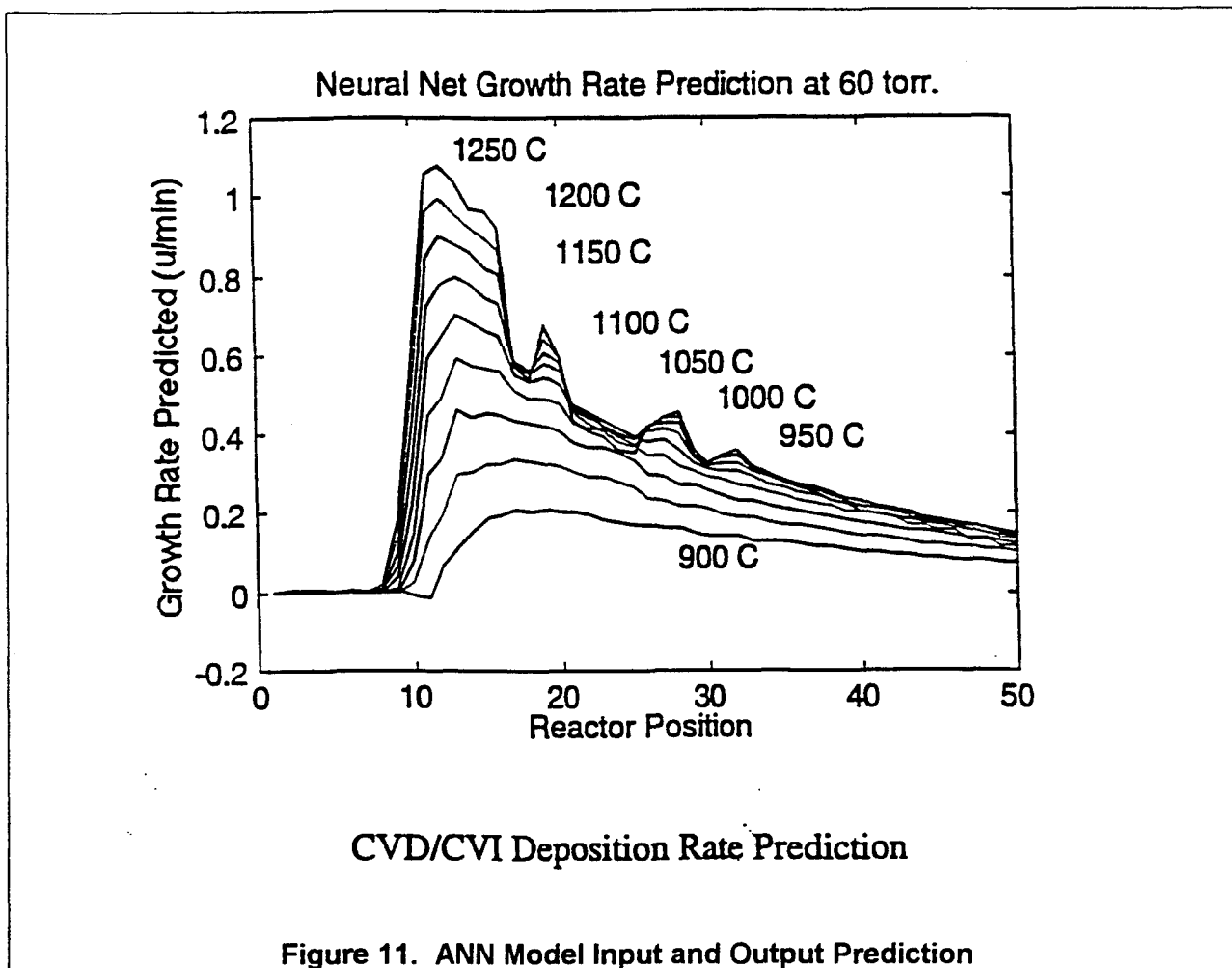
Physics and chemistry first principles are effective and widely employed for the process description purposes of modeling process outputs for specified inputs and conditions, and are readily modifiable to accommodate process changes. Process description models accordingly are a repository of encodable knowledge typically including mathematical algorithms, analytical functions, empirical relationships, and qualitative representations. Unfortunately, their utility for process control purposes is frequently constrained by complexity and execution time requirements in on-line real-time applications. However, a neural network approximator may be trained off-line to emulate independent process description models which may then be used on-line as an intelligent control model for real-time execution. This architecture is illustrated in Figure 9 which also shows system control stability provided by in situ and environmental controllers independent of the intelligent control model.

A two-dimensional example CVD/CVI process model is described in Figure 10 for the transport of energy, mass, and momentum. This first-principles model defines heat transfer, mass transfer, and fluid flow through iteration of its partial differential equations for laminar flow in an axis symmetric reactor. With this data a two-layer ANN structure of 12 input and 100 output neurons is trained by back propagation for use on-line to predict process variable goal trajectories and generate in situ control references representing the intelligent control model.¹⁵ The ANN predicted growth rate shown for beta alumina is a function of specified reactor temperature, pressure and axial position. Predicted variable trajectories may be regenerated along a processing cycle for improved control accuracy as necessary to accommodate a migrating process. This is shown by the sequential intelligent control model episodes of Figure 11.

$v_r \frac{\partial}{\partial r}(\rho v_r) + v_z \frac{\partial}{\partial z}(\rho v_r) = -\frac{\partial P}{\partial r} + \frac{\partial}{\partial r} \left(\mu \frac{1}{r} \frac{\partial}{\partial r}(r v_r) \right) + \frac{\partial}{\partial z} \mu \frac{\partial v_r}{\partial z}$	radial momentum conservation
$v_r \frac{\partial}{\partial r}(\rho v_z) + v_z \frac{\partial}{\partial z}(\rho v_z) = -\frac{\partial P}{\partial z} + \frac{1}{r} \frac{\partial}{\partial r} \left(\mu r \frac{\partial v_z}{\partial r} \right) + \frac{\partial}{\partial z} \mu \frac{\partial v_z}{\partial z} + \rho g_z$	axial momentum conservation
$v_z \frac{\partial}{\partial z}(\rho h) + v_r \frac{\partial}{\partial r}(\rho h) = \frac{\partial}{\partial z} \left[\frac{k}{C_p} \frac{\partial h}{\partial z} \right] + \frac{1}{r} \frac{\partial}{\partial r} \left[\frac{rk}{C_p} \frac{\partial h}{\partial r} \right] + S_h$	energy conservation
$v_z \frac{\partial}{\partial z}(\rho w_j) + v_r \frac{\partial}{\partial r}(\rho w_j) = \frac{\partial}{\partial z} \left[(\rho D_j) \frac{\partial w_j}{\partial z} \right] + \frac{1}{r} \frac{\partial}{\partial r} \left[(r \rho D_j) \frac{\partial w_j}{\partial r} \right] + R_j$	mass conservation
$R_i = -k_f \prod_{i=1}^m [A_i]^{a_i} + k_r \prod_{i=1}^n [B_i]^{b_i}$	deposition rate

FIGURE 10 CVD/CVI TRANSPORT PROCESS DESCRIPTION MODEL

¹⁵ Introduction to Artificial Neural Systems, Zurada, J. M. (1992, West Publishing).



Advanced materials contain specialized properties provided by sophisticated microstructures whose yield are not high when conventional processing methods are employed. Notably, research at the Air Force Materials Directorate has shown that the limitation of nested process representations historically used by IPM vendors can be substantially improved by application of the independence axiom illustrated in Figure 12. This characterization beneficially provides a quantitative description of subprocess variable interactions by the mapping matrices of equation (1). Increased subprocess variable cross coupling typically encountered at upper process levels accordingly necessitates greater control complexity to prevent the inefficiency of extended control complexity to prevent the inefficiency of extended control interactions and resulting process disorder.

Subprocess influence diagrams, like that shown in Figure 13, are conceptualized in terms of the associated physical process apparatus, modeled subprocess variable state transitions, and linkages defining subprocess interactions. The linkages in Figure 13 characterize Navier-Stokes gas dynamics subprocesses on the left-hand side an substrate deposition chemical kinetics on the right-hand side in a simplified one-dimensional model. Inlet reactant mass flows, reactor temperature, and pressure/exhaust flow are at the process environmental level constituting raw material and energy inputs. The B matrix coefficients in the in situ subprocess state-space model of Figure 8 specifically describe the linkages

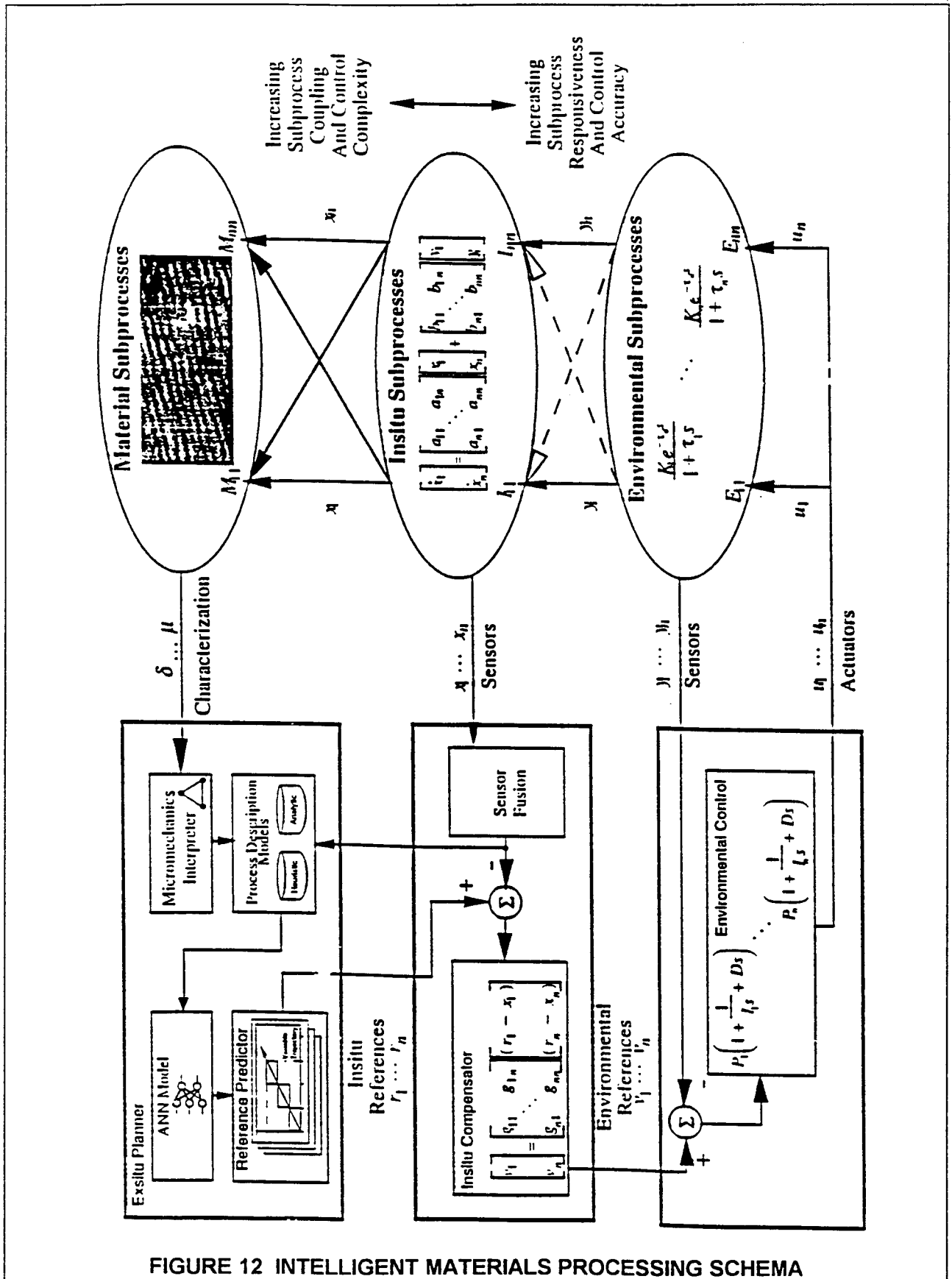


FIGURE 12 INTELLIGENT MATERIALS PROCESSING SCHEMA

between environmental and in situ subprocess variables, with off-diagonal terms indicating cross coupling. The A coefficients correspondingly define the linkages between in situ subprocesses variables and material parameters. For ideal uncoupled subprocess each environmental variable affects only one in situ subprocess variable which, in turn, affects only one material parameter. This ideal is unachievable in most processes, however, but the degree of coupling may be reducible both by process apparatus design and operation. For example, the deleterious influence of gas stream nucleation reactions on material parameters may be reduced by decreasing reactor gas residence time with a multi-port gas injection and scavenging manifold and increased exhaust flow rate. Table 2 defines the parameters of the generalized CVD process description.

TABLE 2 RELEVANT PROCESS PARAMETERS

C_1	inlet reactants concentration	P_x	actuated reactor pressure
C_2	intermediate gas products	\dot{m}_i	actuated inlet reactant mass flow rate
C_3	nucleation gas products	ρ	material density
T_s	substrate temperature	δ	material thickness
P	reactor pressure	μ	material microstructure
T_w	actuated wall temperature	γ	material stoichiometry
D	diffusivity	SRR	surface reaction rate

At the environmental boundary subprocess models are identified as transfer functions in terms of their gains K_n and time constants t_n . The function of the environmental control loops is to satisfy process boundary first-principles including unconditional stability and loop implementations having low instrumentation error to achieve minimum controlled-variable variations. PID controllers are beneficially employed at this level to retain industry standard functions useful for integrated process operations. Controlled variable steady-state error minimization is traditionally obtained by tuning the controller integral term to cancel residual differences between reference inputs and environmental measurements. Contemporary implementations permit a controlled-variable error approaching 0.1% of full scale employing ultra-linear instrumentation.

The fusion of sensor data x_1 to x_n is a frequent requirement for translating the sensed characterization of subprocess parameters into dimensional units interpretable for control purposes. Further, actuation of in situ subprocess variables is relayed through environmental control loops which is practical because of negligible environmental cross coupling permitting an approximate one-to-one correspondence between environmental variable references v_1 to v_n and in situ actuation variables y_n to y_n . However, in situ subprocess model identification must provide for the accommodation of nonlinear state variable trajectories, owing to anticipated complex subprocess interactions, in order to define the in situ compensator described by equation (2). Continuous nonlinear models of the form of equation (3) therefore can approximate the relationship between in situ actuations y_n and controlled variables x_n with nonlinear identification employing the functions of equation (4). Linearization about actuator and controlled variable operating points is achieved by equation (5) to obtain the linear in situ

state model of equation (6). Substitution of controller equation (2) into (6) then yields a closed-loop state equation defining in situ compensator coefficient values G .

In situ compensation and multi-variable subprocess sensing for linear-control of in situ variables provides the merit of substantial reduction in process disorder than is possible in the absence of this intermediate control level. Benefit is achieved by more precise actuation of the x_n and y_n state variables and their in situ subprocess interdependencies, identified by the A and B coefficient matrices, than can be obtained through conventional iteration of the u_n environmental variables. While environmental control references are generated by the in situ compensator shown in Figure 8, in situ references are provided by the ex situ planner described subsequently.

A consequence of our program in intelligent materials processing has been the evolution of a generic blueprint for the design of hierarchical processes and corresponding control structures. Optimum control of many materials processes required initial modeling and periodic remodeling, when in situ and environmental subprocesses migrate, to achieve effective actuation along process variable trajectories describing mappings between material properties of interest and controllable variables. The task of the ex situ planner is to provide this modeling function with output in the form of in situ and environmental references appropriate for real-time process control. Essential elements of the ex situ planner include comprehensive process description models augmented by available in situ sensor data and a materials product characterization interpreter whose combined aggregation is translated into executable control references by an ANN structure.

The utility of Nye's¹⁶ geometric perspective relating thermal, mechanical, and electrical material influences enables a quantitative description of their physical properties in terms of responses to material influences. This perspective is shown by Figure 14 with material entropy, strain and displacement responses to thermal, mechanical, and electrical influences. The merit of this material description provides a definitive characterization for product design and process optimization purposes including improved measurement and control structures. For example, if electrical responses arising from temperature or stress gradients result in undesirable material properties, then material compound modifications may be sought to attenuate these responses.

Tailoring the chemical and physical nature of CVD/CVI deposition requires exact understanding to control the chemical processes occurring in a reactor including knowledge of combined equilibrium, kinetic, and transport subprocesses. Physical and mathematical models may then be usefully employed to provide mechanisms essential for deposition control. Equations capable of describing a CVD reactor are complex, nonlinear, and result in considerable solution difficulty for the general case in the absence of simplifying assumptions for geometry and flow. Beneficially, a neural network approximator has been developed specifically to emulate process description models which may be employed on line for real time control.¹⁷

¹⁶ Physical Properties of Crystals, Nye, J. F. (Oxford University Press, 1989)

¹⁷ Process Advisor, CAD-CHEM IV, AI Ware, Inc., Cleveland, OH.

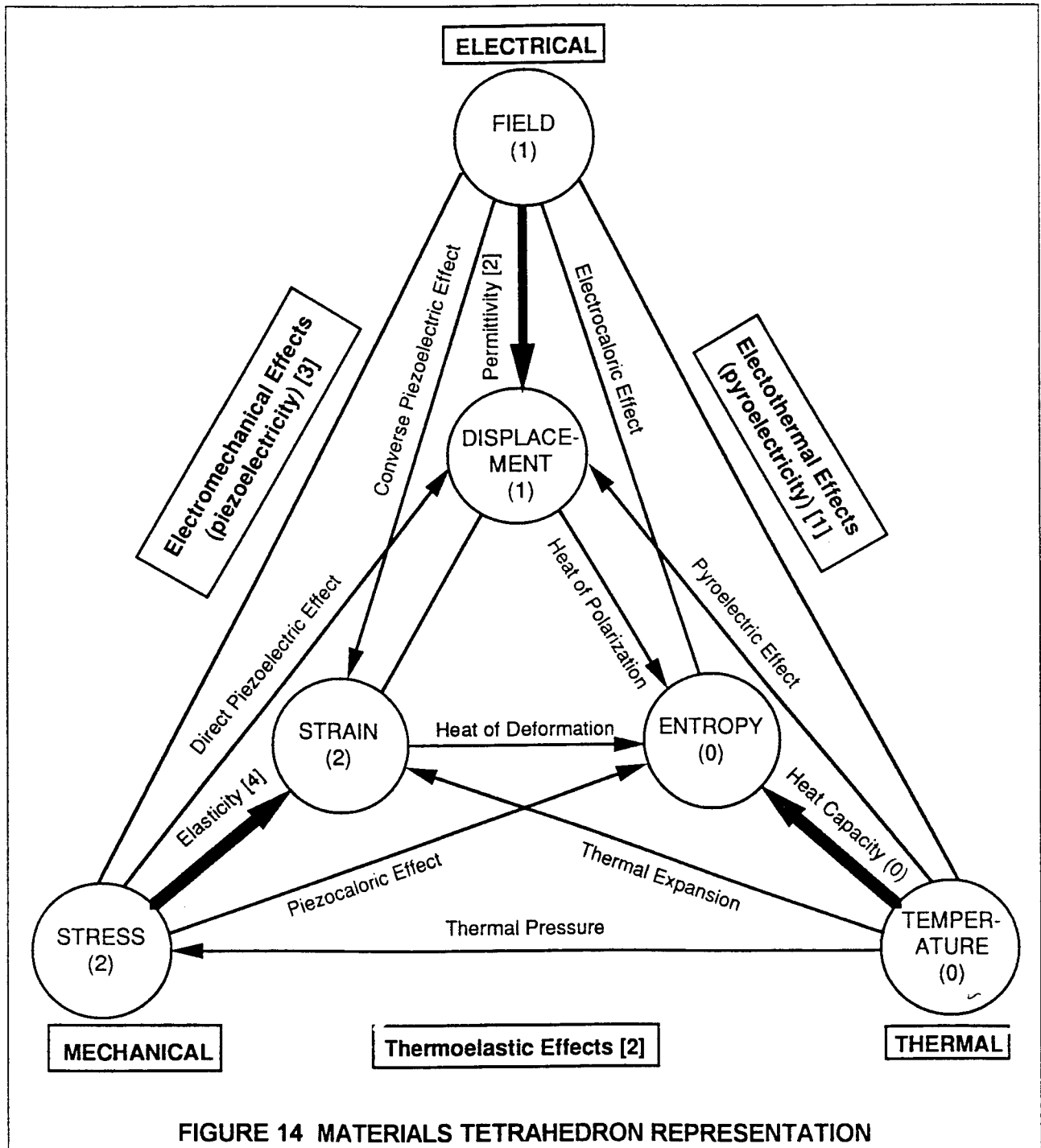


FIGURE 14 MATERIALS TETRAHEDRON REPRESENTATION

IV IN SITU STATE MODEL REQUIREMENTS

Process modeling required development of a semi-quantitative description of the CVI process. The foundations for this work were the models initially proposed by Gupta and

Evans¹⁸, Sotirchos¹⁹, Morell²⁰, and Naslain²¹. The work of Gupta and Evans comprised a starting point for most of this modeling effort. That effort took two directions: simplified, qualitatively correct, and detailed numerical modeling. The first objective of this work was to achieve a process description that would evoke an intuitively clear image of the deposition process. It had to be sufficiently accurate in its predictions to allow process improvement through intelligent adjustment of parameters, and to serve as a guide for sensor development and process automation and control.

This was pursued by an approach of reverse modeling, similar to reverse engineering. The starting point was the creation of a compendium of process models that had appeared in the literature. These published models invariably were assembled from various simplified descriptions of reaction kinetics, fluid flow and diffusion, and heat transfer. For each of the published models, these fundamental concepts were combined to form a set of coupled, linear differential equations that then could be solved numerically. The results that were presented were limited by the author's interests, and by the many approximations deeply imbedded within each submodel. Thus, the sensitivity of the model predictions to these approximations would not be not easy to assess, and confidence in these numerical predictions would be highly suspect.

The approach taken to resolving this problem was to disassemble the published models, assess the underlying approximations, determine the fundamental principles involved, reduce the description to intuitively clear, mechanistically accurate phenomena, and finally to summarize the CVI process in a way that was useful to both the process engineer and the process control engineer. It was hoped that this approach would result in subprocess model descriptions that would fit into the IPM modular approach as it evolved. As background to the effort, it is useful to describe several key terms.

Poiseuille Flow In the continuum regime, also called "*Poiseuille* flow", molecular structure can be ignored and the fluid treated as a classical continuum obeying the nonslip condition at the fluid-pipe wall boundary. This leads to the familiar parabolic fluid velocity profile for flow in round pipes, and a flow rate that varies as the square of the pressure gradient, linearly as the length, and as the fourth power of the pipe radius.

Knudsen Flow In the free molecular flow regime, also called "*Knudsen* flow", the molecular mean free path becomes an appreciable fraction of the pipe radius. As this regime is approached, achieved by reducing the fluid pressure, the flow rate begins to exceed that of Poiseuille flow. This occurs because the boundary layer begins to vanish and, in fact, begins to lose its meaning, as does the concept of a "fluid" in the classical, continuum sense. Therefore, the requirement of a velocity continuum at the fluid-pipe boundary wall also begins to vanish. As the pressure is further reduced, the boundary layer vanishes altogether and the frequency of inter-molecular collisions diminishes until molecules are colliding only with the pipe wall. This condition is defined as fully developed Knudsen, or free molecular, flow.

¹⁸ Gupta, Deepak and Evans, James W., "A Mathematical Model for Chemical vapor Infiltration with Microwave Heating and External Cooling," J. Mater. Res. 6, 810 (1991).

¹⁹ Sotirchos, S. V., "Dynamic Modeling of Chemical Vapor Infiltration," AIChE Journal 37, 1365 (1991).

²⁰ Morell, J. I., et al., "A Mathematical Model for Chemical Vapor Infiltration with Volume Heating," J. Electrochem. Soc. 139, 328 (1992).

²¹ Naslain, R., et al., "The CVI Processing of Ceramic Matrix Composites," J. de Physique 50, 191 (1989).

In this final regime, the "flow" is actually a process of diffusion, and occurs independently for each of the constituents. One consequence of this is that the phenomenon of increasing the flow rate by increasing the pressure gradient is conceptually incorrect. As seen from the point of view of the kinetic theory of gases, increasing the pressure actually increases the species concentration. Thus increasing the pressure gradient actually increases the concentration gradient and it is this that drives the molecular diffusion. It follows that increasing the system pressure by increasing the pressure of a so-called "carrier" gas in the Poiseuille regime will not increase the flow of the reactant gas coexisting in the Knudsen regime because such an increased carrier gas pressure would have no effect on the reactant gas concentration.

Fick Diffusion In the continuum diffusion regime, also called "*Fick* diffusion", the dynamics of individual species subjected to pressure gradients are described by Poiseuille flow. In other words, the species are treated as classical continua. Nevertheless, one species can diffuse through another species. The concentration gradient drives this diffusion in the direction of decreasing mole fraction at a rate that is proportional to a diffusivity of one species through a second so that both species must be specified. Furthermore, if J_{AB} is the flux of species A through species B, and J_{BA} is the flux of species B through species A, then $J_{AB} = -J_{BA}$.

With these three definitions as background, we now can describe some aspects of the CVI process and TA&T's progress toward developing a useful in situ state model for process control.

V CURRENT IN SITU STATE MODEL FOR MICROWAVE CVI

The goal of any CVI process is to achieve high matrix density in a reasonable time. The major impediment to this is premature pore closure that traps voids, i.e. trapped pore spaces, so that these pore spaces can no longer be infiltrated with the reactant gases. We assume that it is adequate to model the fiber preform as a system of parallel cylindrical pores, and to express their interconnectedness in an actual preform using an effective "tortuosity" factor.

The first question is, "Does the initial pore size distribution influence the way the pores close off?"

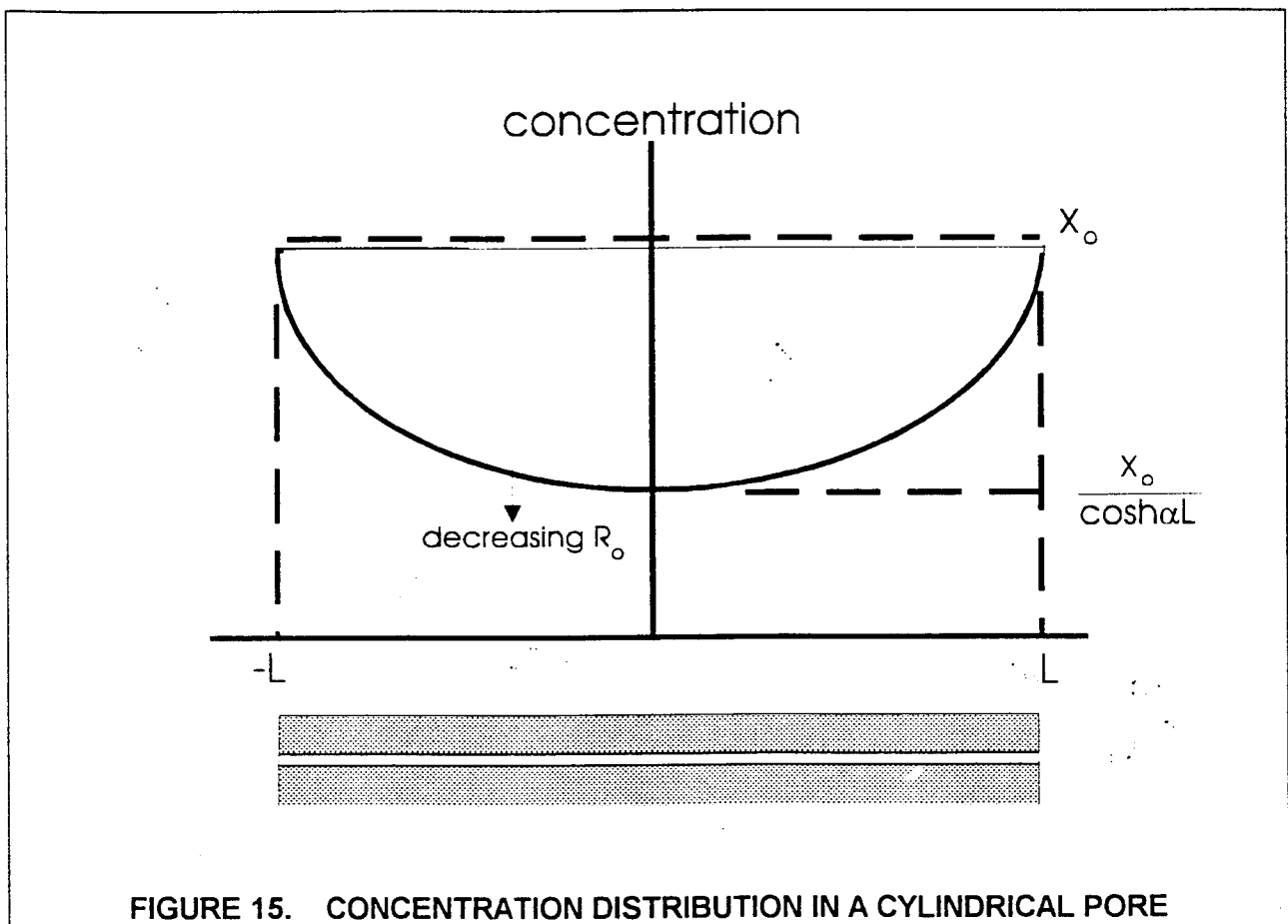
Following Gupta and Evans, the concentration of a species resulting from species diffusion can be expressed as

$$\frac{d}{dz} \left[R^2 D \frac{dX}{dz} \right] - 2kRX = 0 \quad (7)$$

where X is the concentration, k is the reaction rate (with reactions treated here as first-order processes), $R(z)$ the pore radius, and $D(z)$ the diffusivity probably, but not necessarily, Fickian. Initially, the pores are of uniform cross-section so that neither R nor D depend on z , the distance along the pore. Then the equation is easily solved with the result that

$$X(z) = X_0 \frac{\cosh \alpha z}{\cosh \alpha L} \quad (8)$$

where $\alpha = (2k/R_0D)^{1/2}$, R_0 is the initial pore radius, the pore length is $2L$, and X_0 is concentration at each end of the pore. This function is plotted in Figure 15. Not surprisingly, this predicts that the concentration initially is higher at each end of the pore, i.e. at $z = \pm L$. Therefore, if the temperature is uniform in the z -direction so that the reaction rate also is uniform, initially more material will be deposited near the surface than at the middle. If the pore radius initially is large the deposition rate will be limited by the reaction rate. As the process proceeds, ultimately diffusion changes from Fickian to Knudsen. In this case, one might suspect that diffusion into the interior would become increasingly difficult so that the concentration ratio $X_0/X(L)$ would become even larger. Thus the initial reaction limited deposition would change to diffusion limited. This would lead to premature pore closure.



But if the interior temperature is higher than the surface temperature, the rate of reaction at the interior can be increased over that at the surface and premature pore closure can be avoided. For a first-order process, the reaction rate is proportional to the negative of the concentration. The constant of proportionality is the usual heterogeneous rate constant k given by

$$k = k_0 e^{-E_A/RT} \quad (9)$$

The deposition rate can be approximated by the product Xk . This is equivalent to assuming a uniform concentration and thus is strictly applicable only at the beginning of the process. Nevertheless, this suggests that by increasing the temperature of the interior sufficiently over that of the surface, this deposition rate can be increased at the center of the preform. It is clear from the form of α that this temperature gradient depends on the initial pore radius. Using a surface temperature of 917°C and an interior temperature of 1067°C, and an activation energy of 120 kJ/mole for the reaction $\text{CH}_3\text{Cl}_3\text{S} + \text{H}_2 \rightarrow \text{SiC} + 3\text{HCl}$, we have shown that $(Xk)_{\text{center}} = (Xk)_{\text{surface}}$ when $r_0 \cong 0.55 \mu\text{m}$. Since Gupta and Evans had used their full numerical solutions to predict this condition would occur for some value of the initial pore radius $1 < R_0 < 4 \mu\text{m}$, we considered our estimate a good first approximation.

As we continued to develop and expand these ideas, we discovered certain series expansions for the pore radius did not appear to be converging. We investigated this issue at great length and discovered that the expansions were, in fact, converging but were initially diverging. Therefore, a simple approximation to the conditions needed to avoid premature pore closure could not be achieved. This was a crucial discovery because it meant that the only approach was one involving the full set of processing equations -- including the non-linear gas diffusion equation. This observation fully defined the remaining modeling effort.

Simplified examples of the relationships used during the development of subprocess models are the following:

available microwave power density	$S = \frac{1}{2} \omega \epsilon_o E ^2$	(10)
-----------------------------------	---	------

absorbed microwave power density	$P = \kappa'' S$	(11)
----------------------------------	------------------	------

thermal diffusion/temperature distribution	$\kappa \nabla^2 T + P = c \frac{\partial T}{\partial t}$	(12)
--	---	------

mass transport/concentration diffusion	$\frac{d}{dz} \left(r^2 D \frac{dC}{dz} \right) - 2 k r C = 0$	(13)
--	---	------

deposition rate	$\frac{dr}{dt} = - \frac{M b k C}{\rho}$	(14)
-----------------	--	------

definition of first-order reaction	$\frac{dC}{dt} = - k C$	(15)
------------------------------------	-------------------------	------

reaction rate constant	$k = k_o \exp(-E_A / RT)$	(16).
------------------------	---------------------------	-------

The variables and parameters in these expressions have the following meanings:

S = available microwave power density (W/m^3),

ω = angular microwave frequency (s^{-1}),

ϵ_0 = electrical permittivity of free space (farads/m),
 κ'' = dielectric loss factor of the material (dimensionless),
 E = microwave electrical field strength (V/m),
 κ = thermal conductivity of the material (W/m K),
 T = temperature of the material ($^{\circ}\text{C}$ or K),
 P = microwave absorbed volume power density (W/m^3),
 z = distance along a cylindrical pore axis (m),
 r = pore radius (m),
 D = diffusivity of gas along pore (m^2/s),
 C = species concentration (moles/ m^3),
 M = molecular weight of the deposited solid (kg/mole),
 b = stoichiometric coefficient of the deposited species (moles/mole),
 ρ = mass density of the deposited species (kg/m^3),
 k = reaction rate coefficient (m/s),
 k_0 = reaction rate constant (m/s),
 E_A = activation energy for the deposition reaction (kJ/mole),
 R = universal gas constant (kJ/mole K).

These are the basic forms that must appear in any model of the deposition process. For each of the various published models, some form of these equations are combined to produce a set of coupled, linear differential equations. These then are solved numerically to obtain a *global* description of the process. This global description relates the environment of the processing chamber or applicator to aspects of the material product. It does not expose any relationships that might exist among the subprocesses, such as those embodied in equations (10) - (16), the environmental conditions, and the material properties. Furthermore, even at the global level, the results that are presented, and that are available to the designer, are limited by the author's interests, by the many approximations deeply and invisibly imbedded within each submodel, and such a mundane issue as the amount of publication space available. Thus, the sensitivity of the model predictions to these approximations is not easy to assess, and confidence in these numerical predictions is highly suspect. Under these conditions, the prospects for developing advanced process controls are severely circumscribed.

TA&T's approach was to disassemble these published models, assess the underlying approximations, determine the fundamental principles involved, reduce the description to intuitively clear, mechanistically accurate phenomena, and finally to summarize the CVI process in a way that should be useful to both the process engineer and the process control engineer. This approach should result in subprocess model descriptions that will perfectly fit IPM as it evolves.

In addition to these equations, a description of the temperature distribution is necessary. During heating by conventional means, energy is supplied to the sample from its exterior surface. Thus, this surface is at a higher temperature than the interior surface. Since reactant gas also enters the preform across this surface, the gas tends to react on the surface more rapidly than it does toward the interior. Microwave heating is unique in that microwave energy is deposited throughout the material. The equilibrium temperature is reached when the

rate of energy lost through radiation and convection is equal to the rate at which microwave energy is dissipated in the sample. Since energy can be lost only through the exterior surface, and since microwave energy is dissipated uniformly throughout the sample, the exterior surface reaches a lower temperature than the interior surface -- the opposite of that achieved with conventional heating. Thus premature pore closure is avoided. This is the key rationale for microwave heating for CVI processing.

In order to determine the temperature profile achieved with microwave heating, equation (12) is solved. It will be assumed that the material to be processed is shaped as a cylindrical tube with cylindrical pores modeled as capillary tubes lying along the radial axis. In this static case, equation (12) reduces to

$$\kappa \frac{1}{z} \frac{d}{dz} z \frac{dT}{dz} = -P \quad (17).$$

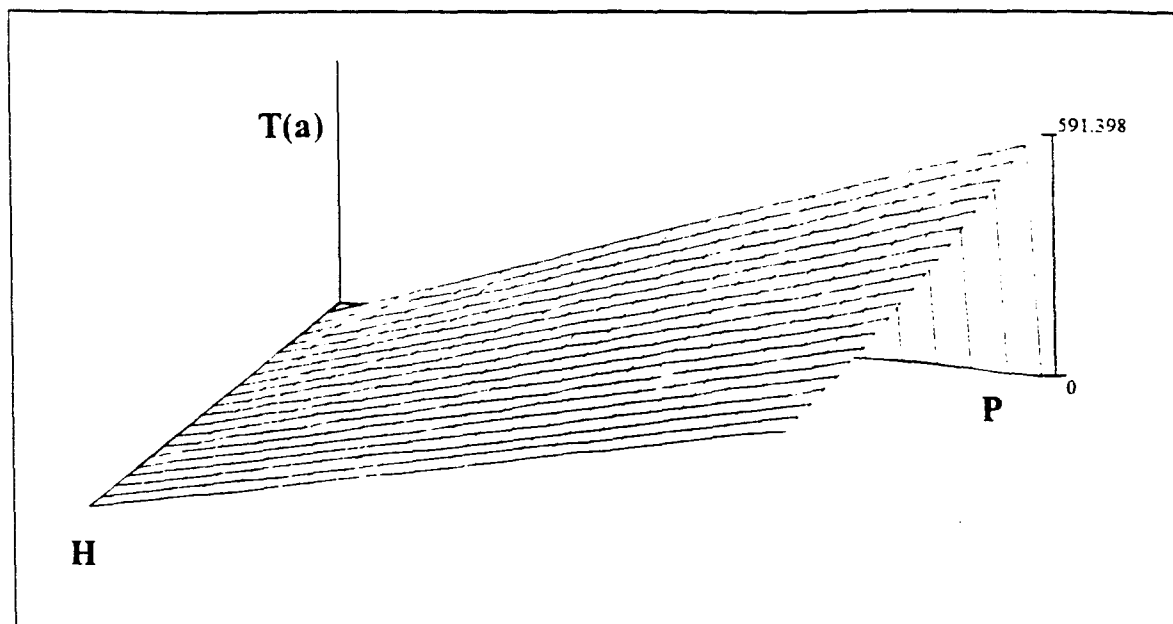
where z is the radial distance along the pore. This also is a good model for a silicon carbide preform wound over a high purity alumina mandrel because the mandrel will not absorb microwave energy, and if no gas flows along the inner axis of the mandrel then, in the steady state, no heat will flow radially from the preform into the mandrel. Therefore, *in the steady state*, the mandrel is thermally "invisible" to the process. The solution to this *static* problem is

$$T(z) = \frac{1}{4\kappa} P (a^2 - z^2) + \frac{1}{2\kappa} P b^2 \ln\left(\frac{z}{a}\right) - \frac{1}{2h} P (b^2 - a^2) + T_\infty \quad (18)$$

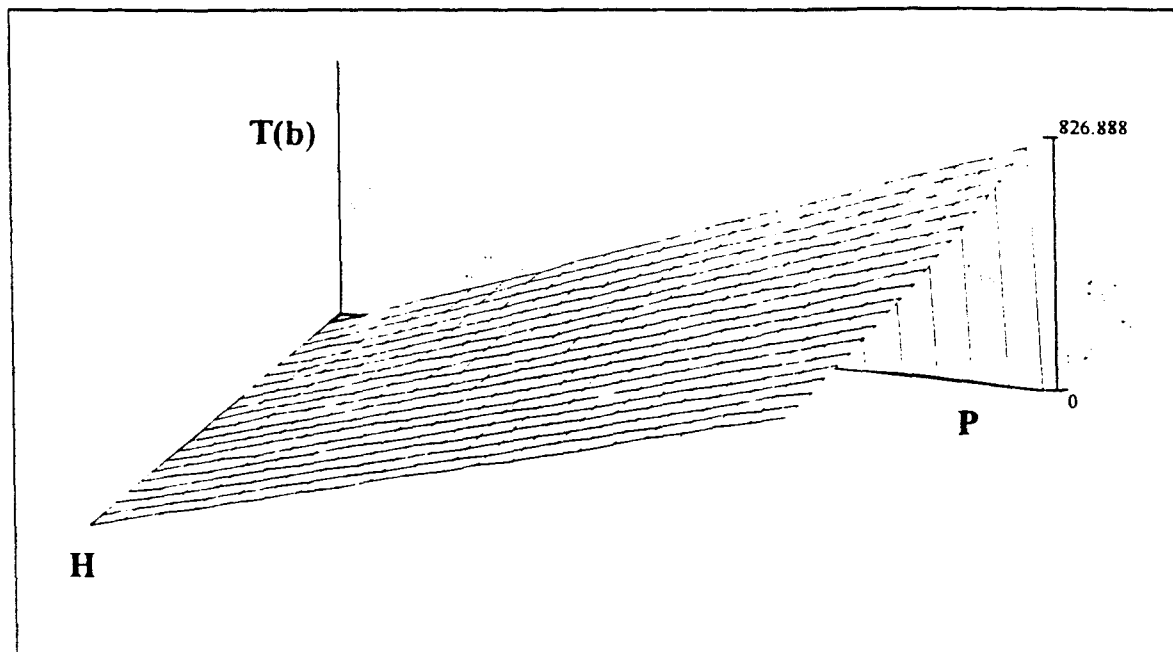
where a and b are the outer and inner radii respectively of the preform, h is the rate of convective cooling at the outer surface in $W/m^2 K$, and the last term is the temperature of the free stream gas that cools this surface at $z = a$. It is worth noting that the temperature difference between the inner and outer surface depends only on the absorbed power and not on the rate of convective cooling.

In order to explore this static temperature profile, it is useful to create a surface map of $T(a)$ and $T(b)$ versus P and h . An example is shown in Figure 16 where the nearly horizontal axes represent P from 0 to 200 MW/m^3 , the axes coming forward to the left represent h from 1500 to 2500 $W/m^2 K$, and the vertical axes represent the differences between the surface temperatures and the free stream temperature. For process control, plots of this type could be stored as tables and used to find specific sets of operating conditions. Alternatively, equation (8) can be inverted to find P and h in terms of a given pair of temperature values, such as $T(a)$ and $T(b)$. As an example, consider developing silicon carbide for which $\kappa = 10$. If we let $a = 3$ cm, $b = 2.5$ cm, $T(a) = 900$ °C, $T(b) = 1100$ °C, and the free stream temperature = 500 °C, then $P = 169$ MW/m^3 and $h = 1945$ $W/m^2 K$. These values then can be inserted into equation (8) to obtain the temperature profile of the heated preform. The results are shown in Figure 17. The reverse temperature gradient that results from this volumetric heating is evident. An obvious question is whether such high microwave power density and such high cooling rates can be achieved.

If the microwave power is pulsed, this approximation must be modified since the alumina will place a thermal load on the preform even if the alumina itself does not absorb microwave energy.



M



N

FIGURE 16 CONTOUR PLOTS OF $T(a)$ AND $T(b)$ VERSUS P AND h

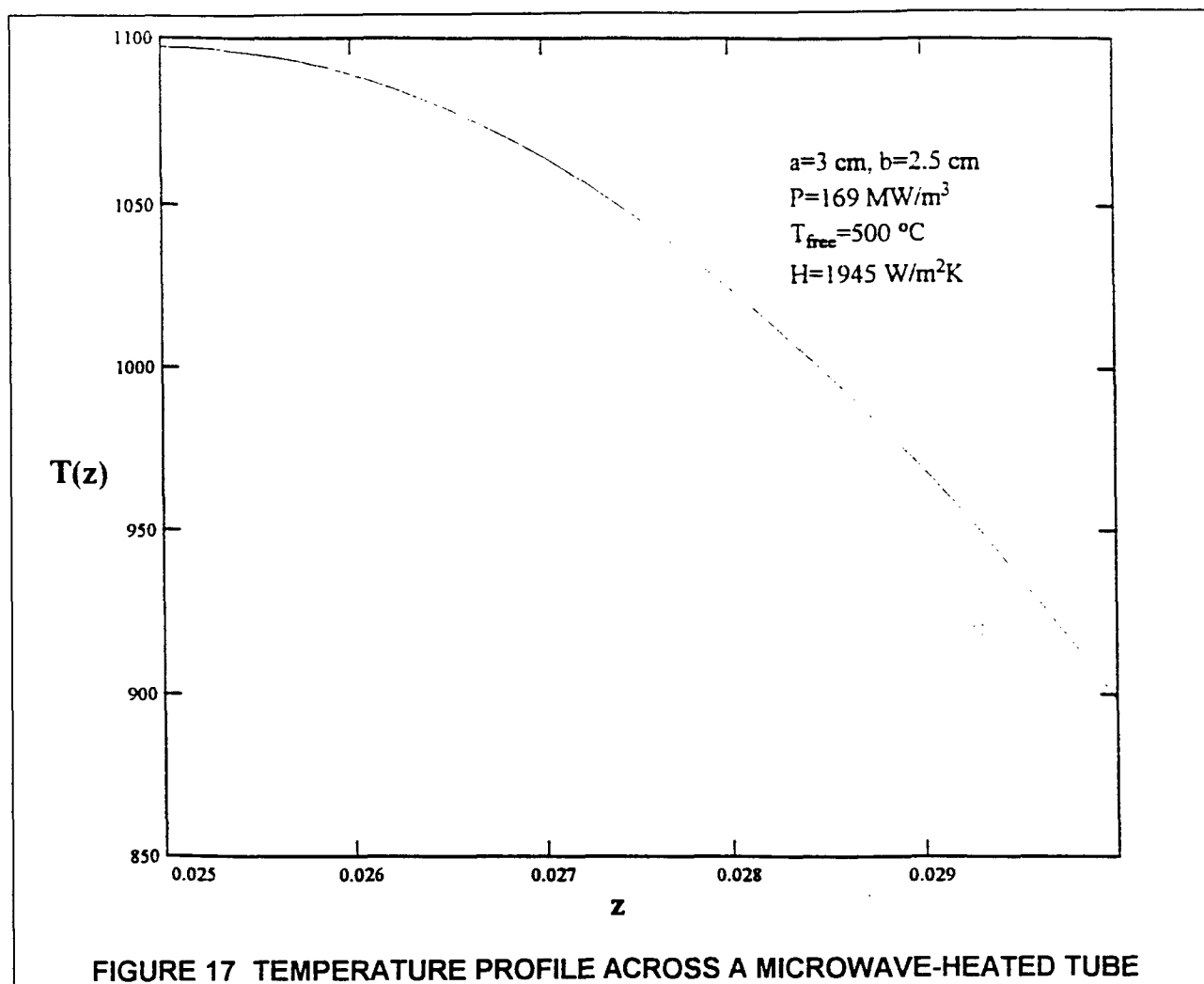


FIGURE 17 TEMPERATURE PROFILE ACROSS A MICROWAVE-HEATED TUBE

TA&T performed extensive, detailed modeling of its CVI microwave applicator. This modeling took account of the microwave feed system, dimensions, wall losses, etc. The results of this analysis are plotted as contour maps of a quantity proportional to the $|E|^2$ term of equation (10). One example is shown in Figure 18. In this particular case the true, maximum available microwave power density, S in Watts per m^3 , is determined using the approximate relationship

$$S = 2 \cdot 10^6 (\text{contour value}) \text{ (W/m}^3\text{)} \quad (19).$$

Thus we see that there is sufficient power to achieve the necessary temperature gradient.

Example of simulated process control

On the basis of the experience described above, Fortran computer code was written to solve the coupled equations (10) through (16). One of the input parameters was the reactant gas pressure. It was mentioned above that the gas pressure normally was between 5 and 20 Torr. This low pressure has to be maintained in a conventional CVI reactor because the walls and the gas itself are at temperatures sufficiently high that homogeneous reactions can occur.

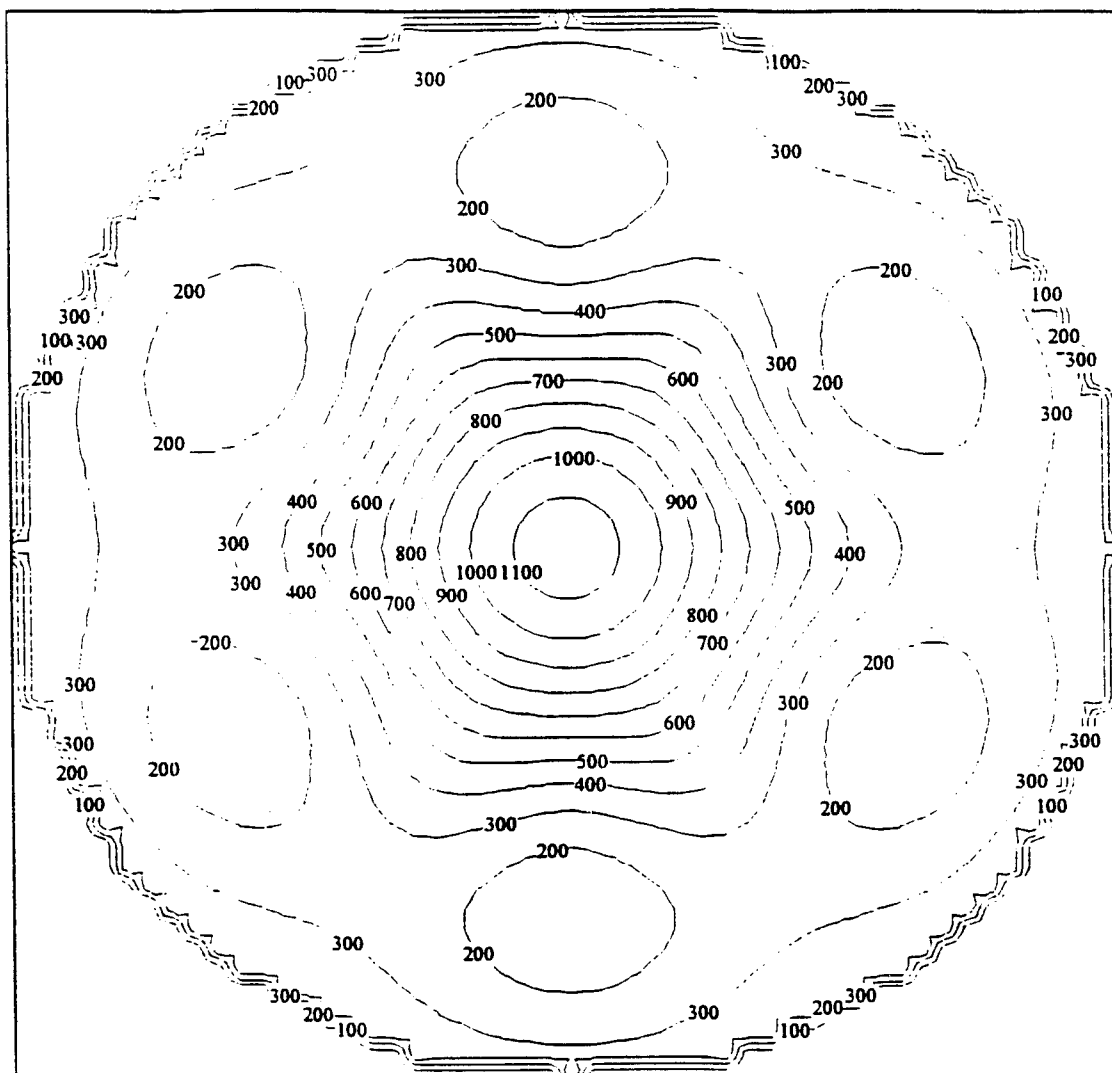


FIGURE 18 CONTOUR MAP OF APPLIED MICROWAVE POWER

Under the conditions of volumetric heating achieved by the absorption of microwave energy the walls and gas remain considerably cooler and the reaction is largely heterogeneous. Thus, the gas pressure can be higher, and in a microwave reactor may be typically 600 Torr. Under conditions of low pressure processing, the molecular mean free path is greater than the typical pore radius and gaseous diffusion is Knudsen. Under conditions of high pressure processing, most molecular collisions are with other molecules and gaseous diffusion is Fickian. The distinction between these two diffusion regimes were accounted for in the computer code.

The code was verified by reproducing the results of Gupta and Evans including those demonstrating the dependence of premature pore closure on initial pore radius. Additional preliminary results are shown in Figure 19 which shows the dependence of trapped porosity and processing time on reactant gas concentration at the surface. Parameter values were typical of CVI processing conditions and are not quoted here because the results of more extensive studies are described below. But these results do show that for nearly an order of magnitude reduction in processing time the trapped porosity falls from about 0.0051 to 0.0023.

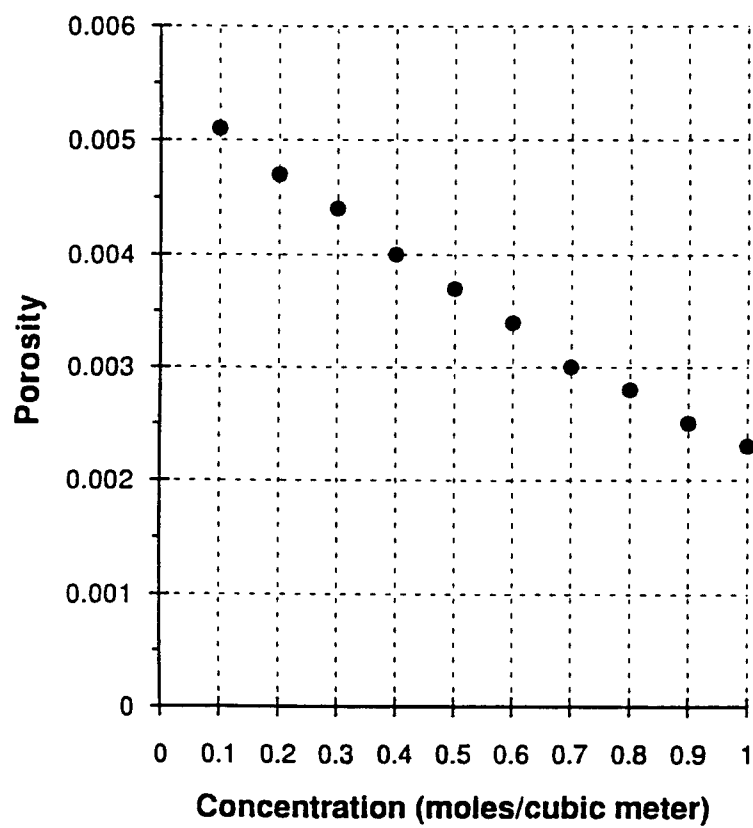
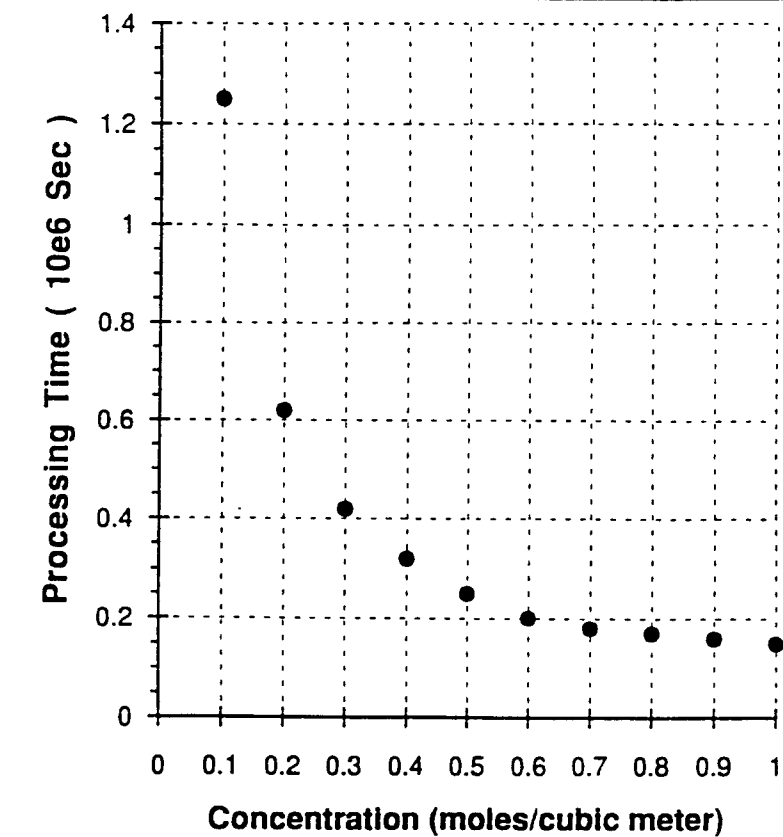


FIGURE 19 TYPICAL CVI SIMULATION PREDICTIONS

In other words, below some porosity, surface gas concentration has a much greater influence on processing time than on porosity. It will be seen below that this tendency is common to most processing conditions. This program then was used in an attempt to find improved processing conditions.

Processing goals are very simple to define. They are:

- achieve minimum trapped porosity (0% is the ultimate goal);
- achieve minimum processing time.

The first assures optimum materials properties; the second assure maximum economic benefit. With these in mind, attempts were made simply to improve processing conditions by changing the conditions in real-time. Since this would require some criteria for change, this simple example would demonstrate the advantage of using an in situ sensor to direct the process. For reasons that will be discussed in the next section, it was imagined that this sensor could provide some measure of the density profile along the length of a pore. Two simulations were compared.

The constant processing conditions were:

surface gas concentration, C_o , = 1 mole/m³
initial pore radius, r_o , = 10 μ m
convective cooling rate, h , = 500 W/m²K
pore length, L , = 5 mm
gas pressure, P , = 1 atm.

The free stream gas temperature was the only adjustable process variable. It is easy to imagine that the temperature of a carrier gas such argon could be varied to change the surface temperature of the preform. The processing time can be estimated by assuming that premature pore closure does not occur so that the pores on exterior surface close last. In that case, integration of equation (14) with C replace by C_o gives the total processing time. The processing time for the parameter values listed above with a free stream gas temperature of 25 °C was computed to be about 34 hours. By solving the coupled set of processing equations, it was shown that the trapped porosity was about 0.002. Within the limits of accumulated computational error, this represents zero trapped porosity. When the free stream gas temperature was raised to 125 °C the processing time fell to 12 hours but the trapped porosity was 0.128. Such a high trapped porosity was unacceptable. Therefore, a modified processing scheme was devised based on a measurement of the density profile.

In this modified scheme, the pore radius was continuously monitored only at the midpoint along the length of the pore. The initial free stream gas temperature was again 25 °C. When the radius of this midpoint pore equaled on half the initial radius of the pore, r_o , the free stream gas temperature was raised to 125 °C. In other words, it was assumed that after the midpoint of the pore had closed sufficiently, the process could be accelerated without fear of premature pore closure. Under these conditions, the processing time was reduced to 18.3 hours leaving a trapped porosity of 0.034. A considerably more elaborate scheme resulted in a processing time of 17.2 hours with a trapped porosity of 0.015. Since the pore radius could be inferred from density measurements, this simulation demonstrated that considerable processing improvement would be possible with in situ sensors.

These numerical solutions required many hours of computer CPU time. They were not, therefore, very suitable for real-time control. Furthermore, they were not especially useful in finding the optimum set of processing conditions. It was decided that a rapidly converging, artificial neural network might offer a viable alternative, and that this could be readily accommodated by the control scheme shown in Figure 12. Thus, the code used above now was used to generate suitable training pairs. It was decided to restrict the adjustable parameters to the four quantities: initial pore radius, reactant species concentration, free stream carrier gas temperature, and convective cooling rate. The values used to define the corners of the parameter hypercube were:

r_o :	1, 10, 100 μm
C_o :	0.5, 1 mole/ m^3
T_∞ :	298, 500 K
h :	400, 600 W/ m^2 K.

Simulations were generated for 25 combinations of these values. The maximum possible processing time was again determined from equation (14). At 10, nearly equally spaced time intervals within this time, the process simulation was stopped and the radial profile recorded at 25 points along the length of the 5mm pore. Process simulation at a point at the center of the parameter space completed the set of data on which the artificial neural network would train.

The neural network was used to predict the trapped porosity and total processing time for a pore residing in a 1-D slab. The neural network was trained using 25 training pairs which contained four parameters and the resulting trapped porosity and total processing time. The neural network structure used consisted of four inputs r_o , C_o , T_∞ , h ; a hidden layer of 8 neurons, and an output layer of only 2 neurons - the processing time, T_{pt} , and the porosity, ϕ . The network was trained using the 25 training pairs provided, consisting of one point at each corner of the training space, for 100,000 epochs. The plots of the training data versus the neural network response after training for T_{pt} and ϕ , shown as the first two figures in Appendix A, indicate that the network provided a reasonable approximation of the points, but that the fit of the training set should be much better.

The learning was based on a gradient descent of the error with small errors making small network changes while large errors make large changes. The training method was evident in the plot of the training data versus the network response for T_{pt} . The data for T_{pt} spanned 5 orders of magnitude - from 16.4 to $1.49 \cdot 10^7$ seconds. The plot showed that for most runs, the fit was far from ideal. However, for the points $1.49 \cdot 10^7$ and $0.74644 \cdot 10^7$ s the fit was reasonable. Hence, a small error in approximating the point $1.49 \cdot 10^7$ would dominate the weight adjustments making it difficult to learn the other points which were orders of magnitude smaller. Attempts were made to train the network after removing the largest 5 points with the result being the ϕ , and T_{pt} could be recalled very accurately. Thus, a reasonable limit should be placed on T_{pt} even though larger trapped porosity values would obviously result.

The trained network, based on all 25 data pairs, was used to predict T_{pt} and ϕ based on the 6 possible combinations of r_o , C_o , T_∞ and h . Plots of these results are shown in Appendix A. The contour maps are not labeled due to the uncertainties discussed above. The surface maps are used in conjunction with these contour maps to locate extrema, although

relative magnitudes remain undetermined. Nevertheless, unexpected regions of the processing space can be seen that suggest substantial improvements in the processing protocols may be developed. Further studies will be pursued to include the local pore density as input, and to use this data to guide real time, in situ process control.

VI EVALUATION OF POTENTIAL IN SITU SENSORS

A measurement of the density profile was assumed to be operative during the simulations discussed above. Decisions on when to change the processing parameters to maintain zero trapped porosity while achieving minimum processing time were based on an effective pore radius that, in turn, could easily be deduced from these density measurements. The decision that a real-time density profile measurement was needed was based on numerous processing simulations combined with continual reassessments of sensor possibilities and advantages. An example of this assessment is shown in the chart, Figure 20. Not included in this figure is a cost comparison.

SENSOR	INFORMATION OBTAINED	FEATURES
beta-source/detector	average porosity	simple to use, average porosity only
gas-phase spectroscopy	average reaction rates	average rate, relatively inexpensive
laser thermal pulse	near-surface porosity	surface temp. only coupling to materials very detailed profile
thermal imaging	porosity, rate of temp. change	
pyrometer	surface temperature	
acoustics	density / porosity	
laser ultrasonics	bulk modulus, density, temp.	
μ -focus x-ray	density / porosity	
broad-beam x-ray	density, porosity	simple to use
microwave scattering	coating thickness, electrical permittivity	thickness & permittivity interrelated


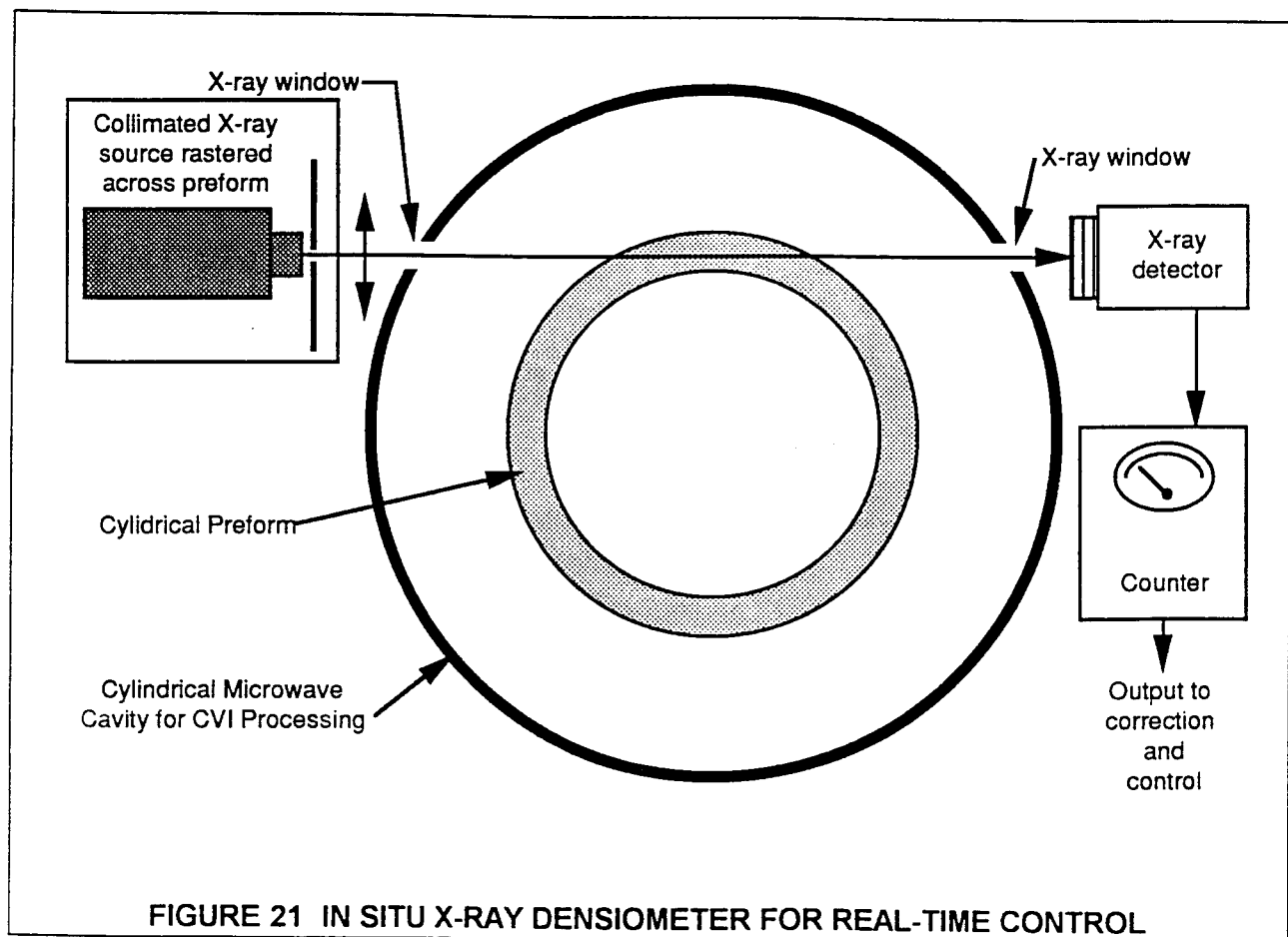
 preferred for CVI subprocess control

FIGURE 20 COMPARISON OF SELECT IN SITU PROCESS CONTROL SENSORS

X-ray radiometry It is the comparison of cost between micro-focus and radiometric x-ray, and the fact that sufficient density information could be obtained from broad-beamed, radiometric x-rays that indicated the later is more suitable for process control. In the current conceptualization of the x-ray density measurement, and x-ray beam would be collimated to a beam width of about 1mm. Manufacturers and users have suggested this dimension is not unreasonable. The collimated beam would intersect the cylindrical preform along a cord, as shown in Figure 21. The x-ray source would be mounted on a motor-driven translation stage that would permit rastering the beam from a line tangent to the outer surface of the preform to a line tangent with the interior of the preform. A simple detector on the receiving side would be used to record count rate as a function of position, and a simple correction would be used to account for the varying amount of material through which the beam had to pass. An algorithm would be developed to convert these measurements into the corresponding radial measurements needed for in situ control. This hardware and software design will be implemented during a Phase II effort.

Gas Analysis Gas phase spectroscopy remains an option to be considered under a Phase II effort. Gas analysis may give valuable information concerning the deposition rate and the rate of the interdiffusion of reactant and product gases. This would not be practical in a conventional, hot wall reactor where homogeneous reaction dominate the production of gas products such as HCl. But during microwave processing, only the preform is heated so that the reactions are, for the most part, heterogeneous and the reaction products are more closely related to reactions occurring in the preform.



Several methods of gas analysis are available. The most direct is by quadrupole mass spectrometry. The advantage is that gas species are readily identifiable. The disadvantage is long data acquisition times and the cost of multi-stage turbo pumping. Laser induced fluorescence is another option. It could be costly and requires relatively long times to obtain sufficient data for analysis. A more direct approach may be atomic absorption. A low power dye laser could be rastered across a bandwidth and a absorption recorded by a broadband detector. Perhaps the simplest method would be one that utilizes the compact gas analyzers used by regulatory agencies to detect gas emissions. Since HCl is both a standard by product of CVI SiC processing and a contaminant, an HCl cell should be available. Other cells could be designed, such as for MTS and the methyl radical, so that instead of a continuous spectrometer, a discrete spectrometer would have been affected. These options will be considered in more detail during a Phase II effort.

VII OUTLINE OF A PHASE II EFFORT

This Phase I effort has achieved the following:

- The broad feasibility of process control for CVI was demonstrated;
- The crucial importance of hierarchical IPM in realizing this control was demonstrated;
- The essential role played by an artificial neural network in building the needed expert system data base was demonstrated;
- An in situ sensor was identified and its role in controlling CVI process control was simulated.

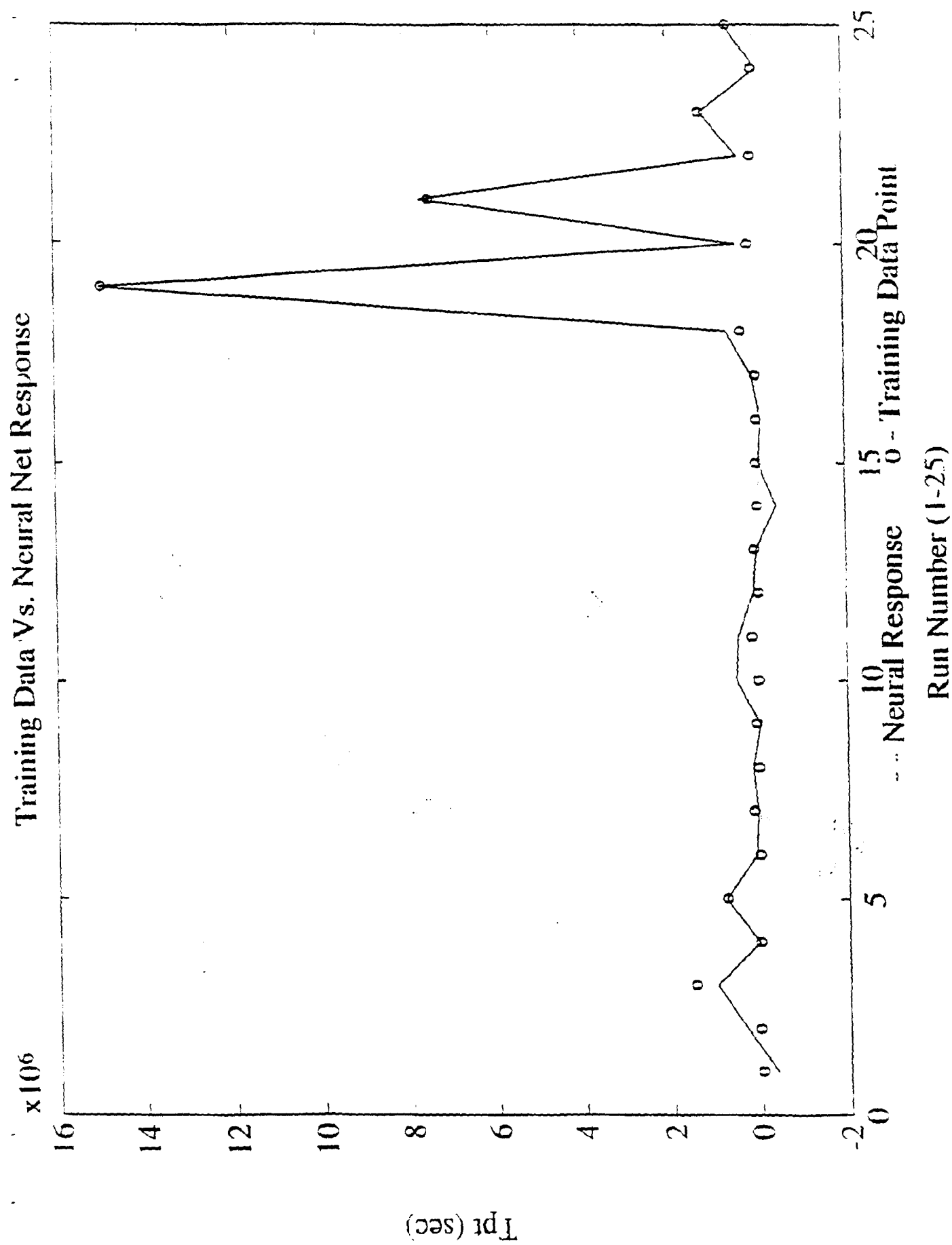
Thus, the goal of each of the four tasks has been reached. This control technology now needs to be implemented on a microwave CVI system. TA&T has two such systems: one operating at 2.6 kW and a large, six-magnetron system supplying 7.5 kW. The larger system was designed and built with computer hooks built in. It is ready to run under process control. This control would be implemented under a Phase II effort. This implementation would, at a minimum, require completing the following tasks.

- Complete design of the hierarchical control scheme;
- Complete the process control hardware interface;
- Implement the software for CVI control;
- Complete implementation of the rapid convergence artificial neural network;
- Install x-ray in situ density sensor;
- Interface x-ray in situ density sensor with control structure;
- Perform extensive ANN training and product evaluation.

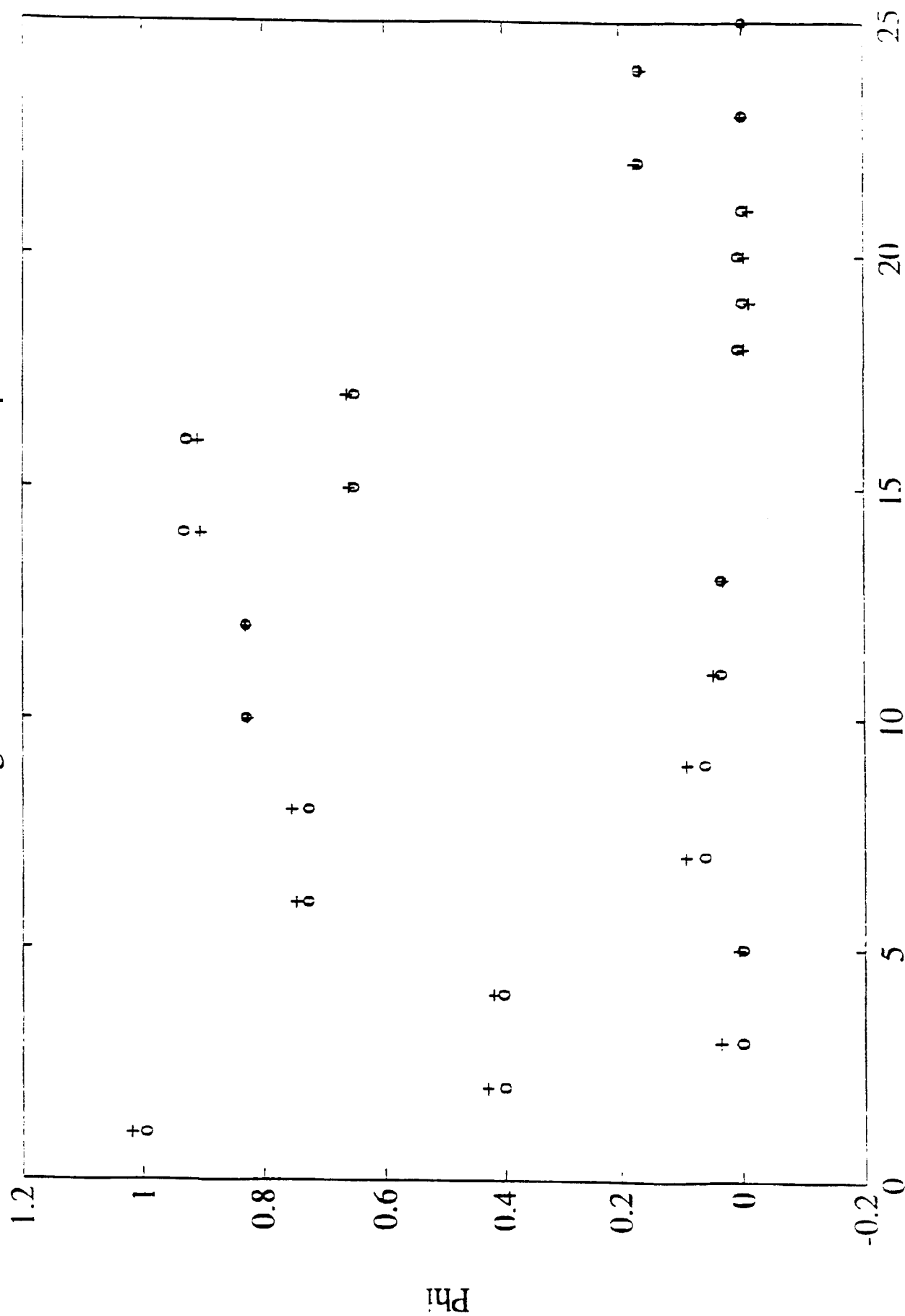
A detailed proposal will be submitted as requested.

APPENDIX

ARTIFICIAL NEURAL NETWORK RESULTS

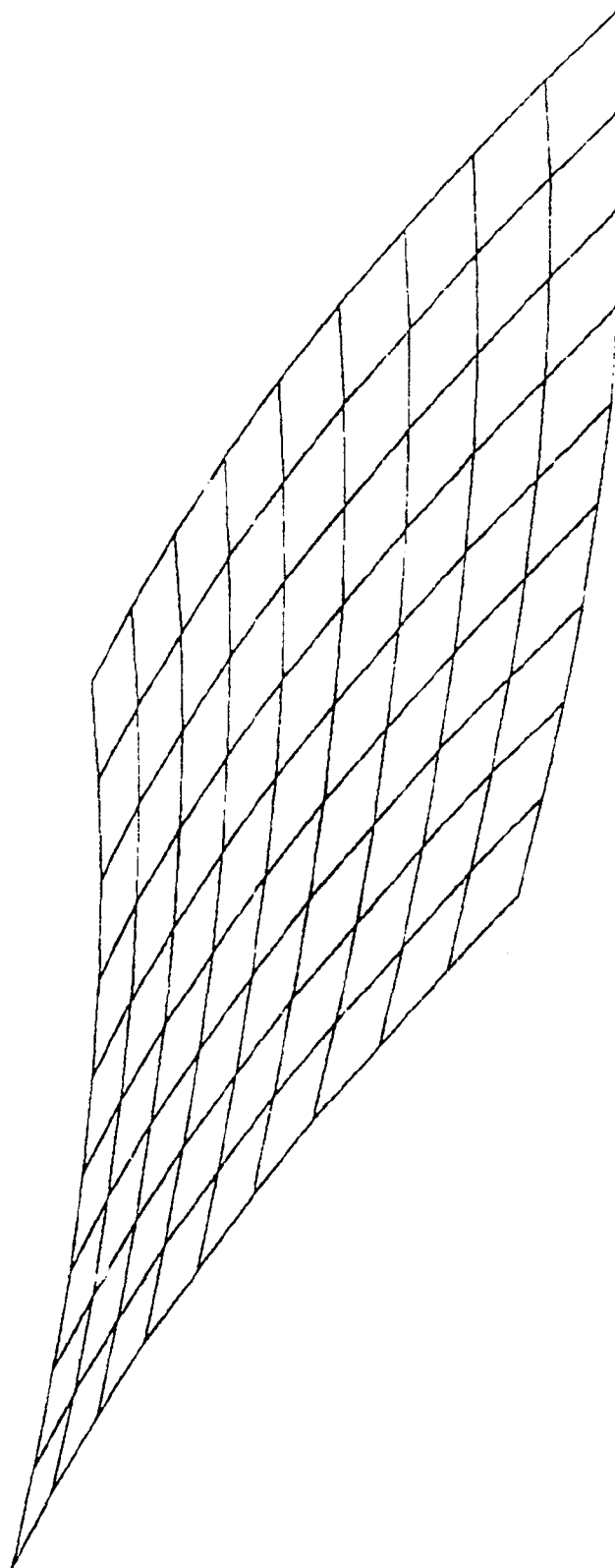


Training Data Vs. Neural Net Response



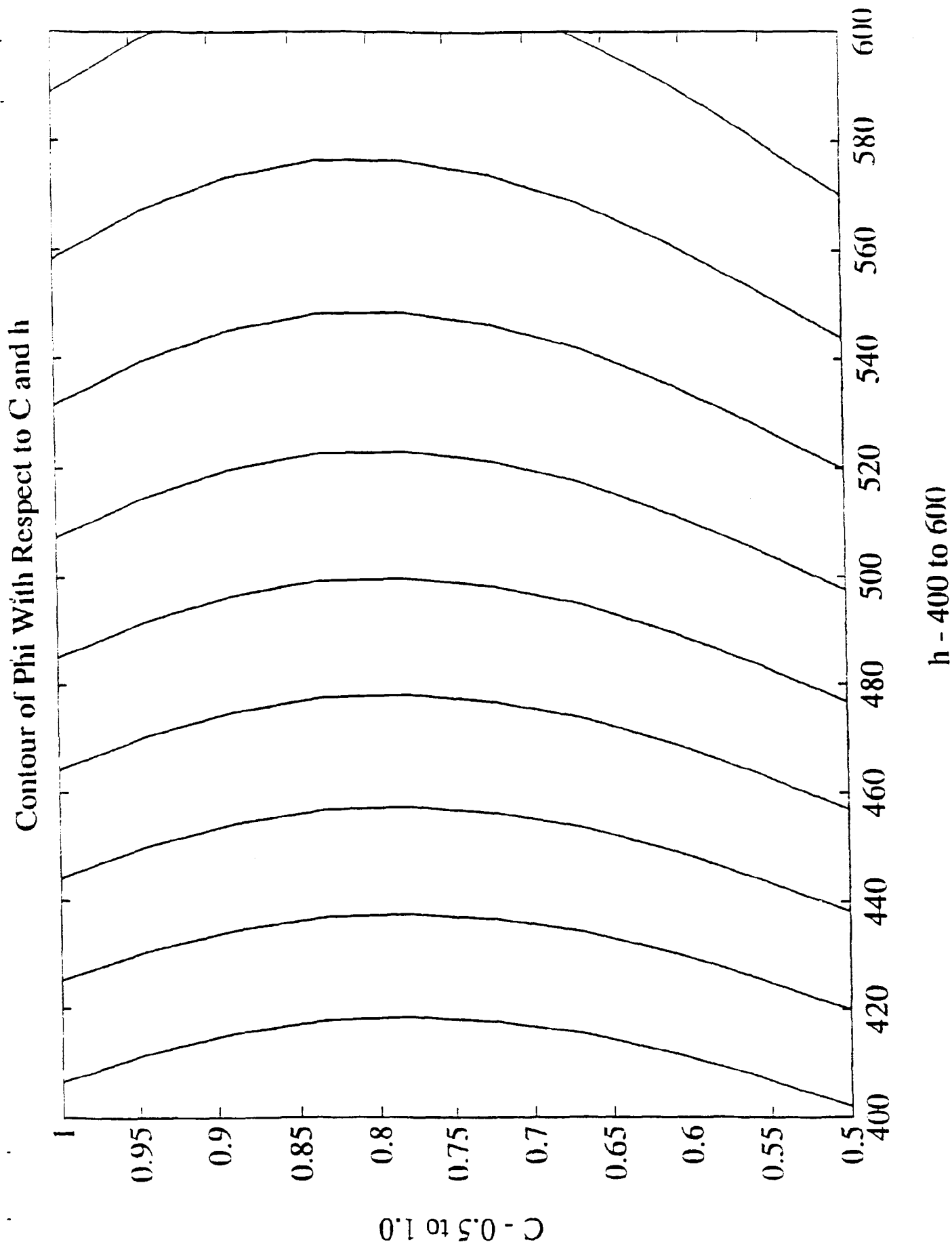
Run Number (1-25)

Phi as a function of C and h

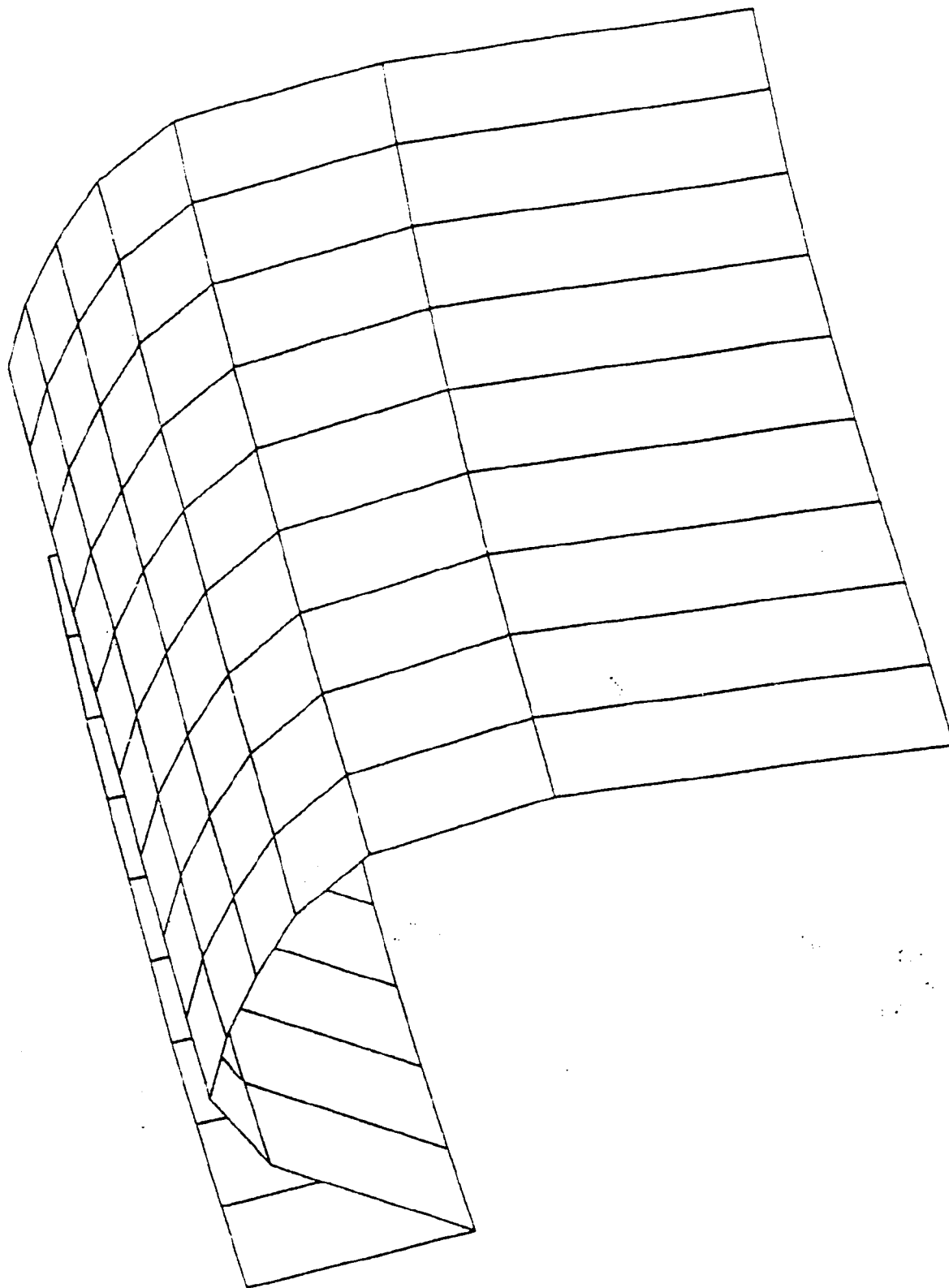


C - 0.5 to 1.0

h - 400 to 600



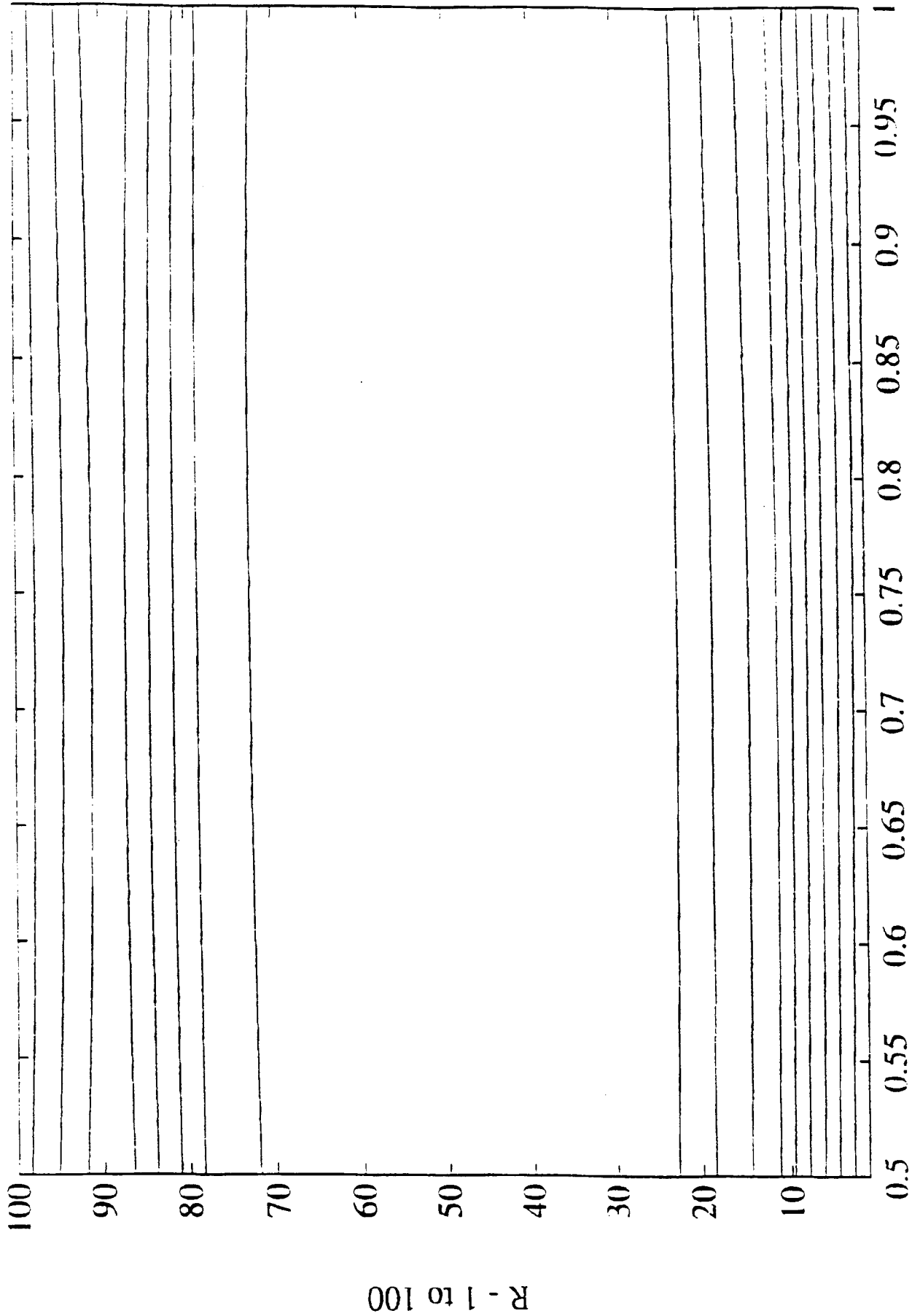
Phi as a function of R and C



R - 1 to 100

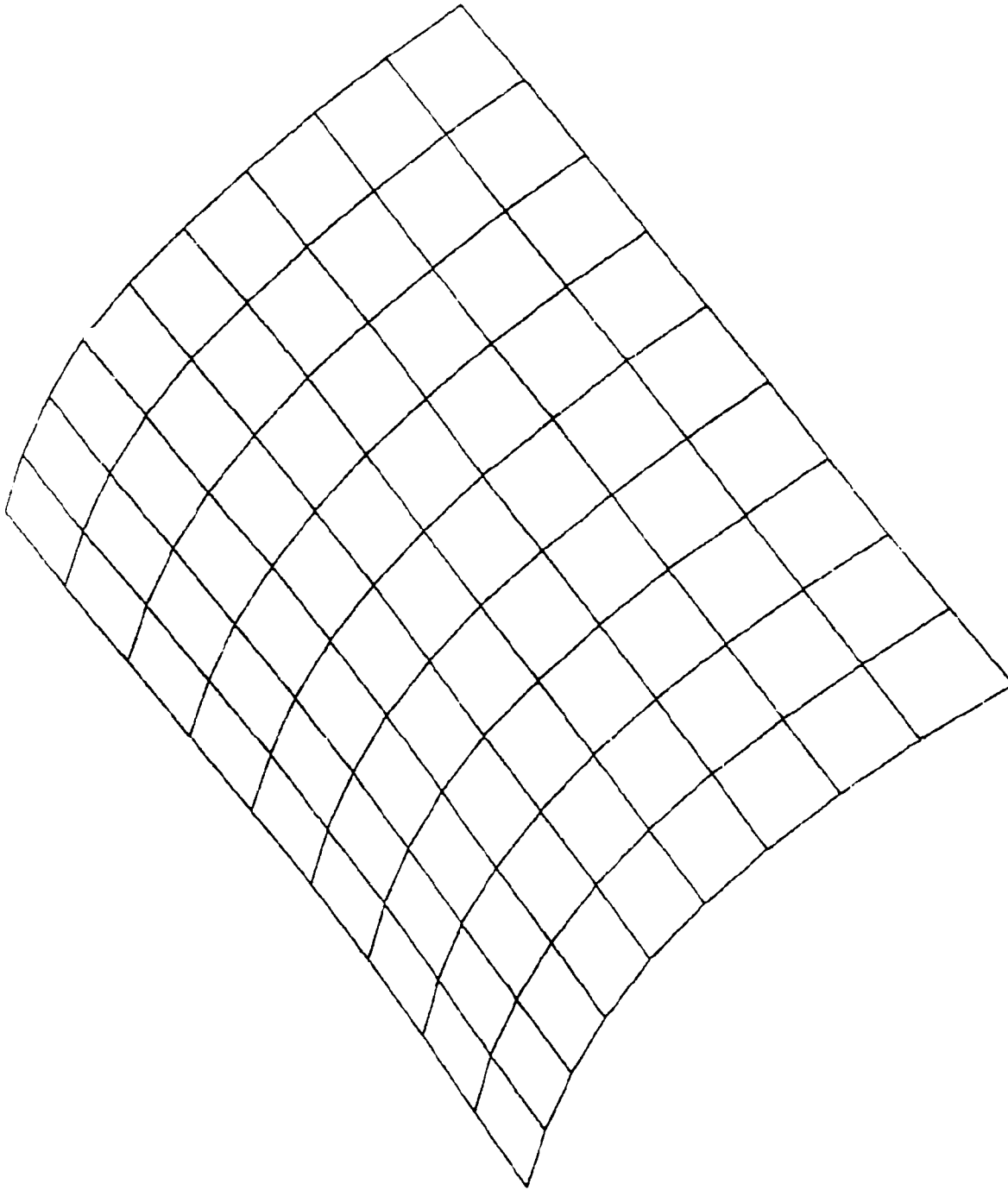
C - 0.5 to 1.0

Contour of Phi With Respect to R and C



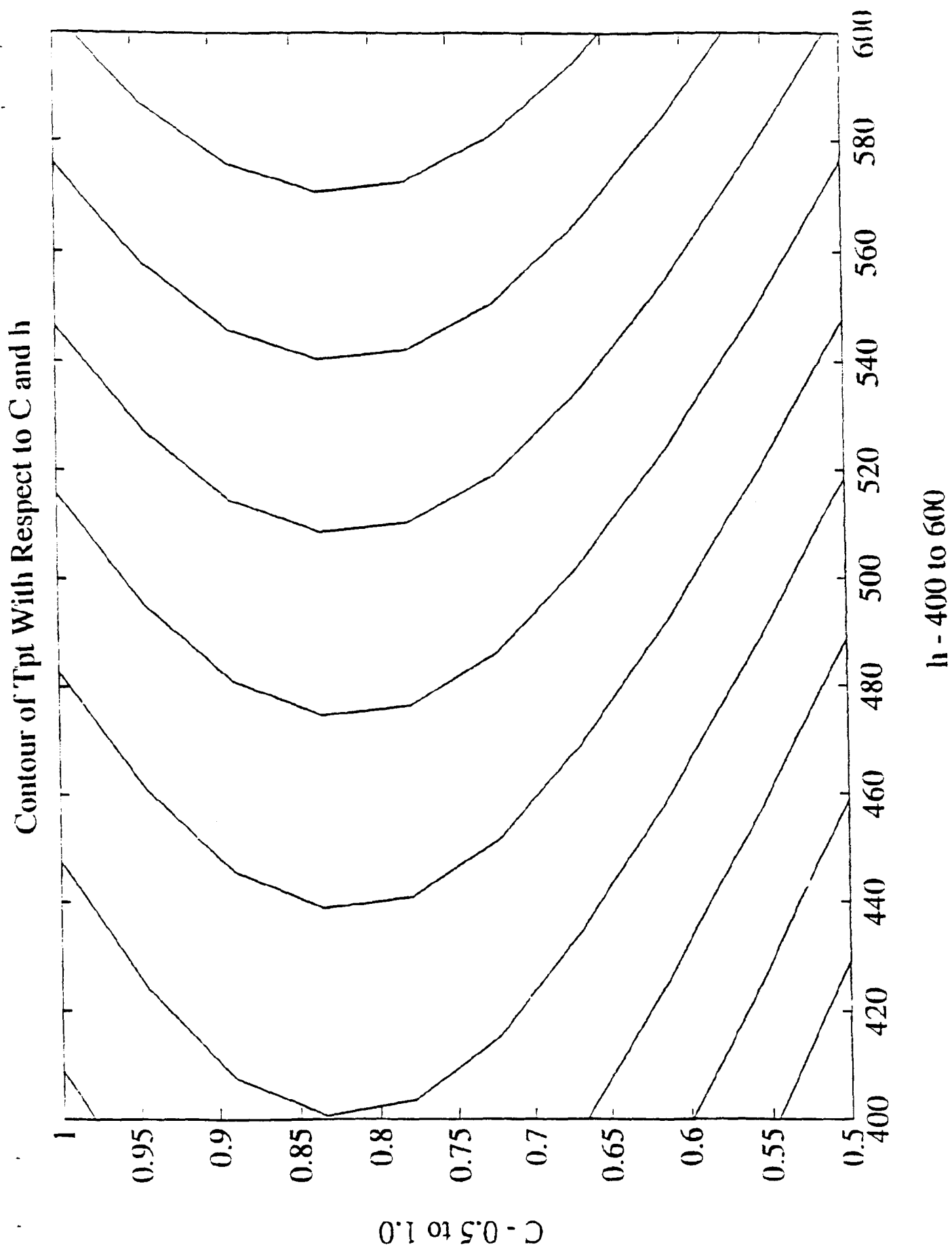
C - 0.5 to 1.0

Tpt With Respect To C and h

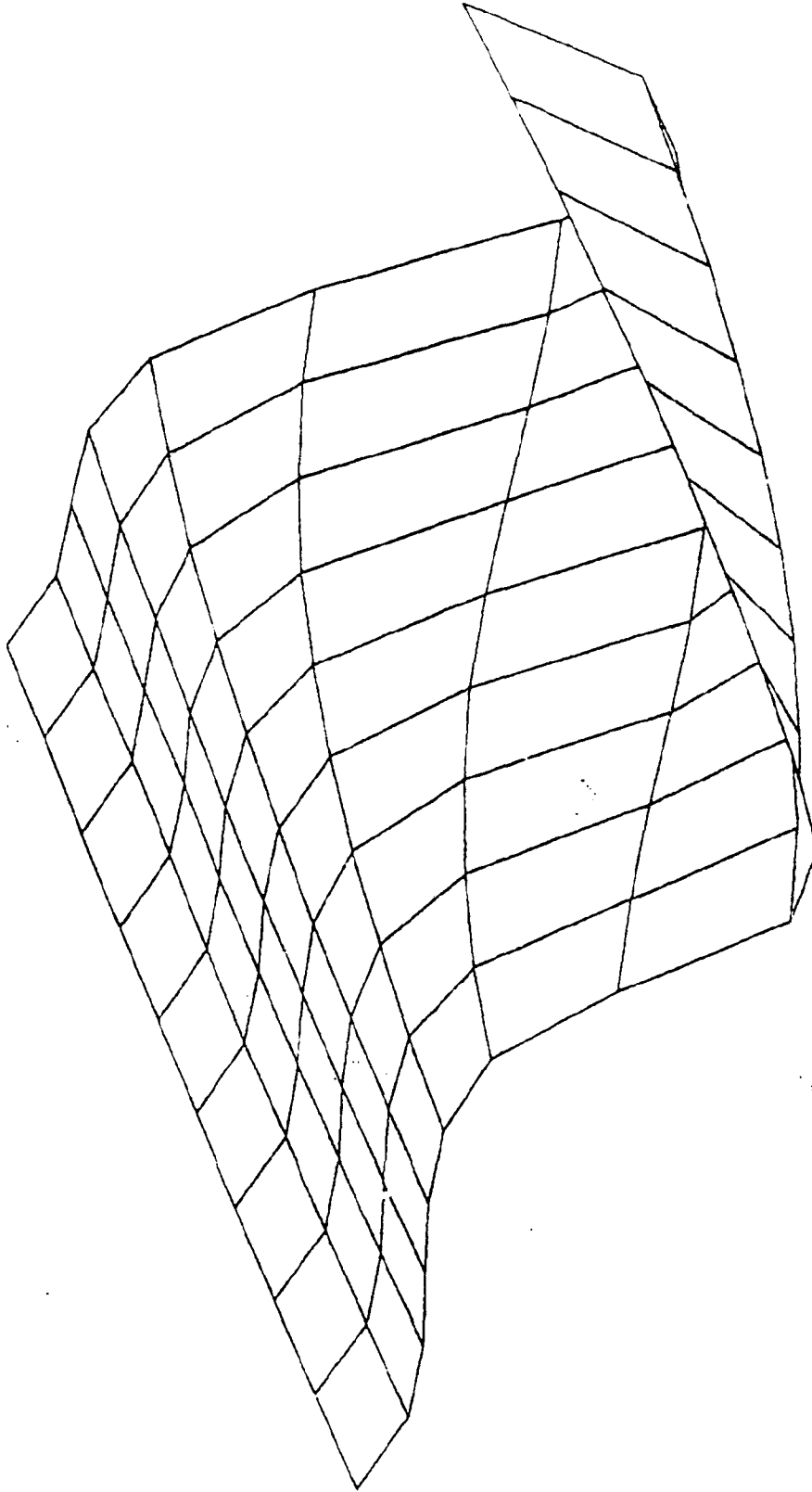


C - 0.5 to 1.0

h - 400 to 600



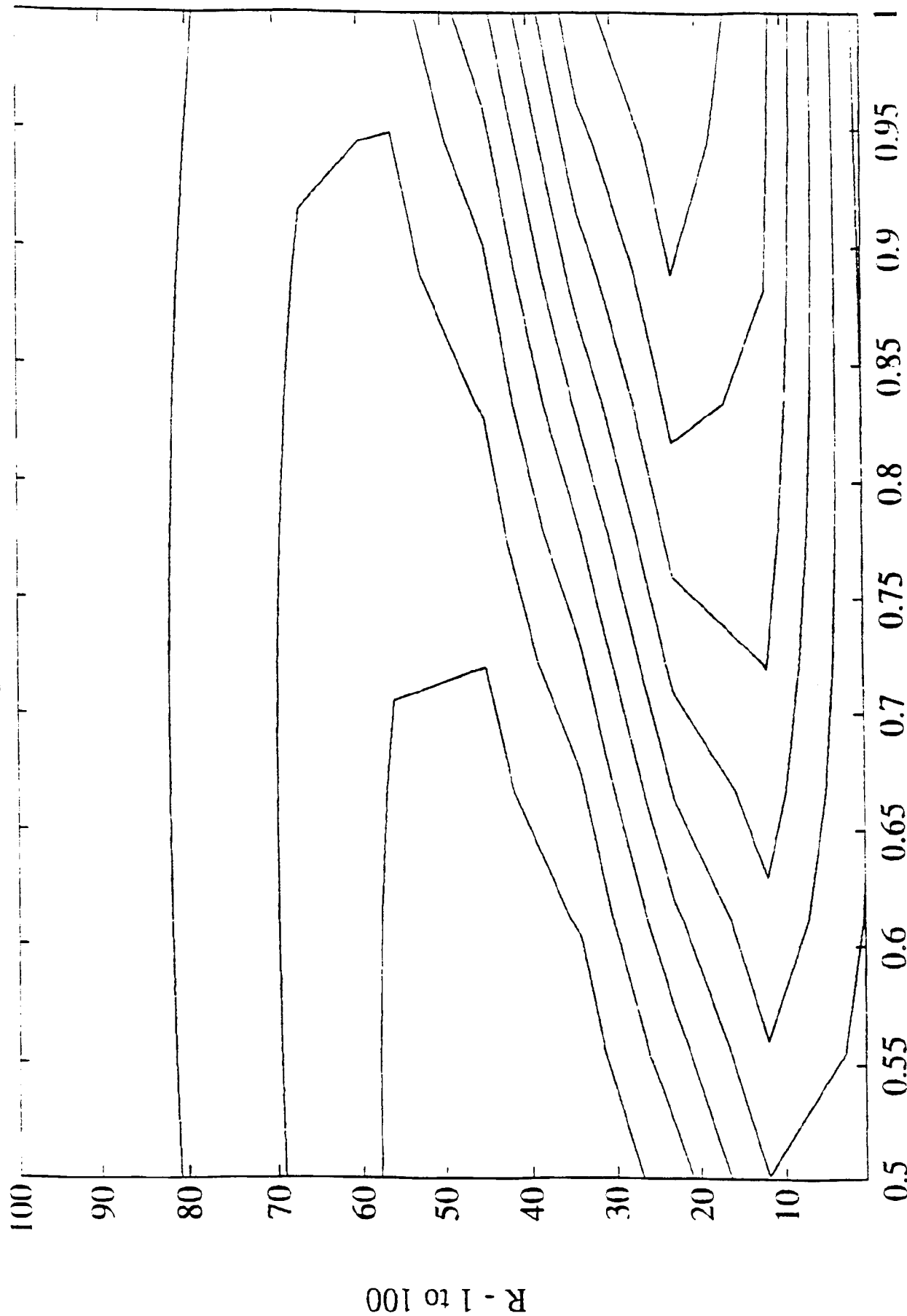
Tpt With Respect To R and C



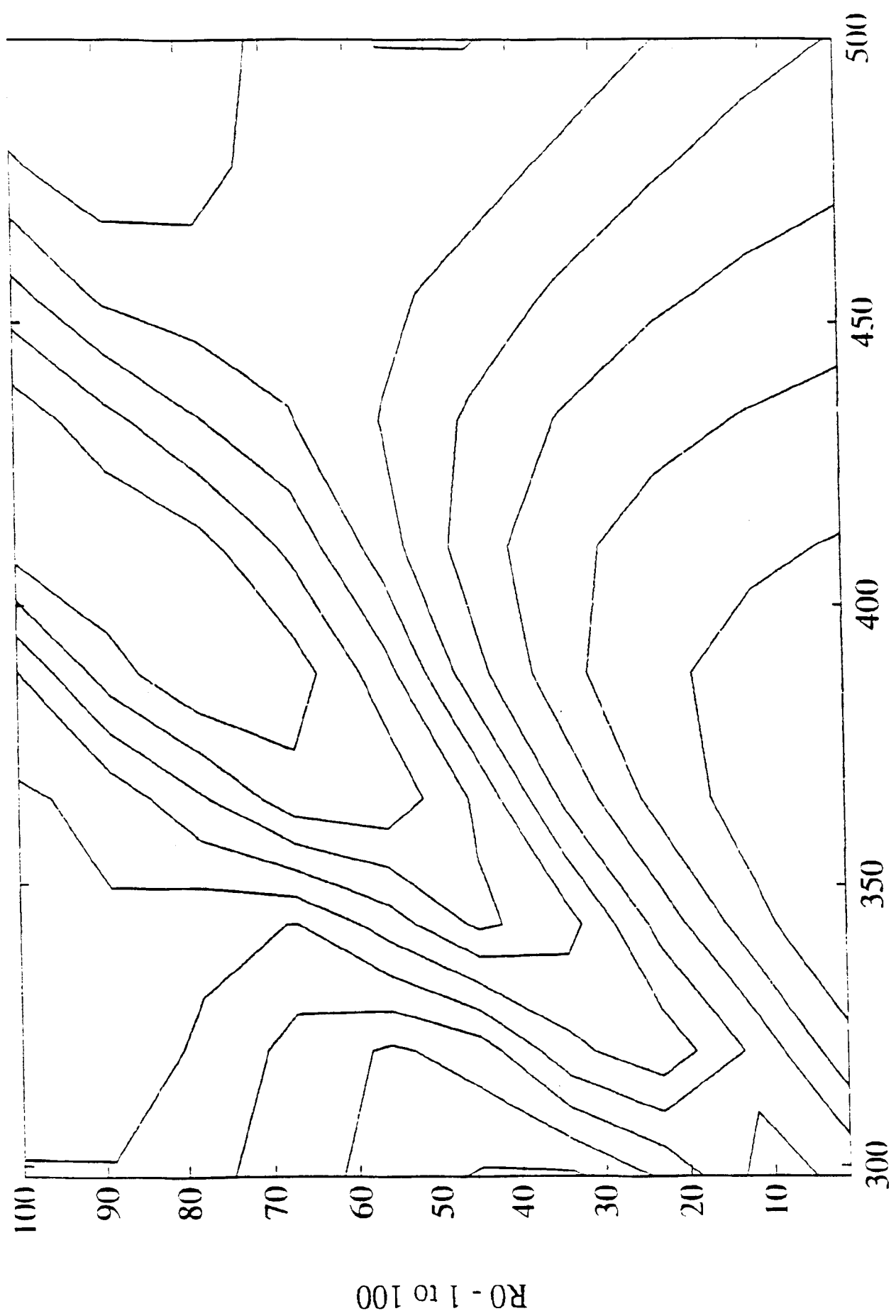
R - 1 to 100

C - 0.5 to 1.0

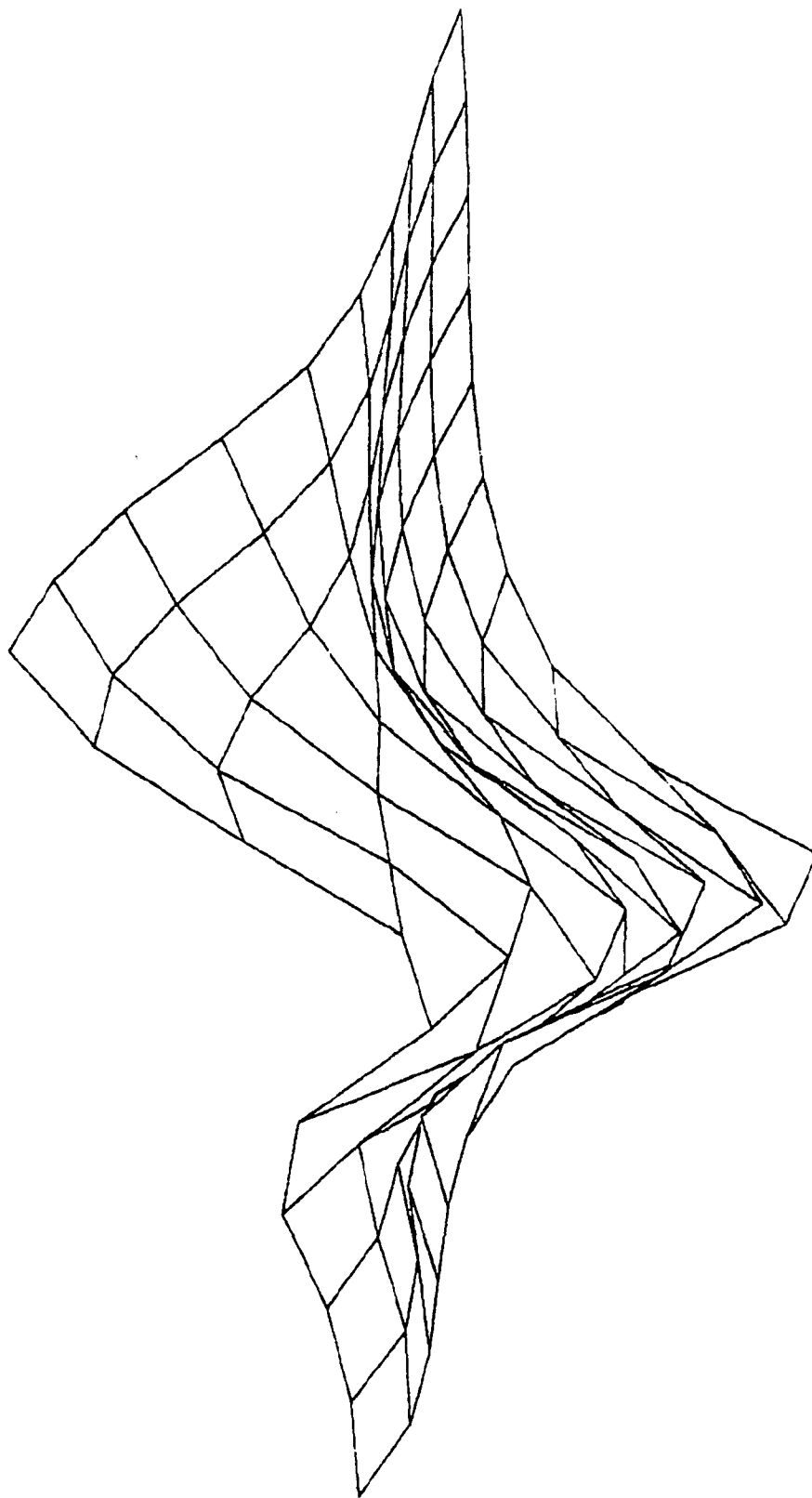
Contour of Tpt With Respect to R and C



Contour of Tpt With Respect to R0 and Tinf



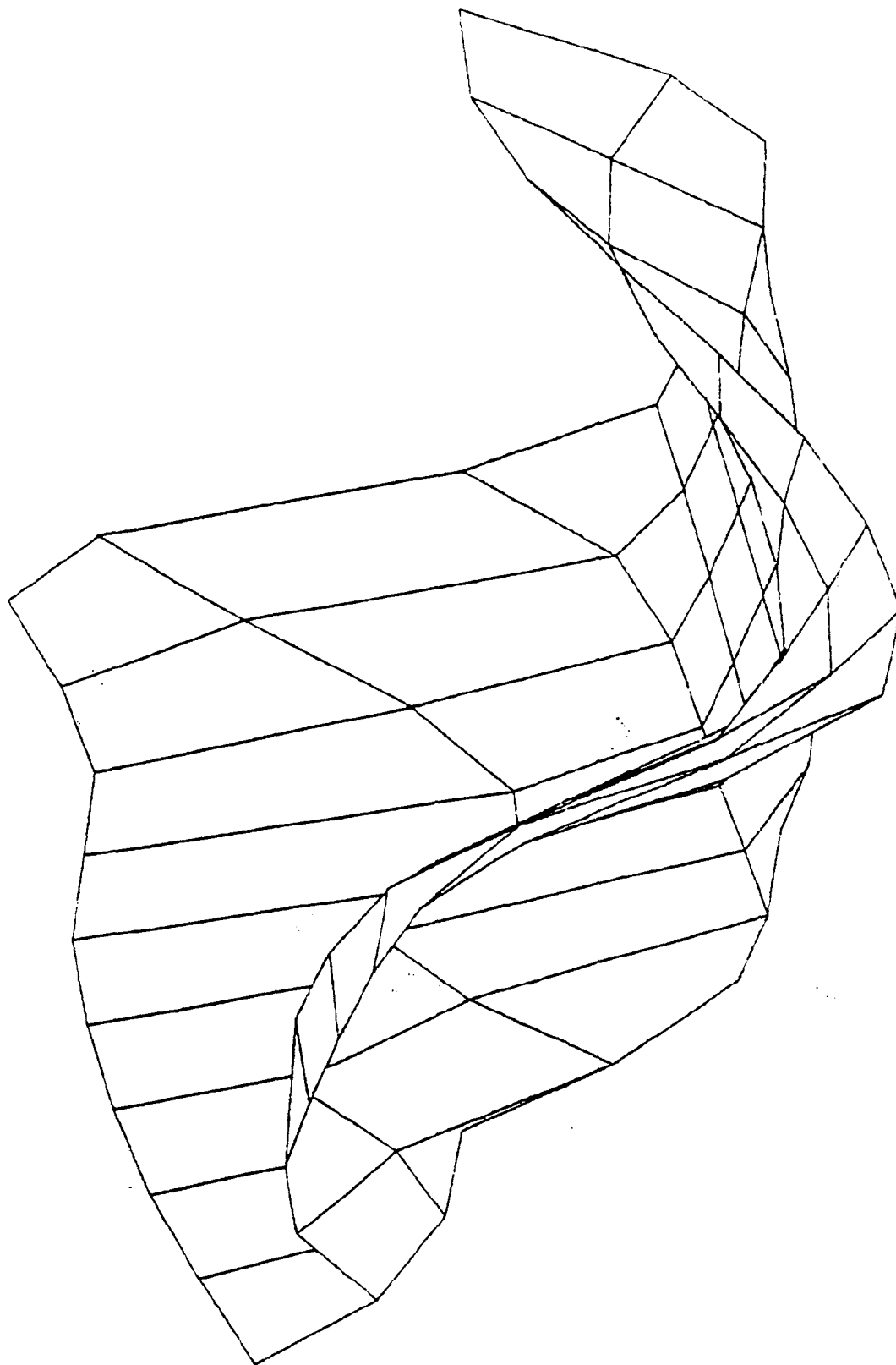
Tpt With Respect To R0 and Tinf



R0 - 1 to 100

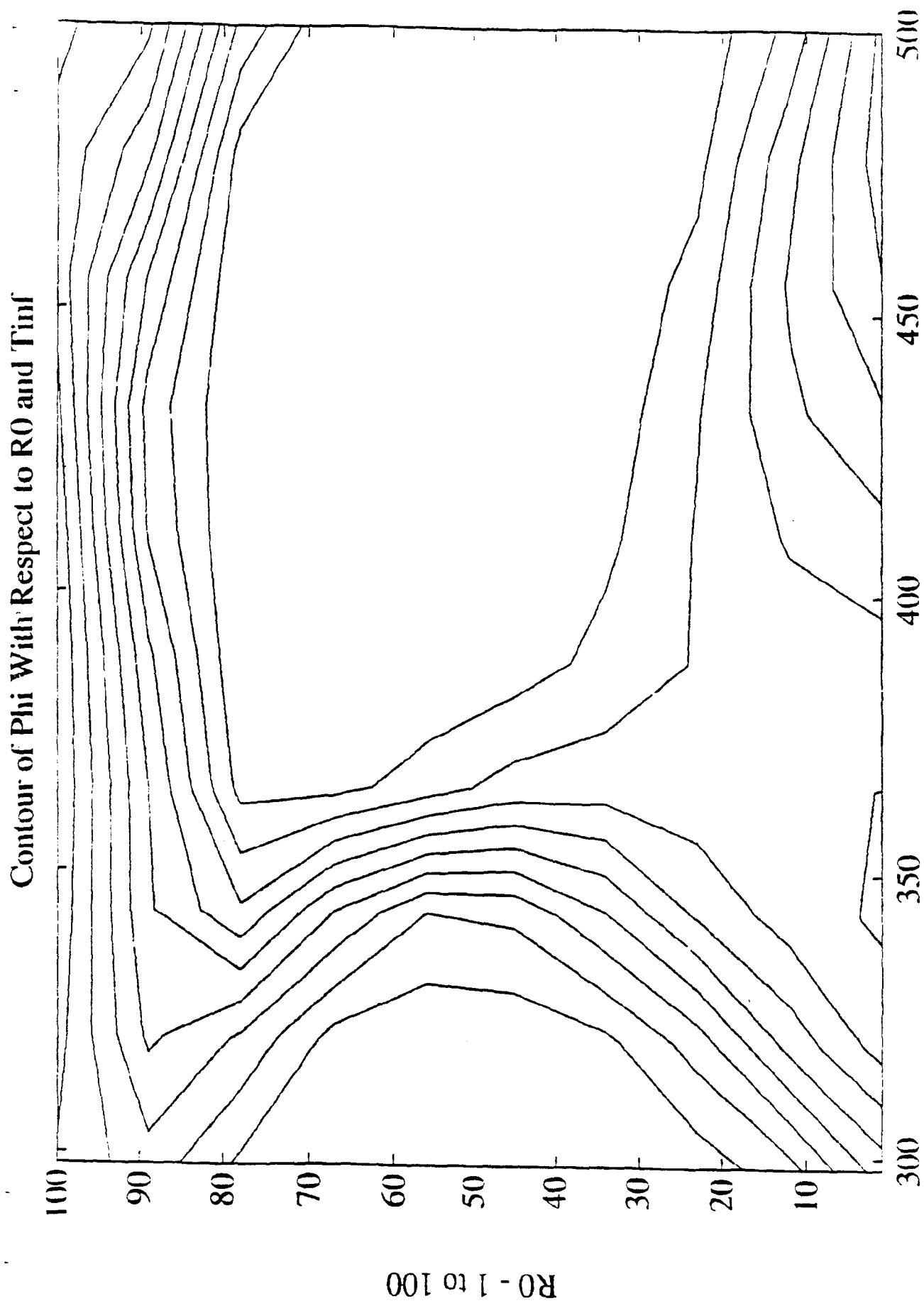
Tinf - 298 to 500

Phi as a function of R0 and Tinf

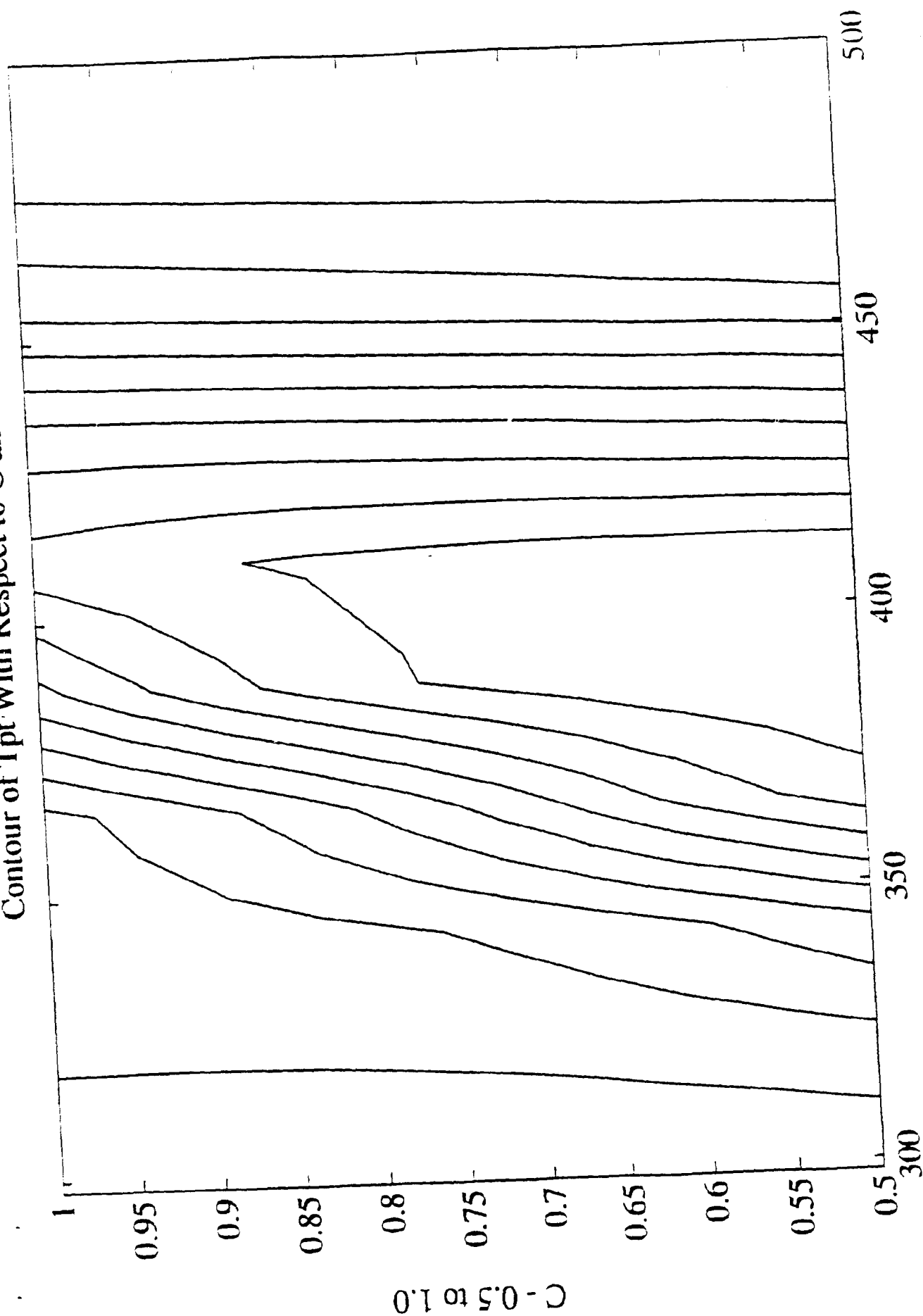


R0 - 1 to 100

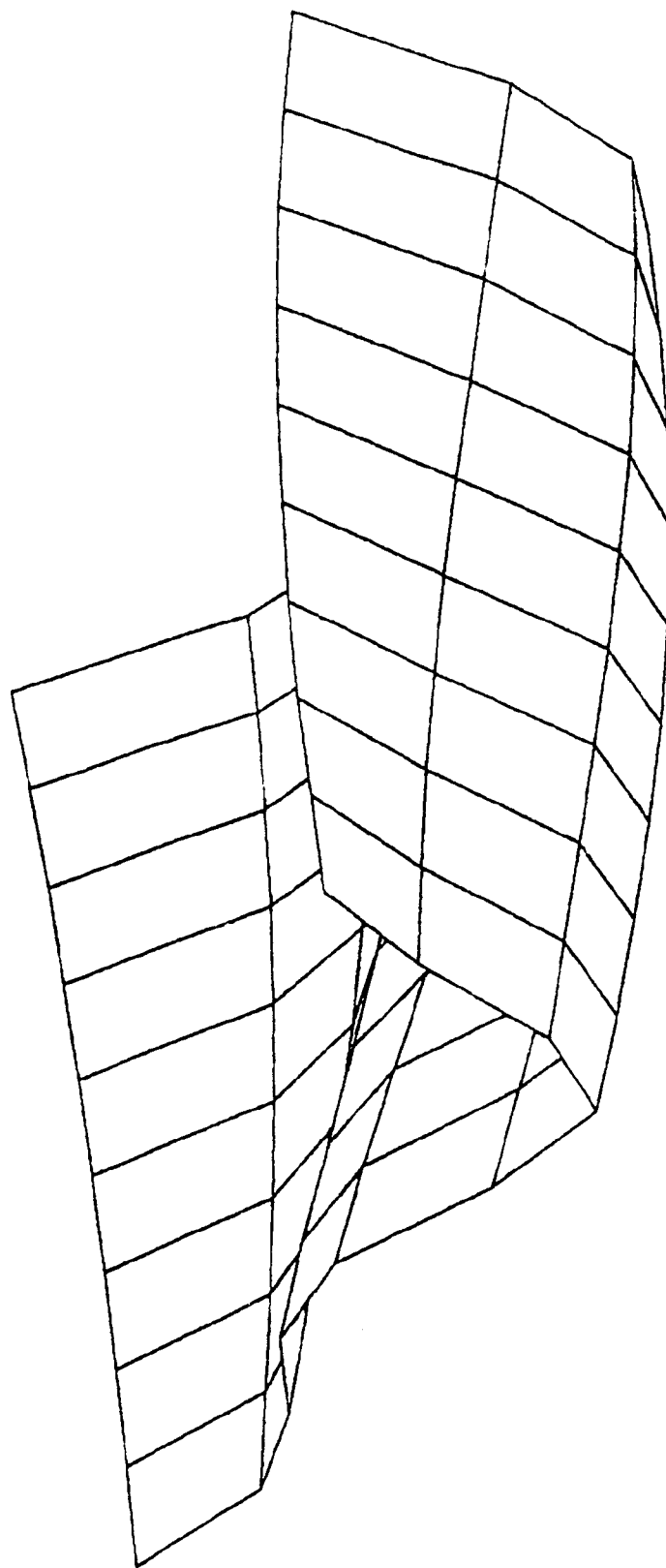
Tinf - 298 to 500



Contour of Tpt With Respect to C and Tinf



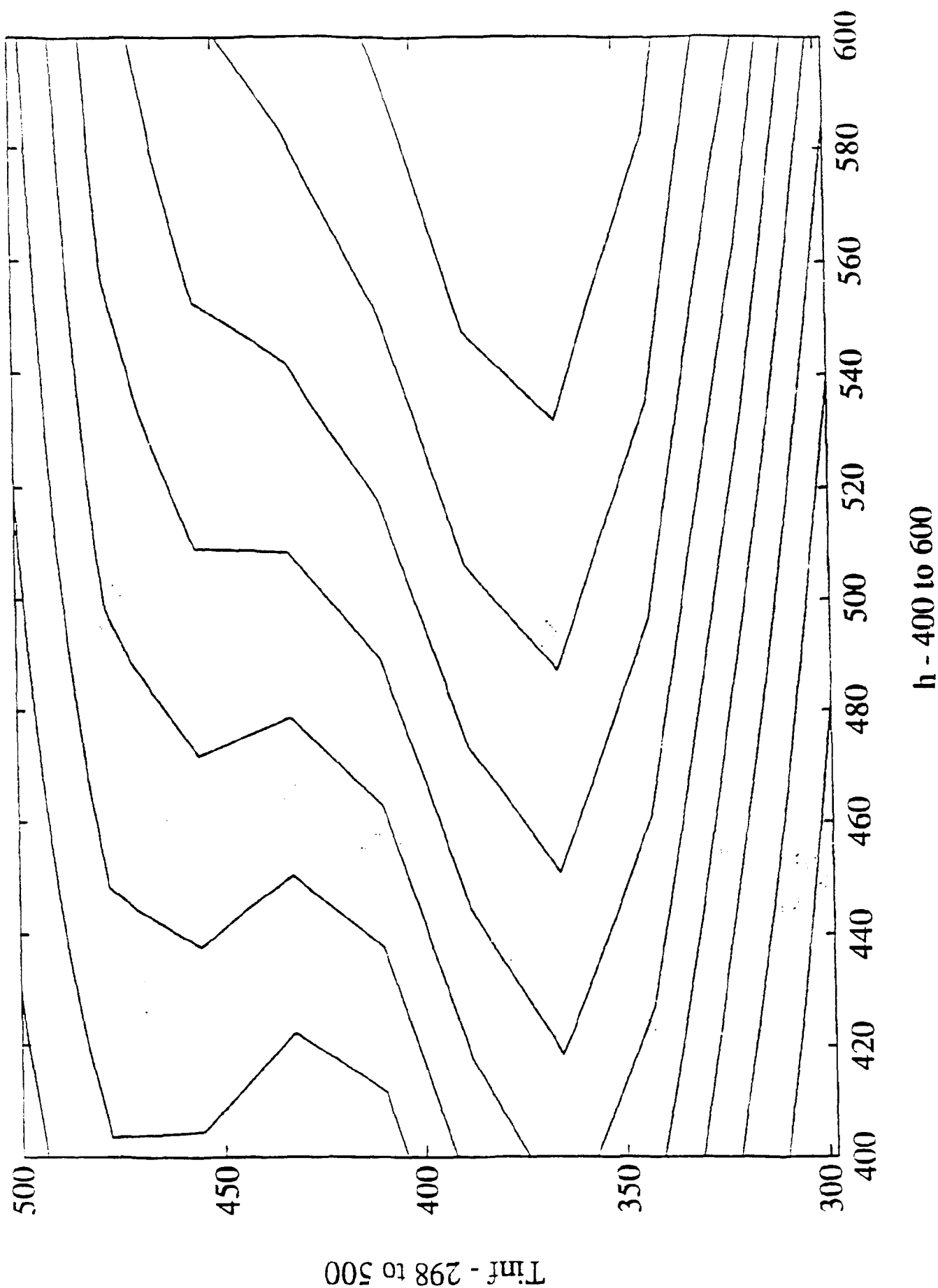
Phi as a function of h and Tinf



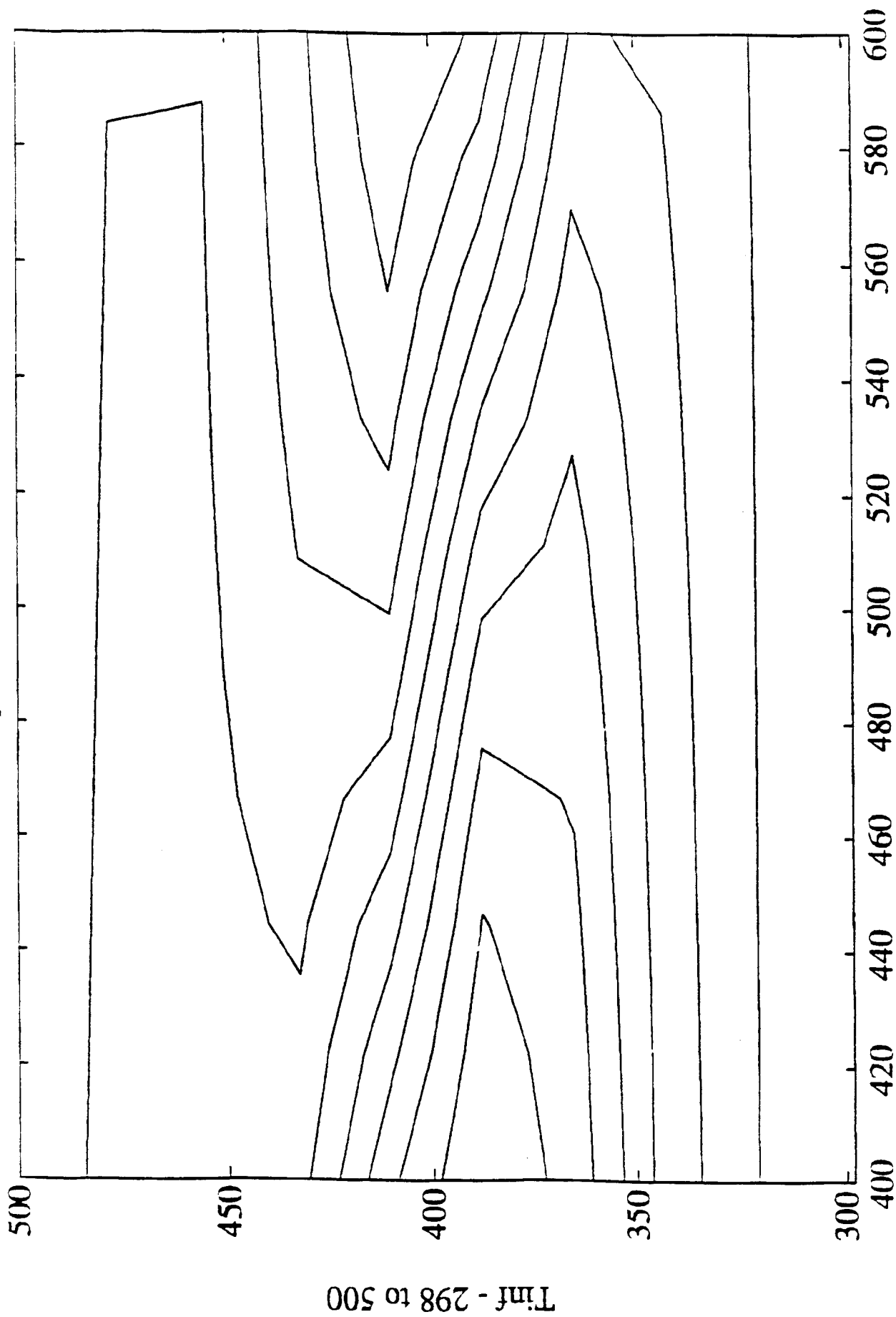
Tinf - 298 to 500

h - 400 to 600

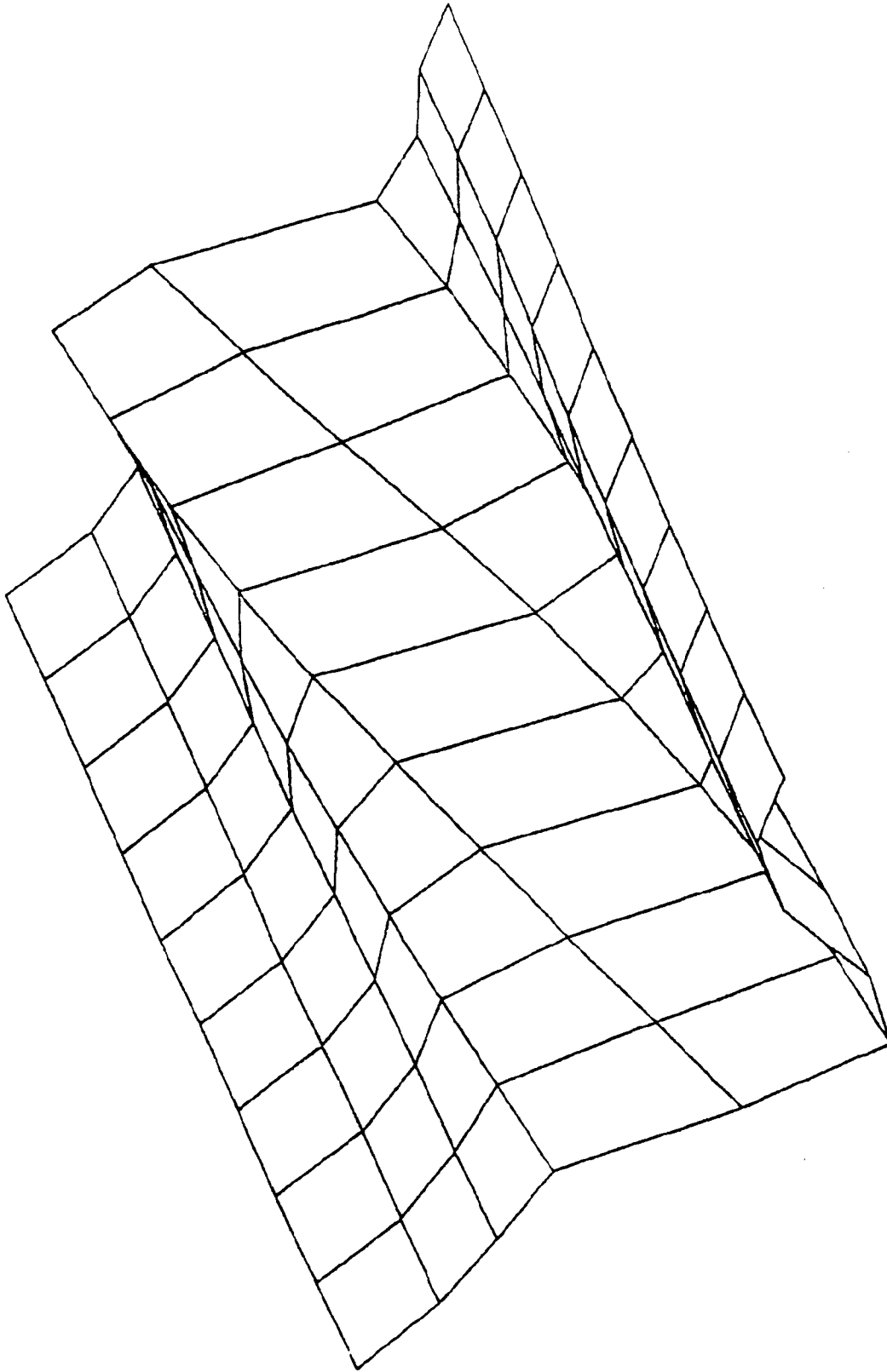
Contour of Phi With Respect to h and Tinf



Contour of Tpt With Respect to h and Tinf



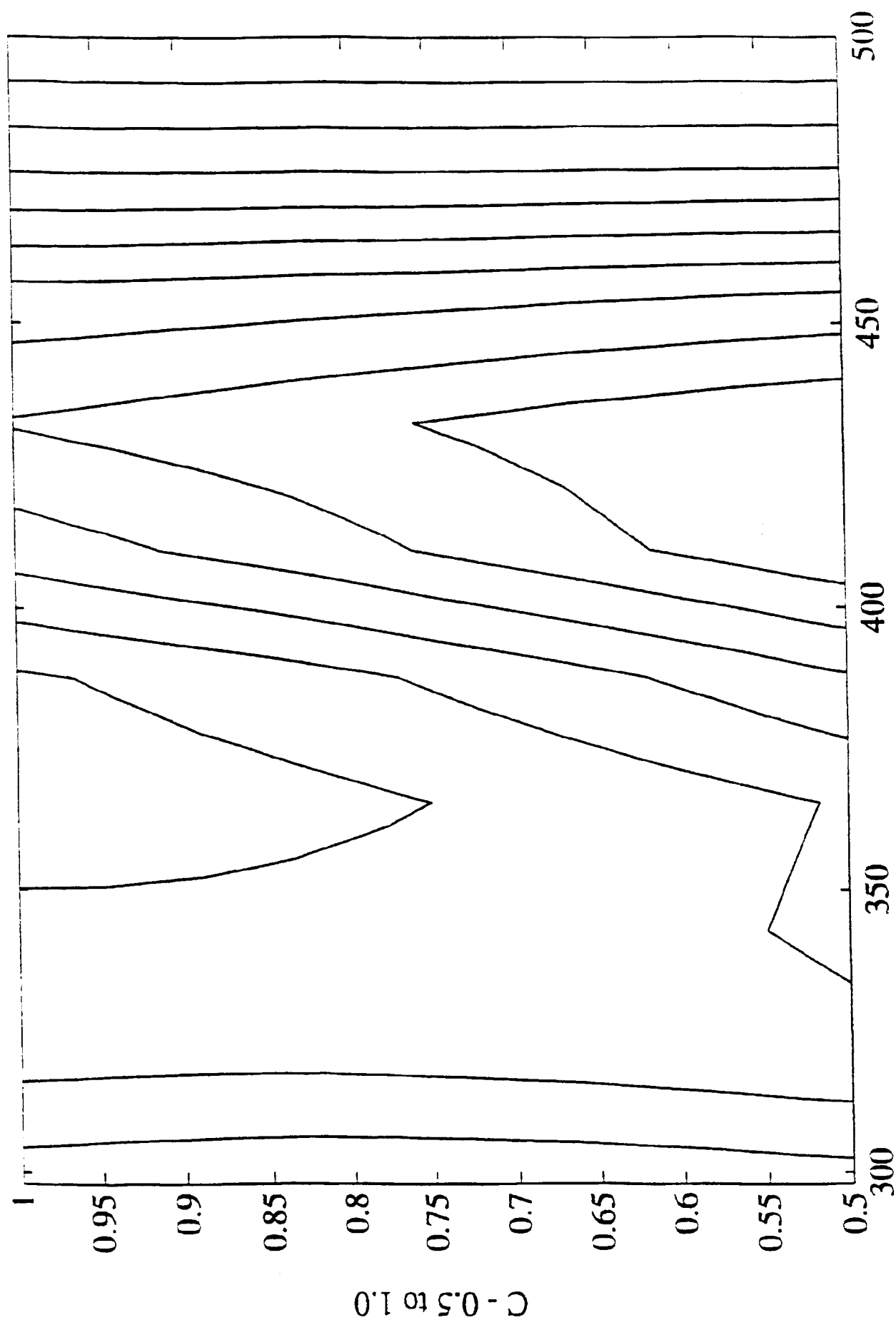
Tpt With Respect To h and Tinf



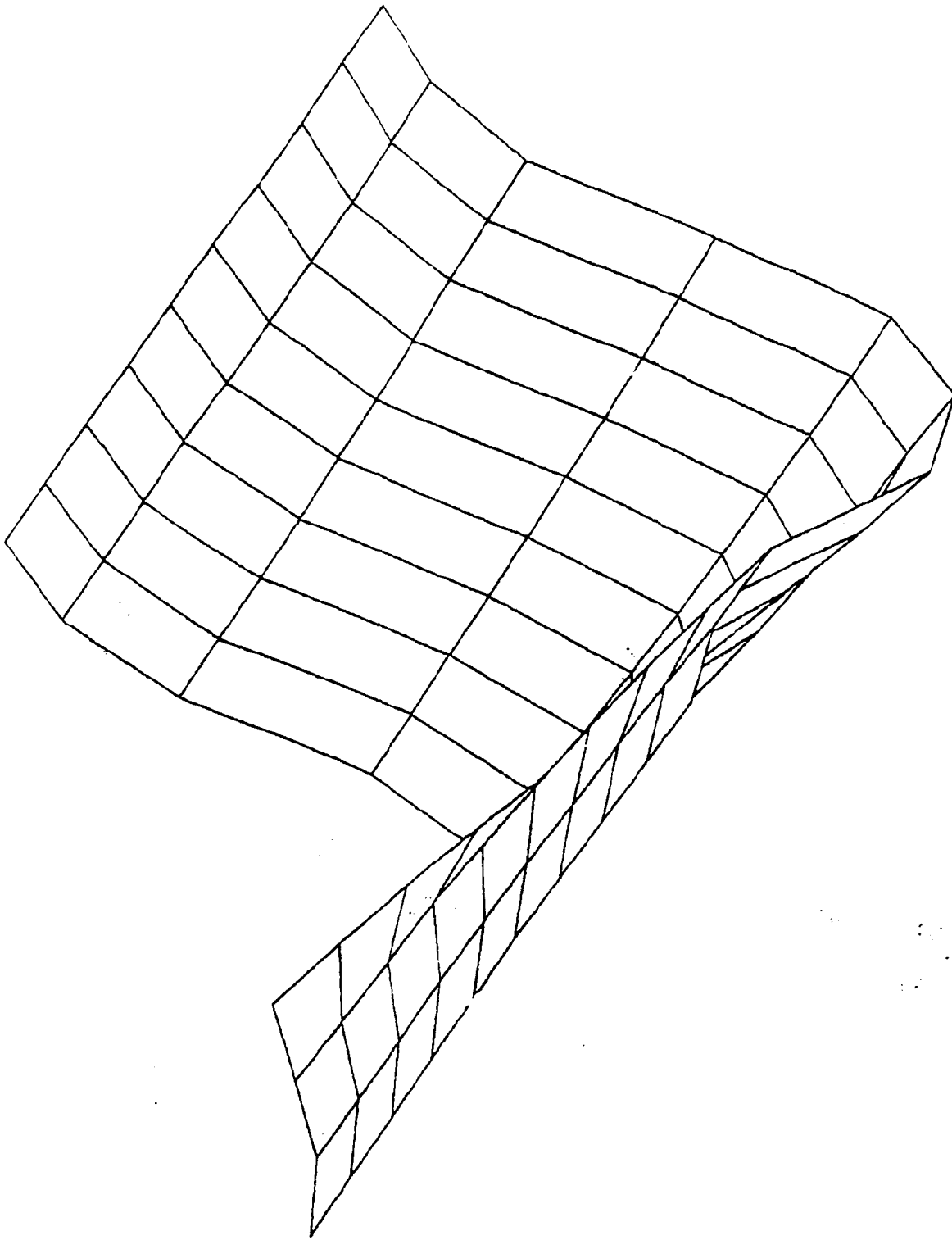
Tinf - 298 to 500

h - 400 to 600

Contour of Phi With Respect to C and Tinf



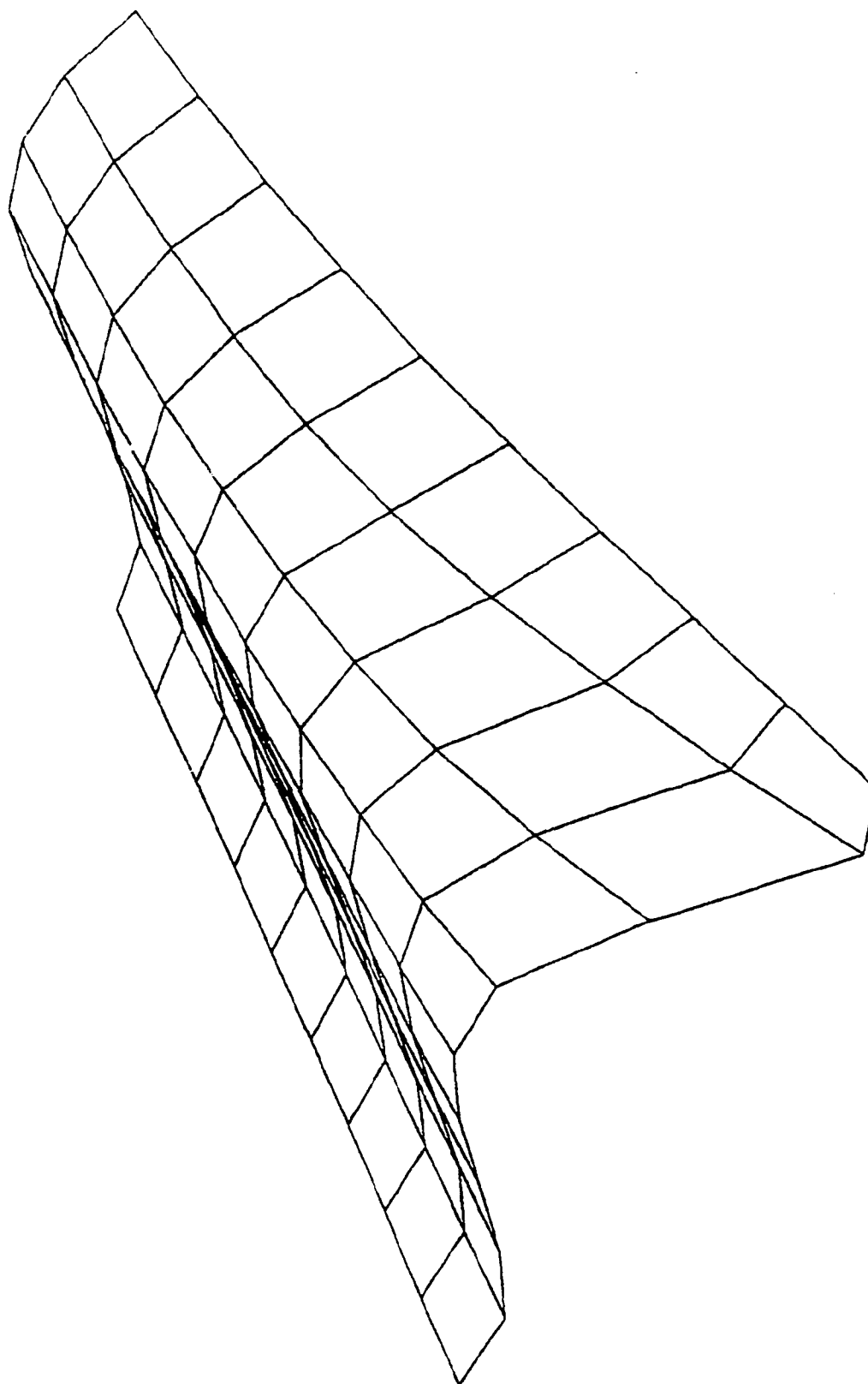
Tpt With Respect To C and Tinf



C - 0.5 to 1.0

Tinf - 298 to 500

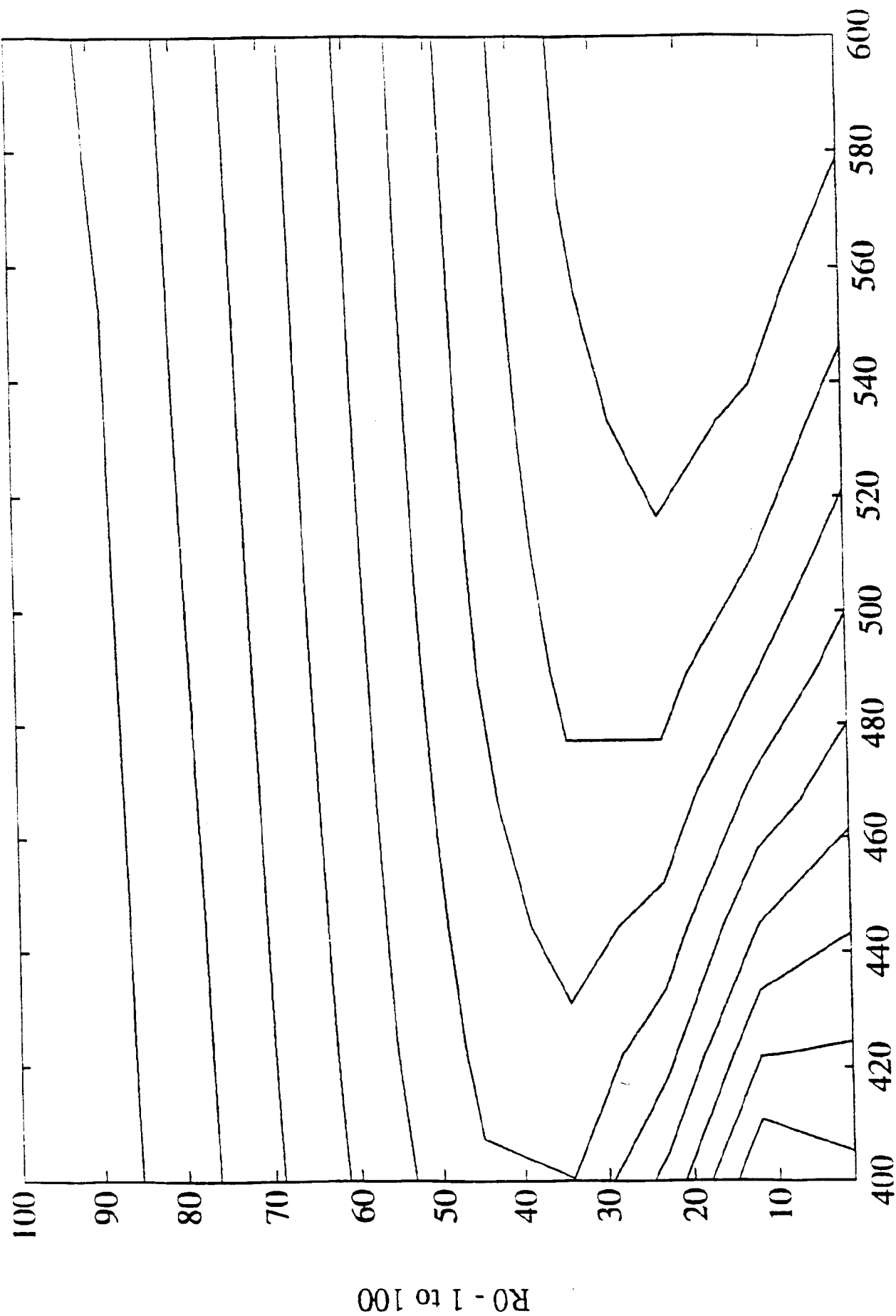
Tpt With Respect To R0 and h



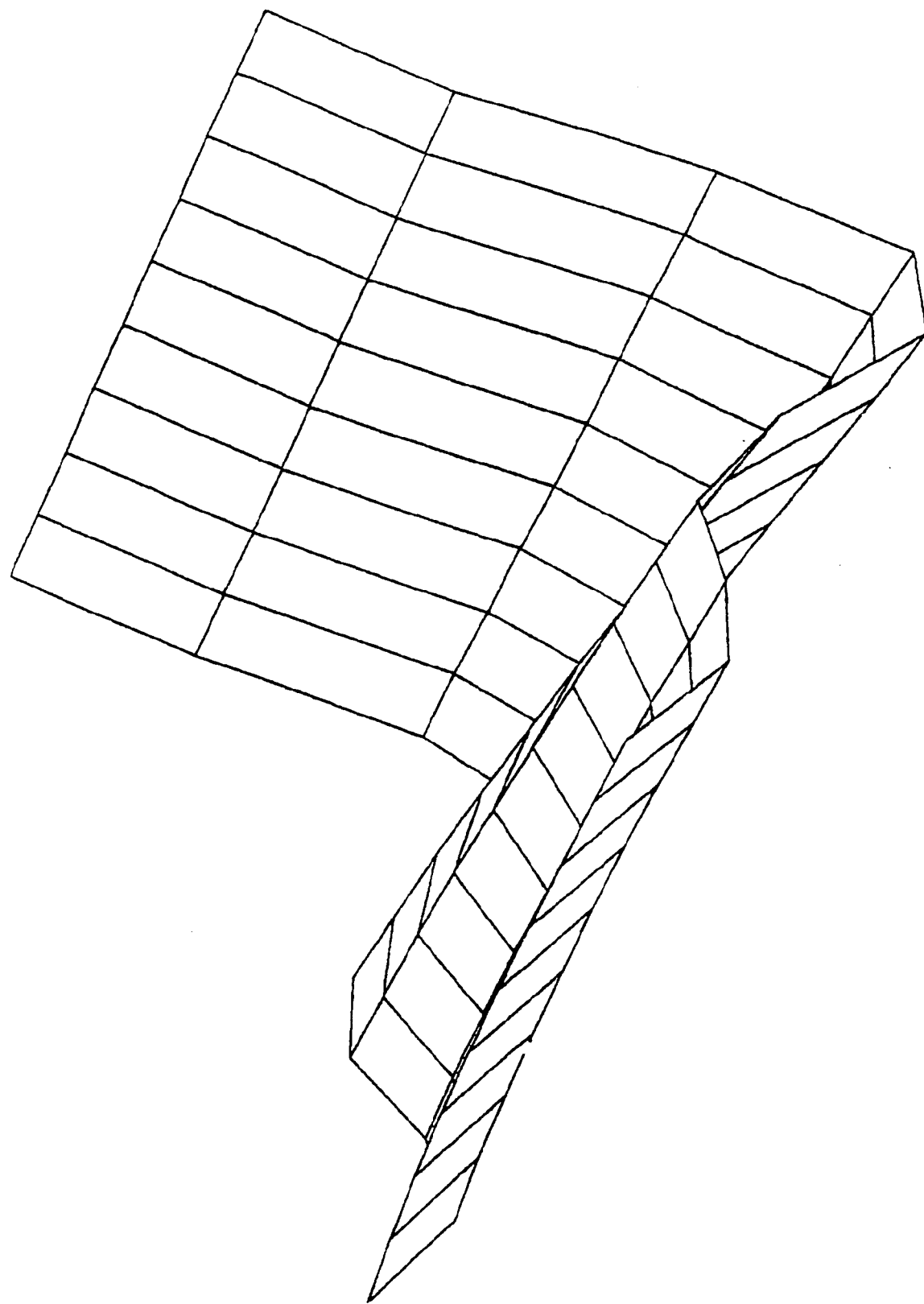
R0 - 1 to 100

h - 400 to 600

Contour of Tpt With Respect to R0 and h



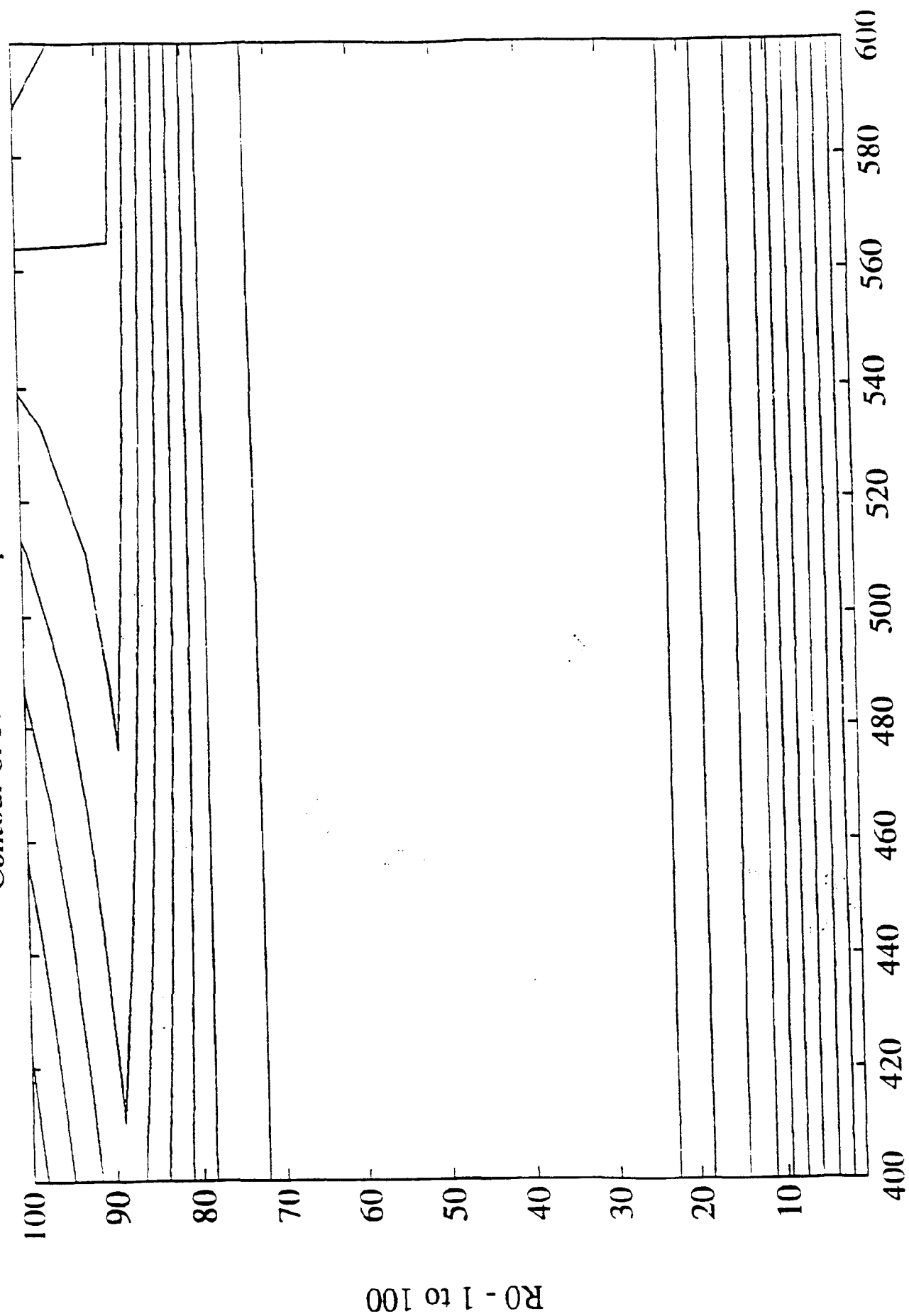
Phi as a function of C and Tinf



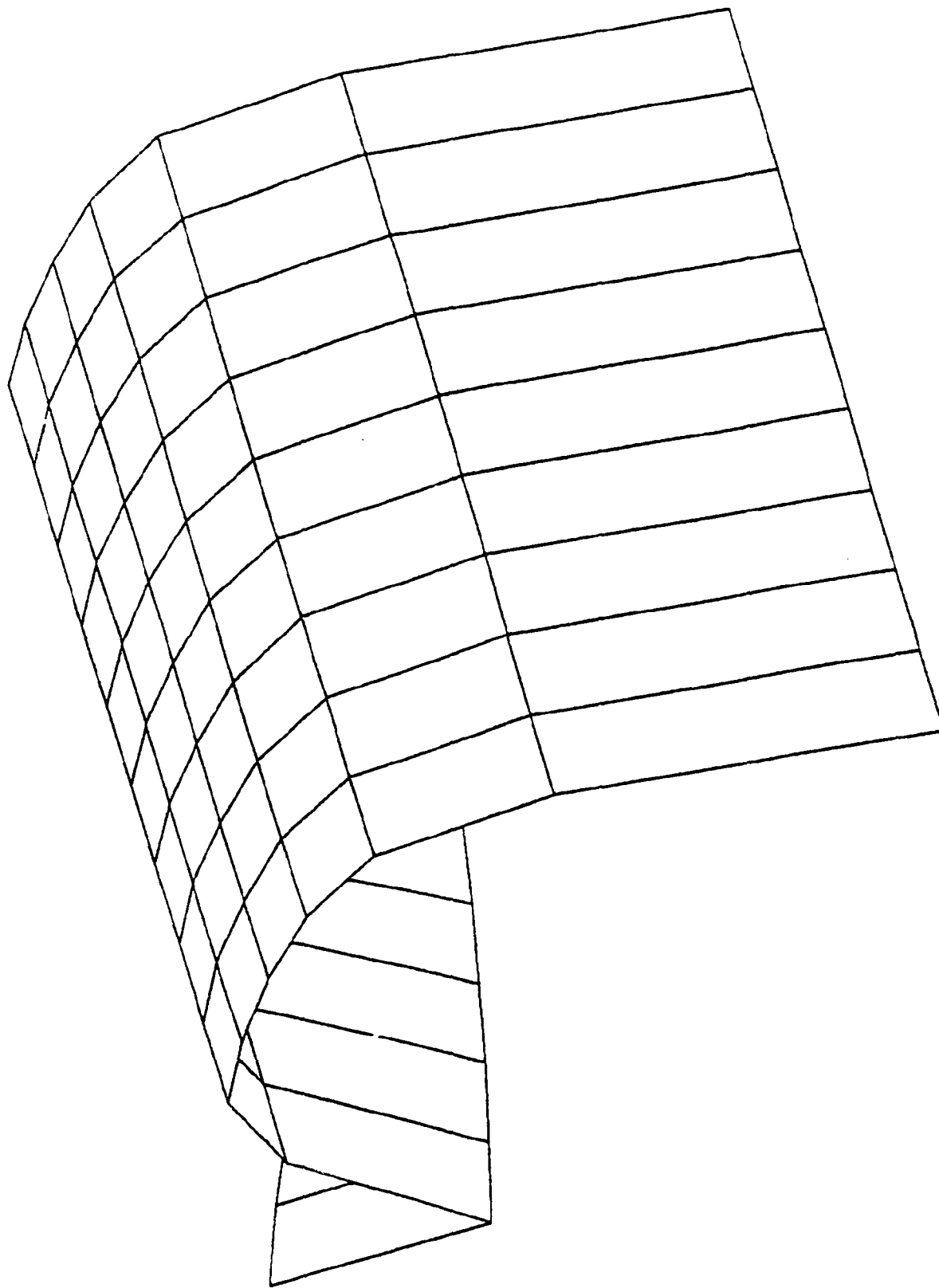
C - 0.5 to 1.0

Tinf - 298 to 500

Contour of Phi With Respect to R0 and h



Phi as a function of R0 and h



R0 - 1 to 100

h - 400 to 600